Copy No._____

Defence Research and Development Canada
Recherche et développement pour la défense Canada

DEFENCE R&D DÉFENSE

VIBRO Software Experimental Validation

Alain Berry
Jean-Luc Wojtowicki
Samuel Berry
Raymond Panneton
Department of Mechanical Engineering

Department of Mechanical Engineering
University of Sherbrooke
Sherbrooke, Quebec
J1K 2R1

Contract Number: W7707-008313/001/HAL

Contract Scientific Authority: J.P. Szabo, Ph.D., (902) 426-0550 ext. 3427

Defence R&D Canada

Contractor Report
DREA CR 2001-054
July 2002

Canada

This page intentionally left blank.

Copy No:

VIBRO Software Experimental Validation

Alain Berry
Jean-Luc Wojtowicki
Samuel Berry
Raymond Panneton
Department of Mechanical Engineering
University of Sherbrooke
Sherbrooke, Quebec, Canada J1K 2R1

Contract Number W7707-008313/001/HAL

Contract Scientific Authority

J.P. Szabo, Ph.D.
Defence R&D Canada – Atlantic
P.O. Box 99000 Stn. Forces
Bldg D-17
Halifax, NS
B3K 5W5
(902) 427-0550 ext. 3427

Defence R&D Canada – Atlantic

Contractor Report
DREA CR 2001-054
July 2002

Scientific Authority

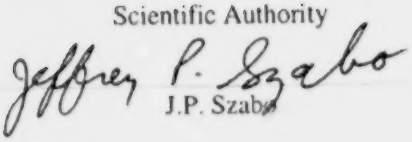

J.P. Szabo

Approved by

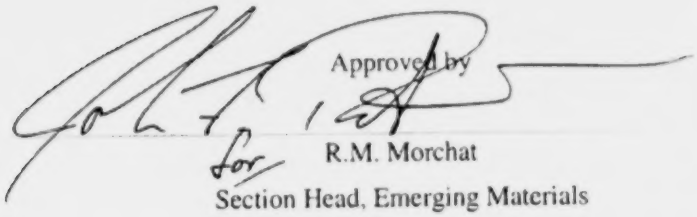

For R.M. Morchat

Section Head, Emerging Materials

Approved for release by

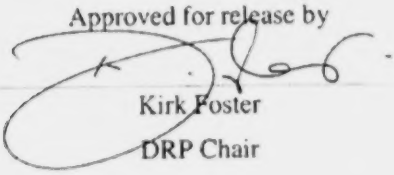

Kirk Foster

DRP Chair

Contractor Report Disclaimer

The scientific or technical validity of this Contract Report is entirely the responsibility of the contractor and the contents do not necessarily have the approval or endorsement of Defence R&D Canada.

Terms of release: The information contained herein is proprietary to Her Majesty and is provided to the recipient on the understanding that it will be used for information and evaluation purposes only. Any commercial use including use for manufacture is prohibited. Release to third parties of this publication or information contained herein is prohibited without the prior written consent of Defence R&D Canada.

© Her Majesty the Queen as represented by the Minister of National Defence, 2002

© Sa majesté la reine, représentée par le ministre de la Défense nationale, 2002

104-06978/

Abstract

The University of Sherbrooke's Acoustics and Vibration Group (GAUS) have developed a computer code called VIBRO for modelling the effect of damping and decoupling coatings on the sound radiation from fluid loaded plates. In this work, laser vibrometry was used to measure the vibration on the both the wet and dry sides of plates backed by a water filled cavity. VIBRO accurately predicted the mean square velocity spectra of bare 2 mm steel plates in air, both in terms of peak positions and magnitudes. The agreement between experimental data and VIBRO model predictions was not quite as good for the corresponding experiment of the bare plate in water, but peak positions still matched closely. A modified Oberst beam method was used to determine the complex Young's and shear modulus of four different types of foam materials: 3 mm neoprene, 6 mm ethylvinylacetate, 12 mm ethylvinylacetate, and 25 mm EPT/SBR foam. For plates coated with these foams, the VIBRO model predictions were generally very good on the water side of the plate. However, the VIBRO model calculations did not capture a dip in the mean square velocity spectum that was observed on the air side of coated plates. The results suggest that VIBRO is a useful tool for prediction of the vibration insertion loss and acoustic insertion loss as vibroacoustic indicators. The experimental results related to the effect of the decoupling coatings on the vibration at the plate/ air interface could not be explained in terms of the VIBRO model.

Résumé

Le Groupe d'acoustique de l'Université de Sherbrooke (GAUS) a mis au point un programme informatique appelé VIBRO servant à modéliser les effets des revêtements d'amortissement et de découplage sur les radiations acoustiques imputables à des plaques chargées de fluides. Dans ces travaux, on a eu recours à la vibrométrie laser pour mesurer les vibrations sur les côtés humides et secs de plaques reposant sur une cavité remplie d'eau. Le VIBRO a permis de prévoir avec précision les spectres de la valeur quadratique moyenne de la vitesse de plaques d'acier non revêtu de 2 mm d'épaisseur dans l'air, en termes de positions et d'amplitude maximales. La concordance entre les données expérimentales et les prévisions du modèle VIBRO n'a pas été aussi bonne que pour l'expérience correspondante réalisée pour des plaques non revêtues dans l'eau, mais les positions maximales étaient très rapprochées. La méthode de faisceau Oberst modifiée a été utilisée pour déterminer le module de Young complexe et le module de rigidité de quatre types différents de mousses : néoprène de 3 mm, acétate d'éthylvinyle de 6 mm, acétate d'éthylvinyle de 12 mm et mousse EPT/SBR de 25 mm. Dans le cas des plaques recouvertes de ces mousses, les prévisions du modèle VIBRO ont été dans l'ensemble très bonnes pour ce qui est du côté eau de la plaque. Cependant, les calculs du modèle VIBRO n'ont pas permis d'observer d'inclinaisons dans le spectre de la valeur quadratique moyenne de la vitesse qui a été observé pour le côté air des plaques revêtues. Les résultats laissent supposer que VIBRO est un outil utile pour la prévision de la perte d'insertion de la vibration et de la perte d'insertion acoustique à titre d'indicateurs vibroacoustiques. Les résultats expérimentaux liés à l'effet des revêtements de découplage sur la vibration à l'interface plaque/air n'ont pas pu être expliqués par le modèle VIBRO.

This page intentionally left blank.

Executive summary

Background

The University of Sherbrooke's Acoustics and Vibration Group (GAUS) have developed a computer code for modelling the effect of damping and polymer based noise reduction coatings on the sound radiation from fluid loaded plates. A full validation of VIBRO would require identical boundary conditions to that presumed by the code: simply supported plate in an infinite rigid baffle, loaded on one side by air and on the other side by water. The plate is excited by point loading or by acoustic excitation from the air side. Free field conditions are presumed for both sides of the plate. The code calculates several relevant variables including radiated sound power, vibration at specified points on the coating and substrate, and mean square velocity on the coating and substrate.

It has been shown that a simply supported plate backed by a water filled cavity gives a similar vibration response to a simply supported plate backed by a semi-infinite water layer, although the acoustic response of the plate will be very different due to acoustic modes in the cavity. In this contract, the vibration response of bare and coated substrates backed by a fluid filled cavity was measured in order to conduct a partial validation of the VIBRO code. Such an approach avoided the requirement of free field conditions and a rigid baffle necessary for acoustic measurements. Determination of the material properties of the coating material was also carried out as part of this work.

Laser vibrometry was used to measure the vibration on the both the wet and dry sides of fluid loaded plates. This report presents in detail a comparison of experimental data with model predictions for several vibroacoustic indicators.

Principal Results

VIBRO accurately predicted the mean square velocity spectra of bare 2 mm steel plates in air, both in terms of peak positions and magnitudes. The agreement between experimental data and VIBRO model predictions was not quite as good for the corresponding experiment of the bare plate in water, but peak positions still matched closely. A modified Oberst beam method was used to determine the complex Young's and shear modulus of four different types of foam materials: 3 mm neoprene, 6 mm ethylvinylacetate, 12 mm ethylvinylacetate, and 25 mm EPT/SBR foam. For plates coated with these foams, the VIBRO model predictions were generally very good on the water side of the plate. However, the VIBRO model calculations did not capture a dip in the mean square velocity spectum that was observed on the air side of coated plates. As a result, VIBRO predictions for vibration insertion loss were quite good, but the predictions for mean square velocity ratio across the coating were not. It was demonstrated that the dip was not related to the finite acoustic volume in the tank, but rather could be explained by an updated 1D model of deJong that accounts for radiation mechanisms of finite plates.

Significance of Results

The technique of using laser vibrometry to measure vibration at the water/ plate interface for bare and coated substrates was demonstrated in this work. A full validation of VIBRO has not been achieved since free field conditions did not apply. However, a partial validation of VIBRO based on the vibration response of bare and coated plates has been carried out. These experiments demonstrated that VIBRO is able to predict the effect of decoupling coatings on the vibration response of finite plates at the plate/water interface. The results also suggest that VIBRO is a useful tool for prediction of the vibration insertion loss and acoustic insertion loss as vibroacoustic indicators. The experimental results related to the effect of the decoupling coatings on the vibration at the plate/ air interface could not be explained in terms of the VIBRO model.

Berry, A., Panneton, R., Wojtowicki, J-L., Berry, S. 2001. VIBRO Software Experimental Validation. DREA CR 2001-054 Defence Research Establishment Atlantic.

Sommaire

Contexte

Le Groupe d'acoustique de l'Université de Sherbrooke (GAUS) a mis au point un programme informatique servant à modéliser les effets des revêtements d'amortissement et des revêtements de réduction du bruit à base de polymères sur les radiations acoustiques imputables à des plaques chargées de fluides. Une validation complète de VIBRO nécessiterait des conditions limites identiques à celles présumées par le programme : une plaque à support simple dans une enceinte à rigidité infinie, comportant une charge d'air d'un côté et une charge d'eau de l'autre. La plaque est excitée par des charges ponctuelles ou par une excitation acoustique du côté air. Des conditions de champ libre sont présumées pour les deux côtés de la plaque. Le programme calcule plusieurs variables pertinentes incluant la puissance acoustique rayonnée, la vibration en des points particuliers du revêtement et du substrat, et la valeur quadratique moyenne de la vitesse sur le revêtement et le substrat.

Il a été démontré qu'une plaque sur support simple reposant sur une cavité remplie d'eau donne une réponse vibratoire semblable à celle d'une plaque à support simple reposant sur une couche d'eau semi-infinie, bien que la réponse acoustique de la plaque soit très différente à cause des modes de transmission acoustique dans la cavité. Dans le présent contrat, la réponse vibratoire des substrats non revêtus et revêtus reposant sur une cavité remplie de fluide a été mesurée afin de réaliser une validation partielle du programme VIBRO. Une telle démarche permettait d'éviter l'exigence des conditions de champ libre et l'enceinte rigide nécessaire pour effectuer les mesures acoustiques. La détermination des propriétés du matériau constituant le revêtement a également été réalisée dans le cadre de ces travaux.

Dans le cadre des travaux, on a eu recours à la vibrométrie laser pour mesurer les vibrations sur les côtés humides et secs de plaques ayant une charge de fluides. Le présent rapport présente une comparaison détaillée des données expérimentales avec les prévisions du modèle pour plusieurs indicateurs vibroacoustiques.

Principaux résultats

Le VIBRO a permis de prévoir avec précision les spectres de la valeur quadratique moyenne de la vitesse de plaques d'acier non revêtu de 2 mm d'épaisseur dans l'air, en termes de positions et d'amplitude maximales. La concordance entre les données expérimentales et les prévisions du modèle VIBRO n'a pas été aussi bonne que pour l'expérience correspondante réalisée pour des plaques non revêtues dans l'eau, mais les positions maximales étaient très rapprochées. La méthode de faisceau Oberst modifiée a été utilisée pour déterminer le module de Young complexe et le module de rigidité de quatre types différents de mousses : néoprène de 3 mm, acétate d'éthylvinyle de 6 mm, acétate d'éthylvinyle de 12 mm et mousse EPT/SBR de 25 mm. Dans le cas des plaques recouvertes de ces mousses, les prévisions du modèle VIBRO ont été dans l'ensemble très bonnes pour ce qui est du côté eau de la plaque. Cependant, les calculs du modèle VIBRO n'ont pas permis d'observer d'inclinaisons dans le spectre de la valeur quadratique moyenne de la vitesse qui a été observé pour le côté air des

plaques revêtues. Ainsi, les prévisions de VIBRO pour la perte d'insertion de vibration ont été très bonnes, mais les prévisions pour le rapport de la valeur quadratique moyenne de la vitesse ont été moins intéressantes. On a démontré que l'inclinaison n'était pas liée au volume acoustique fini dans le réservoir, mais plutôt qu'elle pouvait être expliquée par un modèle 1D de deJong mis à jour qui tient compte du rayonnement dans les plaques finies.

Importance des résultats

La technique utilisant la vibrométrie laser pour mesurer les vibrations à l'interface eau/plaque pour les substrats non revêtus et revêtus a été démontrée dans les présents travaux. Une validation complète de VIBRO n'a pas été réalisée puisque les conditions de champ libre ne s'appliquaient pas. Cependant, une validation partielle de VIBRO fondée sur la réponse vibratoire des plaques non revêtues et revêtues a été réalisée. Ces expériences ont démontré que VIBRO permet de prévoir l'effet des revêtements de découplage sur la réponse vibratoire de plaques finies à l'interface plaque/eau. Les résultats laissent également supposer que VIBRO est un outil utile pour la prévision de la perte d'insertion de vibration et pour la perte d'insertion acoustique à titre d'indicateurs vibroacoustiques. Les résultats expérimentaux liés à l'effet des revêtements de découplage sur la vibration à l'interface plaque/air n'ont pas pu être expliqués par le modèle VIBRO.

Berry, A., Panneton, R., Wojtowicki, J-L., Berry, S. 2001. Validation expérimentale du logiciel VIBRO. CRDA CR 2001-054 Centre de recherches pour la défense Atlantique.

Table of Contents

INTRODUCTION 1

CHARACTERIZATION OF FOAM MATERIALS 2
1.1 Poisson's ratio measurements 2
1.2 Complex young's modulus measurements 2
1.2.1 Modified Oberst beam technique 2
1.2.2 Analytical model 5
1.2.3 Inversion of the model 8
1.2.4 Test specimens 13
1.2.5 Results 14

VIBRATION MEASUREMENTS AND COMPARISONS WITH VIBRO 22
2.1 Experimental set-up 22
2.2 Acquisition and analysis 27
2.2.1 Acquisition 27
2.2.2 Analysis 29
2.2.3 Preliminary tests 31
2.2.4 Characteristics of test plates and of measurements 33
2.3 Comparisons with VIBRO predictions 36
2.3.1 VIBRO parameters 36
2.3.2 Steel plate in air 36
2.3.3 Steel plate in water 37
2.3.4 2mm steel plate with 3mm neoprene foam 40
2.3.5 2mm steel plate with 6mm EVA foam 51
2.3.6 9.5mm steel plate with 25mm EPT/SBR foam 59

CONCLUSION 67

APPENDIX A : SHEAR DAMPING EQUATIONS 68

APPENDIX B : THEORY-EXPERIMENT COMPARISON FOR VARIOUS MATERIAL CHARACTERIZATION DATA 70

APPENDIX C : INFLUENCE OF THE VOLUME OF WATER ON THE VIBRATION RESPONSE 83

INTRODUCTION

The University of Sherbrooke's Acoustics and Vibration Group (GAUS) have developed a computer code for modelling the effect of damping and polymer based noise reduction coatings on the sound radiation from fluid loaded plates. The code was originally written using a locally reacting model for decoupling materials, and was later refined to include the full three dimensional behaviour of the coating, using a wave approach.

A full validation of VIBRO would require identical boundary conditions to that presumed by the code: simply supported plate in an infinite rigid baffle, loaded on one side by air and on the other side by water. The plate is excited by point loading or by acoustic excitation from the air side. Free field conditions are presumed for both sides of the plate. The code calculates several relevant variables including radiated sound power, vibration at specified points on the coating and substrate, and mean square velocity on the coating and substrate.

It has been shown that a simply supported plate backed by a water filled cavity gives a similar vibration response to a simply supported plate backed by a semi-infinite water layer, although the acoustic response of the plate will be very different due to acoustic modes in the cavity. Therefore, it was suggested that validation of VIBRO could be carried out by measuring the vibration response of bare and coated substrates backed by a fluid filled cavity. Such an approach avoids the requirement of free field conditions and a rigid baffle necessary for acoustic measurements.

The purpose of this contract is to validate VIBRO by carrying out vibration measurements on bare and coated substrates. Acoustic properties of the coating materials are also determined as part of this work.

CHARACTERIZATION OF FOAM MATERIALS

*I.1 Poisson's ratio measurements**

I.2 Complex Young's modulus measurements

I.2.1 Modified Oberst beam technique

The Oberst beam technique The «Oberst beam» is a classical method for the characterization of viscoelastic or damping materials based on measurements on a composite cantilever beam made of a base metallic beam and free or constrained layers of the material under test. The method usually consists of measuring the FRF between the external force applied to the composite beam and the response at a given location; The FRF measured on both the base beam and the composite beam allows extraction of the material properties, generally at the resonances of the composite beam. As the base beam is made of a rigid and lightly damped material (steel, aluminum), one critical aspect of this method is to properly excite the beam without adding weight or damping. Therefore, exciting the beam with an electrodynamic shaker is not recommended because of the added mass (moving mass, stinger misalignment, force transducer) brought by the shaker. Alternative solutions are suggested in the ASTM E576 standard[1], see figure I.1. An electro-magnetic non-contacting transducer (tachometer pick-up, for example) can provide a proper excitation but it is limited to ferro-magnetic materials. As aluminum or plastic materials are widely used for the base beam, a small piece of magnetic material must be glued to achieve specimen excitation.

---

* Note by Scientific Authority: No Poisson's ratio measurements were carried out.

1. ASTM E756 – 98, Standard Test Method for Measuring Vibration-Damping Properties of Materials, American Society for Testing and Materials

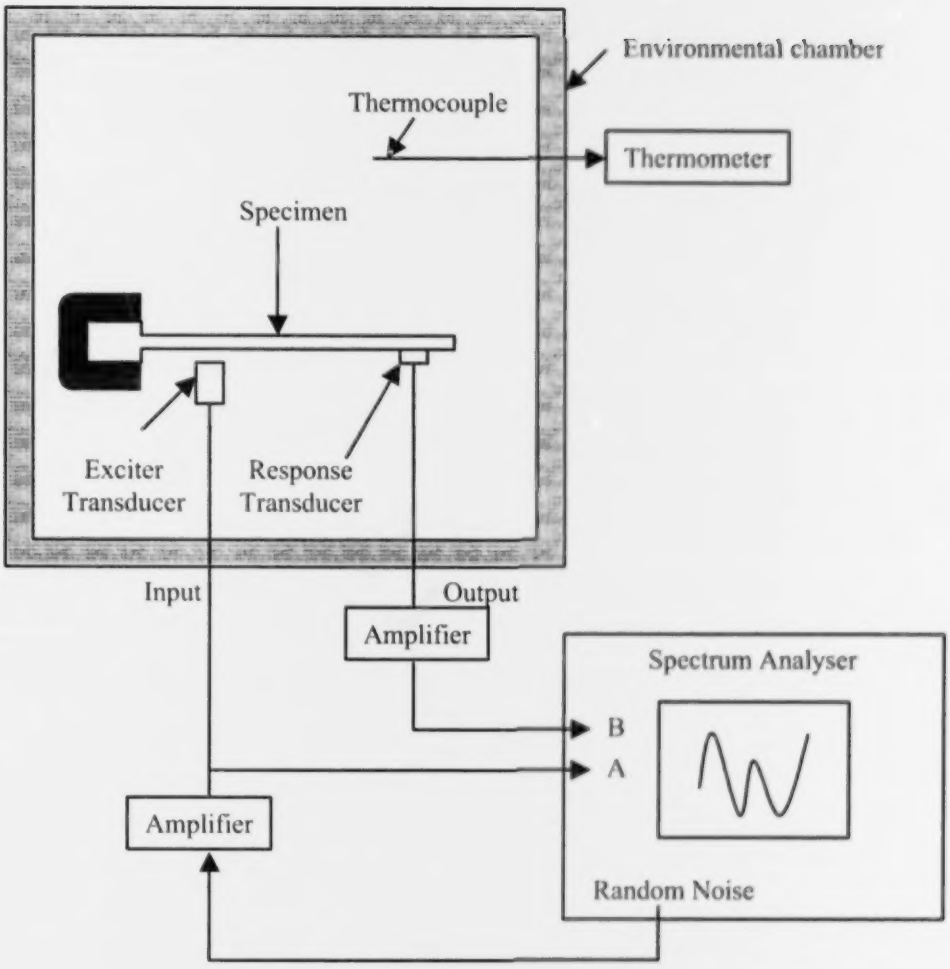

Figure I.1: Experimental set-up as described in the ASTM E576 standard

Potential difficulties of the technique are to properly measure the excitation force in the case of a non-contacting excitation device, and the modified dynamics due to the added piece of ferro-magnetic bonded to the structure (added damping due to the bonding, mass of the added piece). Also, the response measurement of the beam usually involves an accelerometer. Even if the problem of added damping and mass is much less critical because small and light accelerometers are available, it is preferable to avoid this solution for the same reasons as above. A straightforward solution is to use a laser vibrometer, which can accurately measure dynamic velocities without contact. However, this equipment is much more expensive than a simple accelerometer. Other problems can occur because of the clamped side of the beam (see figure I.2). The clamping is simulated by an increase of the thickness of the beam (the root). This root is wedged into a heavy and stiff clamping system. Usually this system is satisfactory, but problems can occur in the case of misalignment, insufficient clamping force, bad machining of the root.

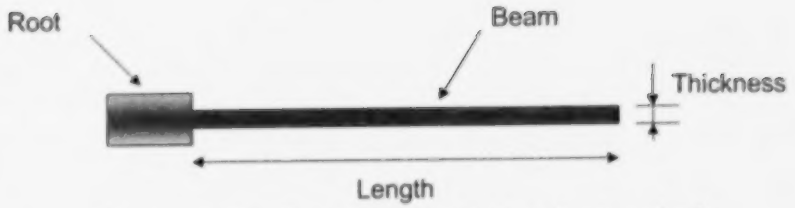

Figure I.2: Cantilever beam used in the Oberst method

Several attempts made at the GAUS laboratory[2] showed that the suggested experimental set-up led to large experimental errors, making the accurate evaluation of the mechanical properties of damping materials an interesting challenge. Therefore, an alternative to the ASTM E576 standard was investigated in this project, in order to avoid experimental uncertainties and increase accuracy of the measurements.

The modified Oberst beam technique The principle of the modified technique is shown on Figure I.3; it involves a free-free beam excited at its center by an electrodynamic shaker. The use of a free-free beam alleviates the experimental difficulties associated with clamping of the beam. The beam under test (with or without damping material) is simply screwed in its center to the shaker with a threaded rod. In practice, this is a very simple mechanical set-up (care must be brought on precisely locating the excitation point at the beam center to avoid unbalance problems).

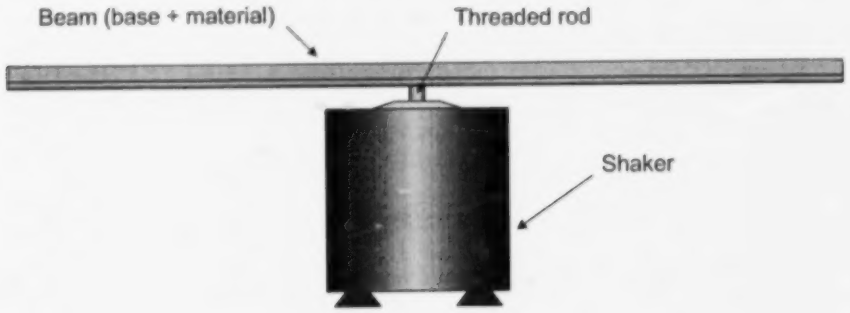

Figure I.3: Proposed experimental set-up

Furthermore, a free-free beam of length L excited at its center is dynamically equivalent to a clamped-free beam of length $L/2$ excited at its base (Figure I.4) , so that the analytical background and results should be essentially similar to the Oberst beam configuration. Finally, the experimental method consists of measuring the FRF between the beam transverse velocities at the driving point and at a free end of the beam, using a non contact laser measurement; in contrast with the Oberst beam technique, no excitation force measurement is needed in the modified technique.

2. J-L Wojtowicki, (2000) *Oberst Beam Excitation Using Piezo Electric Actuators,* GAUS internal report.

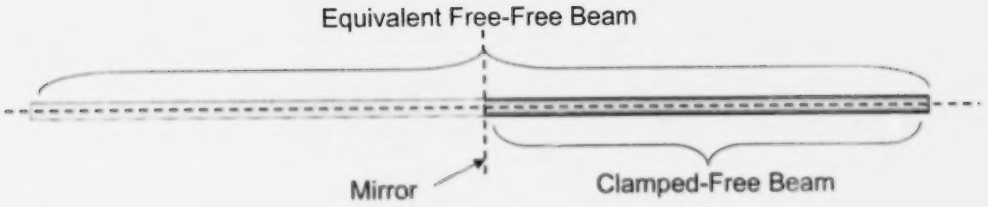

Figure I.4: Oberst beam and its equivalent double length free-free beam

I.2.2 Analytical model

The basic assumption of the characterization technique is that the composite beam behaves like an equivalent homogeneous flexural beam; under this assumption, it is a straightforward task to derive an equivalent model of the composite beam. The transverse displacement of a flexural beam is described by equation I.1, where A, B, C and D are four constants determined by the boundary conditions:

$$Y(x) = C.\cosh(\beta.x) + D.\sinh(\beta.x) + E.\cos(\beta.x) + F.\sin(\beta.x) \quad \text{(I.1)}$$

where $0 \le x \le L$ and β is the flexural wavenumber given by $\beta^4 = \frac{\rho.A.\omega^2}{E.I}$, where

ρ: density of the composite beam (kg/m³)
A: area of beam's cross-section (m²)
ω: pulsation (rad/s)
E: Young's modulus of the composite beam (Pa)
I: area moment of inertia of composite beam (m⁴)

The free boundary conditions at $x=0$ and $x=L$ express the nullity of the bending moment and shear force:

$$E.I.\frac{\partial^2 Y}{\partial x^2} = 0 \text{ at } x=0 \text{ and } x=L \quad \text{(I.2)}$$

$$\frac{\partial}{\partial x}\left(E.I.\frac{\partial^2 Y}{\partial x^2}\right) = 0 \text{ at } x=0 \text{ and } x=L \quad \text{(I.3)}$$

The boundary conditions lead to the relations $C = E$ and $D = F$ and to the following frequency equation for a free-free beam,

$$\cosh(\beta.L).\cos(\beta.L) = 1 \quad \text{(I.4)}$$

The imposed excitation at mid-span provides the additional condition that the bending slope is zero at that location,

$$\frac{\partial Y(L/2)}{\partial x} = 0 \tag{I.5}$$

Finally, if $H(\omega,x) = \dfrac{Y(\omega,x)}{Y(\omega,L/2)}$ denotes the ratio of the beam response at location x to the beam response at the forcing point, the following expression can be derived from equations (I.1)-(I.5):

$$\begin{aligned} H(\omega,x) = {} & \frac{1}{2}\cdot\frac{\cosh(\beta.L/2)+\cos(\beta.L/2)}{1+\cosh(\beta.L/2).\cos(\beta.L/2)}.[\cosh(\beta.x).\cos(\beta.x)] \\ & -\frac{1}{2}\cdot\frac{\sinh(\beta.L/2)+\sin(\beta.L/2)}{1+\cosh(\beta.L/2).\cos(\beta.L/2)}.[\sinh(\beta.x).\sin(\beta.x)] \end{aligned} \tag{I.6}$$

The denominator of equation (I.6) shows the term $1+\cosh(\beta.L/2).\cos(\beta.L/2)$, which also appears in the frequency equation of a clamped-free beam with a length *L/2*; therefore, a free-free beam of dimension *L* excited by a point force at its center essentially behaves like a clamped-free beam of dimension *L/2* with a base excitation. Equation I.6 is the «compact» model of the beam because it does not involve any modal summation of the test structure.

Validation of the direct model Since the experimental characterization is based on the inversion of the above analytical model, it is important to check the accuracy of this model, and especially equation (I.6). The equation (I.6) has been experimentally tested on a simple aluminum beam of length 300 mm, width 19 mm and thickness 3 mm. Constant, frequency-independent material properties have been assumed for aluminum (Young's modulus of 70 Gpa and loss factor of 0.08%), and the predicted FRF is compared to the measured FRF. The results are shown on figure I.5 for a measurement point at the tip of the beam.

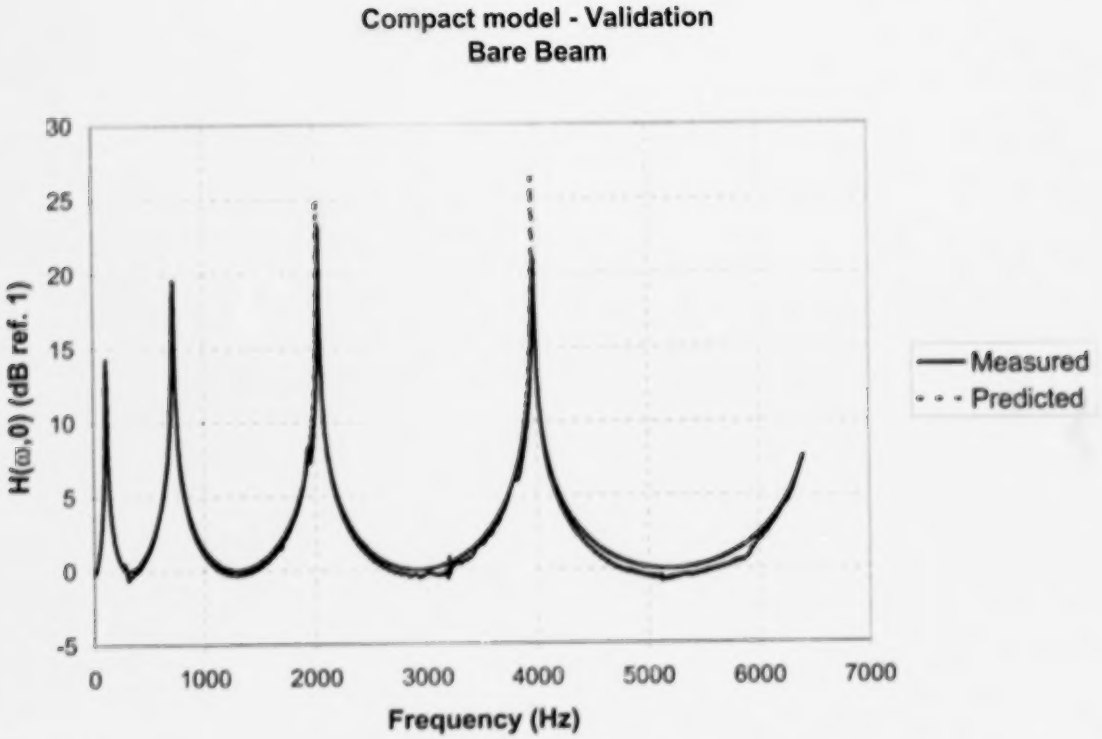

Figure I.5: Validation of the compact model, bare aluminum beam (l = 30mm, w = 19 mm, h = 3 mm)

The agreement between the experiment and the prediction is very good, the modal peaks are well located and the two curves almost coincide. However, significant deviations appear on resonance of the 3rd and 4th modes; this is because the loss factor as been kept constant against frequency in the model, whereas it should increase in practice.

Figure I.5 also shows that the FRF between the center point (where the beam is excited) and the tip of the beam tends towards 1 (0 dB) between two modes. At the corresponding frequencies, the two points vibrate in phase with the same amplitude. Near a mode, the response reaches a maximum controlled by structural damping. The frequencies of the modes could be predicted using the classical formulation for a cantilever beam. Conversely, those FRFs can be used directly to calculate the mechanical properties of materials using the ASTM E756 standard for example.

I.2.3 Inversion of the model

In the following, experimental data of $H(\omega,0)$ (free end measurements) are used in conjunction with the above model to extract the properties of foam materials added to a base aluminum beam. The FRF $H(\omega,0)$ is measured from two transverse *velocity* measurements with a laser Doppler vibrometer. It must be noted that the same model is used for both the bare beam and the composite beams. In the second case, the beam is regarded as a homogenous equivalent beam. The extraction procedure follows two steps:

- In a first step, an optimization procedure extracts the bending stiffness $\widetilde{E}\,I(\omega)$ of the beam under test where $\widetilde{E}$ is the complex equivalent Young's modulus and I is the equivalent area moment of inertia. This is done for the base beam alone ($\widetilde{E}_b I_b(\omega)$) and for the composite beam ($\widetilde{E}\,I(\omega)$);
- The extraction of the mechanical properties of the material (Young's modulus E_{mat}, loss factor η_{mat}) is performed in a second step.

Extraction of the equivalent bending stiffness The calculation of the rigidity $\widetilde{E}\,I$ of the composite beam is performed from experimental FRF on limited frequency bands including only one vibration mode. The order of the mode, dimensions and weight of the beam must be determined before extracting $\widetilde{E}\,I$.

Step 1: The software identifies the maximum value of the experimental FRF, and estimates the modal frequency. The structural loss factor is deduced for each mode using the 3 dB bandwidth method. From the values of the modal frequency and loss factor, a first estimation of the flexural rigidity is performed using the relation $\widetilde{\omega}_n = \kappa_n^2 \sqrt{\frac{\widetilde{E}I}{\mu}}$, where $\widetilde{\omega}_n$ is the complex frequency, μ is the lineic mass of the beam and κ_n are the modal wavenumbers of the beam, given by

$n = 1$	$\kappa_n = 1.875$
$n = 2$	$\kappa_n = 4.694$
$n = 3$	$\kappa_n = 7.854$
$n = 4$	$\kappa_n = 10.995$
$n > 4$	$\kappa_n = (2n - 1)(\pi/2)$

Step 2: The initial estimate of $\widetilde{E}\,I$ is adjusted (real and imaginary parts) iteratively in order to minimize a cost function which is defined as the difference between the experimental and theoretical FRF in the frequency range considered.

Figure I.6 shows an example of the model inversion for the same base aluminum beam as before (length 300 mm, width 19 mm, thickness 3 mm) with a free layer of auto-adhesive damping material (thickness 1 mm); a Young's modulus of 70 Gpa and a constant loss factor of 0.08% have been assumed for the aluminum beam. In this case,

the complex composite bending stiffness $\widetilde{E}I$ has been adjusted in the model at each frequency so that the experimental and theoretical FRF coincide over the whole frequency range. The extracted $\widetilde{E}I$ therefore varies with the frequency. Note when comparing figures I.5 and I.6 that the addition of a free layer of damping material significantly changes the structural damping of the composite beam, but only slightly affects the resonant frequencies; therefore the FRF has significant sensitivity to the loss factor of the damping material, but much less to the Young's modulus of the damping material. A way to increase the sensitivity of the FRF to the Young's modulus of the tested material is to use a constrained layer configuration; this is detailed in a forthcoming section. In all subsequent experiments, the optimization of $\widetilde{E}I$ is carried on limited frequency bands around resonance instead of large frequency bands, in order to obtain one value for the loss factor and Young's modulus per mode.

One advantage of the proposed method is to calculate the properties of the composite beam using a large number of experimental data points and the exact analytical formulation. In comparison, the ASTM E756 standard uses the values of the modal frequencies (measured at the peaks) and loss factor (measured typically with the 3dB bandwidth method). The modal frequency is equal to the peak frequency as long as the damping is small; in the case of large damping, a correction factor should be applied. Also, the 3dB bandwidth method is a quick , but usually not very accurate way to evaluate the structural loss factor. A curve fitting method is preferable. However, curve-fitting algorithms are based on trial functions, which are not the analytical FRF as proposed in this present work. Therefore, another potential interest of the present approach is to perform optimization on an analytical expression which depicts the real physical problem.

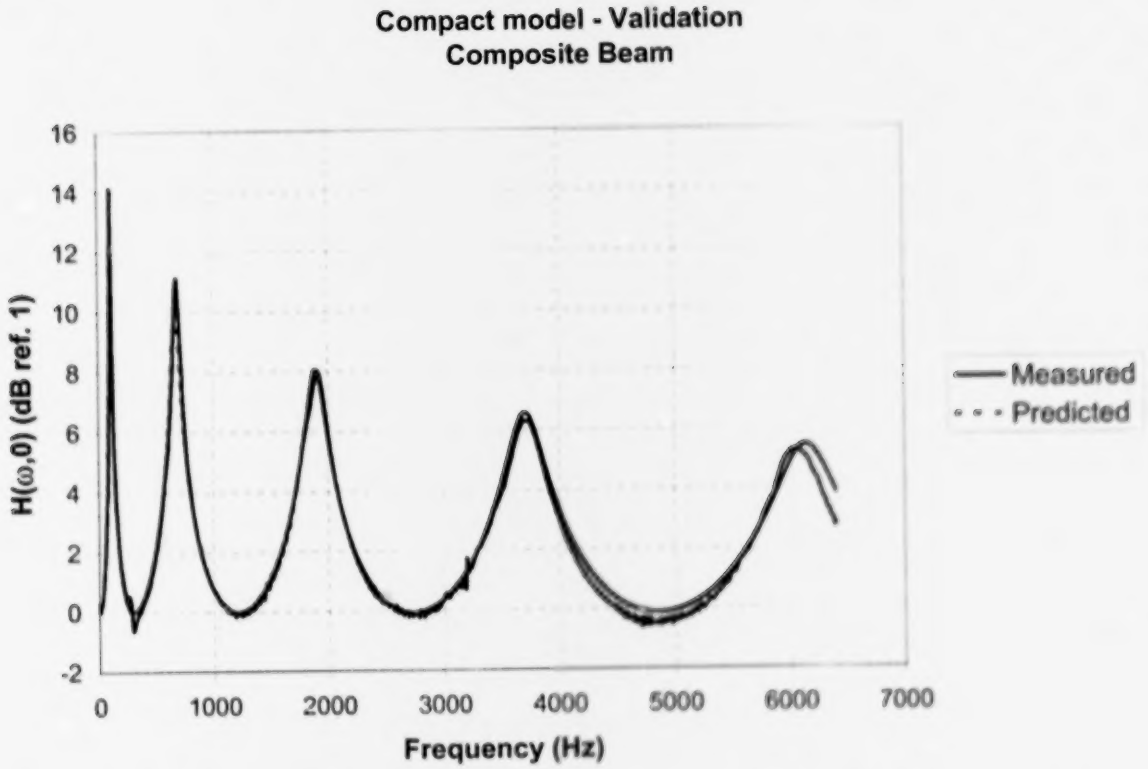

Figure I.6: Example of the model inversion for a composite beam (base beam + free layer of viscoelastic material)

Extraction of the mechanical properties of the material Once $\widetilde{E}_b I_b(\omega)$ has been determined for the base beam and $\widetilde{E}I(\omega)$ for the composite beam, the material properties, i.e. Young's modulus $E_{mat}(\omega)$ and loss factor $\eta_{mat}(\omega)$ are extracted. Two cases are considered:

- Extensional damping (Figure I.7)

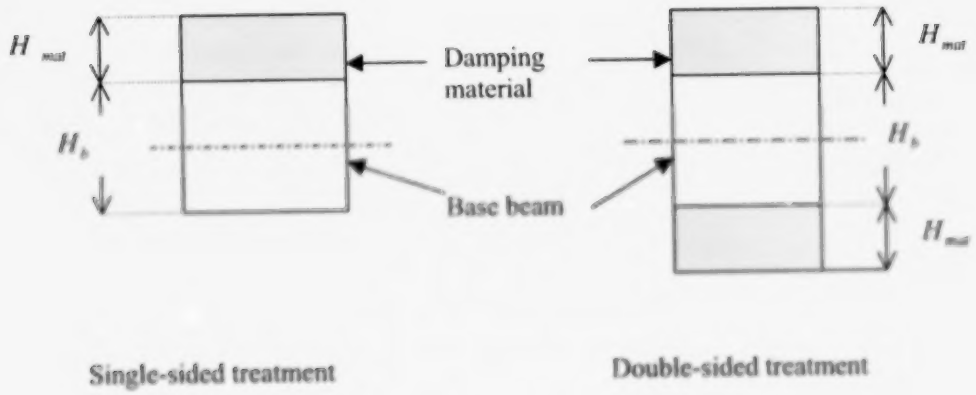

Figure I.7: Extensional damping configurations for material characterization

When the damping material is unconstrained (glued on one or two faces of the base beam), the treatment is called extensional damping. As one of the faces of the material is free, the added rigidity is due to bending deformation of the material. It is assumed that the composite beam is subjected to pure bending deformation. The neutral axis of the composite beam is somewhat moved upwards from the position of the neutral axis of the base beam in the case of a single-sided treatment; for symmetry reasons, it remains unchanged for the double-sided treatment. The determination of the material properties is based on the Ross, Ungar and Kerwin[3] model for a multi-layer structure. This model allows the flexural rigidity $\widetilde{E}I$ of a multi-layer beam or plate to be calculated using the properties of the different layers (density, thickness, width, length, Young's modulus). The following equation gives the equivalent flexural rigidity for a single sided damped beam:

$$\widetilde{E}.I = \widetilde{E}_b.I_b \times \left(1 + e_2 h_2^3 + 3 \times (1 + h_2)^2 \times \left(\frac{e_2 h_2}{1 + e_2 h_2}\right)\right) \qquad (I.7)$$

The following equation applies for a double sided damped beam.

$$\widetilde{E}.I = 2.\widetilde{E}_{mat}.I_{mat} + \widetilde{E}_b.I_b \qquad (I.8)$$

with e_2: Young's modulus ratio $\widetilde{E}_{mat} / \widetilde{E}_b$

h_2: Thickness ratio H_{mat} / H_b

$\widetilde{E}_b$: Young's modulus of the base beam (Pa)

I_b: Area moment of inertia of the base beam with respect to its neutral axis (m^4)

H_b: Thickness of the base beam (m)

3. A. D. Nashif, D.I.G. Jones, J.P. Henderson, *Vibration Damping*, John Wiley & Sons, 1985.

$\widetilde{E}_{mat}$: Young's modulus of the tested material (Pa)
I_{mat}: Area moment of inertia of the tested material with respect to the neutral axis of the composite beam (m^4)
H_{mat}: Thickness of the tested material (m)

The experiments for extensional damping involved only single sided materials, so that only equation (I.7) was used. The calculation of the complex modulus of the material $\widetilde{E}_{mat}$ using equation I.7 leads to the solution of an algebraic equation of degree 2 (two complex roots). Only the root with positive real and imaginary parts is selected. The calculation of $\widetilde{E}_{mat}$ using equation I.8 is trivial. The Young's modulus and loss factor of the material are determined by identifying the real and imaginary part of $\widetilde{E}_{mat}$ using $\widetilde{E}_{mat} = E_{mat}(1 + j\eta_{mat})$

Shear damping (Figure I.8)

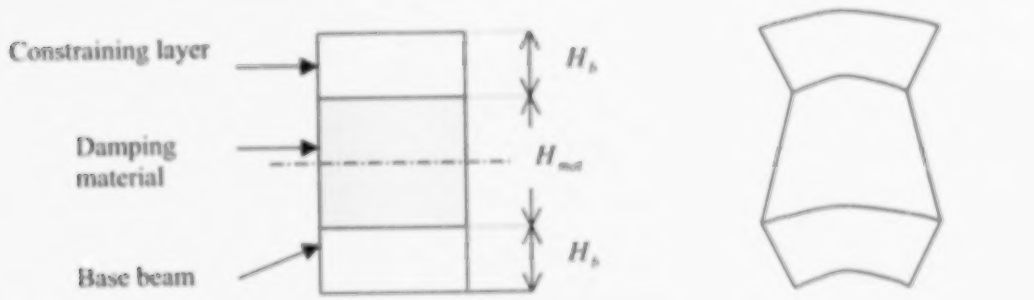

Constrained-layer treatment Deformation of a beam element

Figure I.8: Shear damping configurations for material characterization

When the damping material is sandwiched between the base beam and a rigid constraining layer, the treatment is called shear damping. In this case, the composite beam has a significantly larger flexural rigidity due to the shear deformation of the sandwiched material, which is usually much larger than the bending deformation. Equation I.9 gives the flexural rigidity for a composite beam with a shear damping treatment assuming that the base beam and the constraining layer are identical:

$$\widetilde{E}.I = 2.\widetilde{E}_b.I_b + \widetilde{E}_{mat}.I_{mat}\left(\frac{H_b}{H_{mat}}\right)^2 + \frac{1}{\kappa_n^2}.\widetilde{G}_{mat}.A_{mat} \times \left(1 + \frac{H_b}{H_{mat}}\right)^2 \qquad (I.9)$$

with $\widetilde{G}_{mat}$: Shear modulus of the tested material (Pa)

A_{mat}: Cross-sectional area of the tested material (m^2)

κ_n: modal wavenumbers of a clamped-free beam of length $L/2$,

$n = 1$ $\kappa_n = 1.875$

$n = 2$ $\kappa_n = 4.694$

$n = 3$ $\kappa_n = 7.854$

$n = 4$ $\kappa_n = 10.995$

$n > 4$ $\kappa_n = (2n - 1)(\pi/2)$

I_{mat}: Area moment of inertia of the tested material with respect to its neutral axis (m^4); note that for shear damping, the definition of I_{mat} is therefore different to extensional damping.

The derivation of equation I.9 is detailed in Appendix A. The second term in the right-hand side of equation I.9 is due to the flexural rigidity of the sandwiched material, while the third term is related to shear. For soft materials, the flexural term can usually be neglected for the first modes. However, it is interesting to note that the shear rigidity rapidly decreases as the frequency increases due to the division by κ_n^2 whereas the flexural rigidity has a slower frequency dependence. When the flexural term of equation (I.9) is neglected, it simplifies to

$$\widetilde{E}.I = 2.\widetilde{E}_b.I_b + \frac{1}{\kappa_n^2}.\widetilde{G}_{mat}.A_{mat} \times \left(1 + \frac{H_b}{H_{mat}}\right)^2 \qquad (I.10)$$

Therefore, equation (I.10) allows extraction of the complex shear modulus of the material, $\widetilde{G}_{mat}$. The real-valued shear modulus and loss factor of the material are determined by identifying the real and imaginary part of $\widetilde{G}_{mat}$ using $\widetilde{G}_{mat} = G_{mat}(1 + j\eta_{mat})$. If it is further assumed that the material is homogeneous and isotropic, $\widetilde{G}_{mat} = \frac{\widetilde{E}_{mat}}{2(1+\upsilon_{mat})}$; the complex Young's modulus of the material can therefore be extracted from equation I.10 provided the Poisson's ratio of the material is known.

I.2.4 Test specimens

Various tests specimens were prepared in order to measure the material properties of foams supplied by DREA. The length of the specimens were 150mm, 270mm or 350mm, depending on the material under test. The base beams were made of aluminum, with a thickness of 1mm or 0.25mm. It was found that for the soft materials considered, thin base beams had to be used in order to obtain a sufficient sensitivity of the measured FRF to the material properties. Also, the material was bonded on the base beam as a free layer (extensional damping), or sandwiched between two identical base aluminum beams

(shear damping). Figure I.9 shows an example of a composite beam (the material is constrained between 1mm aluminum beams) attached to the test shaker.

Figure I.9: A test specimen (shear damping configuration) attached to the shaker

I.2.5 Results

Tables I.1 to I.4 below detail the measured properties of the foams (Young's modulus or shear modulus, and loss factor).

Table I.1 Material characterization using a 1mm base beam and single-sided extensional damping

3 mm neoprene foam

Beam		
Length		mm
Width		mm
Thickness		mm
Density		kg/m³
Material		
Thickness		mm
Density		kg/m³

Mode	Frequency (Hz)	E (Pa)	η
1			
2			
3			
4			
5			
6			

6 mm EVA foam

Beam		
Length	270	mm
Width	25,5	mm
Thickness	0,92	mm
Density	2830	kg/m³
Material		
Thickness	6,38	mm
Density	74,7	kg/m³

Mode	Frequency (Hz)	E (Pa)	η
1	41,375	1,74E+06	0,2392
2	263	2,05E+06	0,2568
3	741	2,22E+06	0,2210
4	1450	1,85E+06	0,3084
5	2386	1,25E+06	0,4687
6	3546	1,19E+06	0,2397

12 mm EVA foam

Beam		
Length	270	mm
Width	25,5	mm
Thickness	0,93	mm
Density	2797	kg/m³
Material		
Thickness	13,5	mm
Density	71	kg/m³

Mode	Frequency (Hz)	E (Pa)	η
1	44,0	2,32E+06	0,1301
2	276,8	2,28E+06	1,46E-01
3	761,5	1,87E+06	1,64E-01
4	1453,0	1,36E+06	2,23E-01
5	2329,0	8,23E+05	3,66E-01
6	3386,0	3,78E+05	1,72E+00

6 mm PVC foam

Beam		
Length	270	mm
Width	25,6	mm
Thickness	0,93	mm
Density	2784	kg/m³
Material		
Thickness	6,15	mm
Density	167,2	kg/m³

Mode	Frequency (Hz)	E (Pa)	η
1	37,875	5,35E+05	0,2884
2			
3			
4			
5			
6			

25 mm EPT/SBR foam

Beam		
Length	350	mm
Width	25,4	mm
Thickness	1,57	mm
Density	2739	kg/m³
Material		
Thickness	26,8	mm
Density	158	kg/m³

Mode	Frequency (Hz)	E (Pa)	η
1	41,75	2,86E+06	0,2016
2	259	2,66E+06	0,1860
3	672	1,76E+06	0,2757
4	1324	1,81E+06	0,5739
5			
6			

Table I.2 Material characterization using a 0.25mm base beam and single-sided extensional damping

3 mm neoprene foam

Beam		
Length	150	mm
Width	25,5	mm
Thickness	0,28	mm
Density	2633	kg/m³
Matérial		
Thickness	3,22	mm
Density	309	kg/m³

Mode	Frequency (Hz)	E (Pa)	η
1	32,72	3,21E+06	0,0809
2	205,11	3,21E+06	0,1625
3	563	2,84E+06	0,2790
4	1053,28	2,27E+06	0,3875
5	1523,42	1,47E+06	0,6470
6			

6 mm EVA foam

Beam		
Length		mm
Width		mm
Thickness		mm
Density		kg/m³
Matérial		
Thickness		mm
Density		kg/m³

Mode	Frequency (Hz)	E (Pa)	η
1			
2			
3			
4			
5			
6			

12 mm EVA foam

Beam		
Length		mm
Width		mm
Thickness		mm
Density		kg/m³
Matérial		
Thickness		mm
Density		kg/m³

Mode	Frequency (Hz)	E (Pa)	η
1			
2			
3			
4			
5			
6			

6 mm PVC foam

Beam		
Length	150	mm
Width	38,18	mm
Thickness	0,28	mm
Density	2614	kg/m³
Matérial		
Thickness	6,12	mm
Density	159	kg/m³

Mode	Frequency (Hz)	E (Pa)	η
1	35,89	8,04E+05	0,2396
2	225,55	8,78E+05	0,5000
3	548,81	5,82E+05	0,6815
4	1473,5	3,52E+05	1,4782
5			
6			

25 mm EPT/SBR foam

Beam		
Length		mm
Width		mm
Thickness		mm
Density		kg/m³
Matérial		
Thickness		mm
Density		kg/m³

Mode	Frequency (Hz)	E (Pa)	η
1			
2			
3			
4			
5			
6			

Table I.3 Material characterization using a 1mm base beam and shear damping

3 mm neoprene foam

Beam		
Length		mm
Width		mm
Thickness		mm
Density		kg/m³
Matérial		
Thickness		mm
Density		kg/m³

Mode	Frequency (Hz)	G (Pa)	η
1			
2			
3			
4			
5			
6			

6 mm EVA foam

Beam		
Length	270	mm
Width	25,5	mm
Thickness	0,92	mm
Density	2830	kg/m³
Matérial		
Thickness	6,38	mm
Density	74,7	kg/m³

Mode	Frequency (Hz)	G (Pa)	η
1	100,52	1,13E+06	0,1145
2	400,44	1,87E+06	0,1707
3	886,3	1,51E+06	0,1878
4	1615	1,30E+06	0,2248
5	2572,55	8,89E+05	0,3718
6	3745,07	3,35E+05	1,0677

12 mm EVA foam

Beam		
Length	270	mm
Width	25,5	mm
Thickness	0,93	mm
Density	2797	kg/m³
Matérial		
Thickness	13,5	mm
Density	71	kg/m³

Mode	Frequency (Hz)	G (Pa)	η
1	118,3	1,05E+06	0,1291
2	438,5	1,70E+06	0,1702
3	916,8	1,50E+06	0,1685
4	1613,4	1,36E+06	0,1547
5	2509,5	1,02E+06	0,2450
6	3589,6	3,47E+05	0,5468

6 mm PVC foam

Beam		
Length		mm
Width		mm
Thickness		mm
Density		kg/m³
Matérial		
Thickness		mm
Density		kg/m³

Mode	Frequency (Hz)	G (Pa)	η
1			
2			
3			
4			
5			
6			

25 mm EPT/SBR foam

Beam		
Length	270	mm
Width	25,4	mm
Thickness	0,93	mm
Density	2739	kg/m³
Matérial		
Thickness	26,8	mm
Density	158	kg/m³

Mode	Frequency (Hz)	G (Pa)	η
1	524,14	1,86E+07	0,3790
2	989,49	1,01E+07	0,2535
3	1591,14	8,39E+06	0,1715
4	2291,19	7,59E+06	0,1407
5			
6			

Table I.4 Material characterization using a 0.25mm base beam and shear damping

3 mm neoprene foam

Beam

Length	150 mm
Width	25,5 mm
Thickness	0,28 mm
Density	2633 kg/m³

Matérial

Thickness	3,22 mm
Density	309 kg/m³

Mode	Frequency (Hz)	G (Pa)	η
1	88,36	2,72E+05	0,1537
2	363,9	5,69E+05	0,3351
3	765,31	5,29E+05	0,3495
4	1350,25	5,85E+05	0,3304
5	1961,5	7,41E+05	0,2793
6			

6 mm EVA foam

Beam

Length	mm
Width	mm
Thickness	mm
Density	kg/m³

Matérial

Thickness	mm
Density	kg/m³

Mode	Frequency (Hz)	G (Pa)	η
1			
2			
3			
4			
5			
6			

12 mm EVA foam

Beam

Length	mm
Width	mm
Thickness	mm
Density	kg/m³

Matérial

Thickness	mm
Density	kg/m³

Mode	Frequency (Hz)	G (Pa)	η
1			
2			
3			
4			
5			
6			

6 mm PVC foam

Beam

Length	150 mm
Width	38,18 mm
Thickness	0,28 mm
Density	2614 kg/m³

Matérial

Thickness	6,12 mm
Density	159 kg/m³

Mode	Frequency (Hz)	G (Pa)	η
1	103,83	2,21E+05	0,3669
2	452,45	5,77E+05	0,6742
3	928,12	7,36E+05	0,4660
4			
5			
6			

25 mm EPT/SBR foam

Beam

Length	mm
Width	mm
Thickness	mm
Density	kg/m³

Matérial

Thickness	mm
Density	kg/m³

Mode	Frequency (Hz)	G (Pa)	η
1			
2			
3			
4			
5			
6			

Figures I.10 and I.11 show the frequency dependence for the Young's modulus and loss factor of the various materials and compares the values obtained with extensional (single-sided) and shear (constrained layer) techniques (the shear modulus G measured with the constrained layer technique was used to derive a Young's modulus E according to the isotropic relation $E = 2(1+\nu)G$; a value of $\nu = 0.35$ was assumed for the Poisson coefficient). Both techniques give values of the Young's modulus in the Mpa range for the various materials investigated, although significant differences are observed between extensional and shear measurements of E (in general, the shear technique gives larger values of E than the extensional measurement). The very large differences found in the case of the 25mm EPT/SBR foam may be due to the non-respect of the thin beam hypothesis in this case. As far as loss factor is concerned, we note that extensional and shear measurements are in fairly good agreement at the low frequency end of the spectrum.

As a general comment, the extensional technique was found to be much less sensitive than the shear technique for the materials investigated.

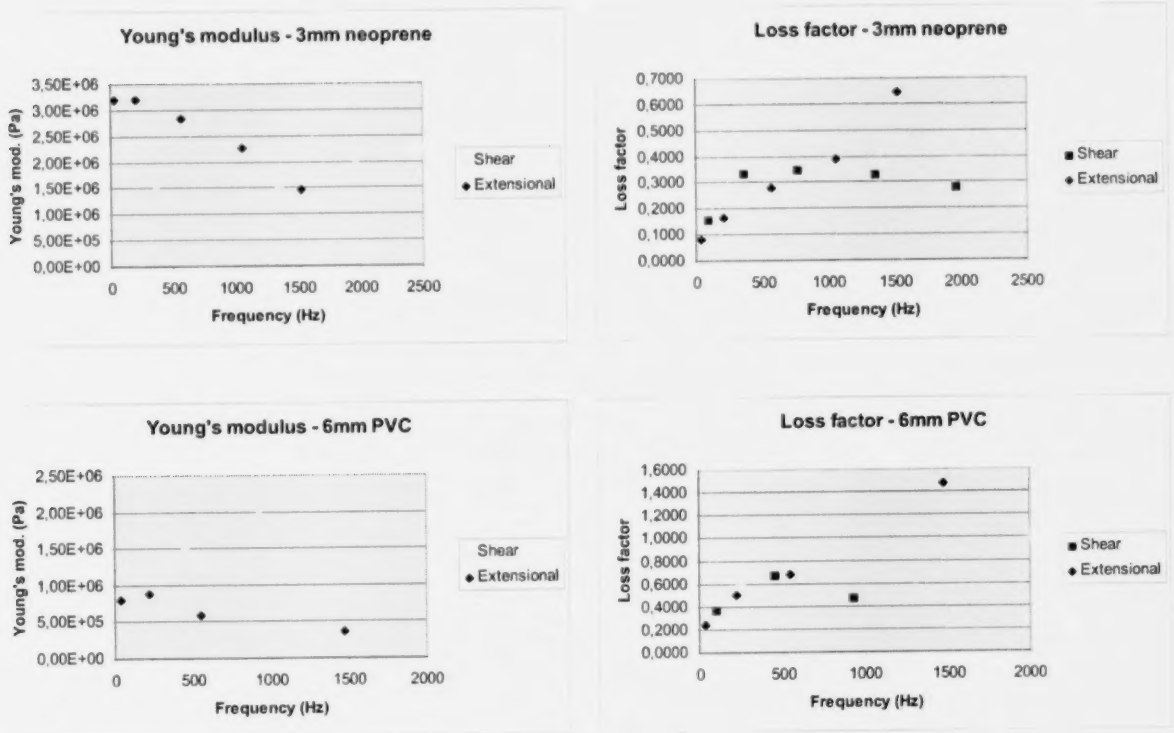

Figure I.10: Comparison of Young's modulus and loss factor frequency dependence obtained with extensional (single-sided) and shear (constrained layer) techniques: 3mm neoprene and 6 mm PVC

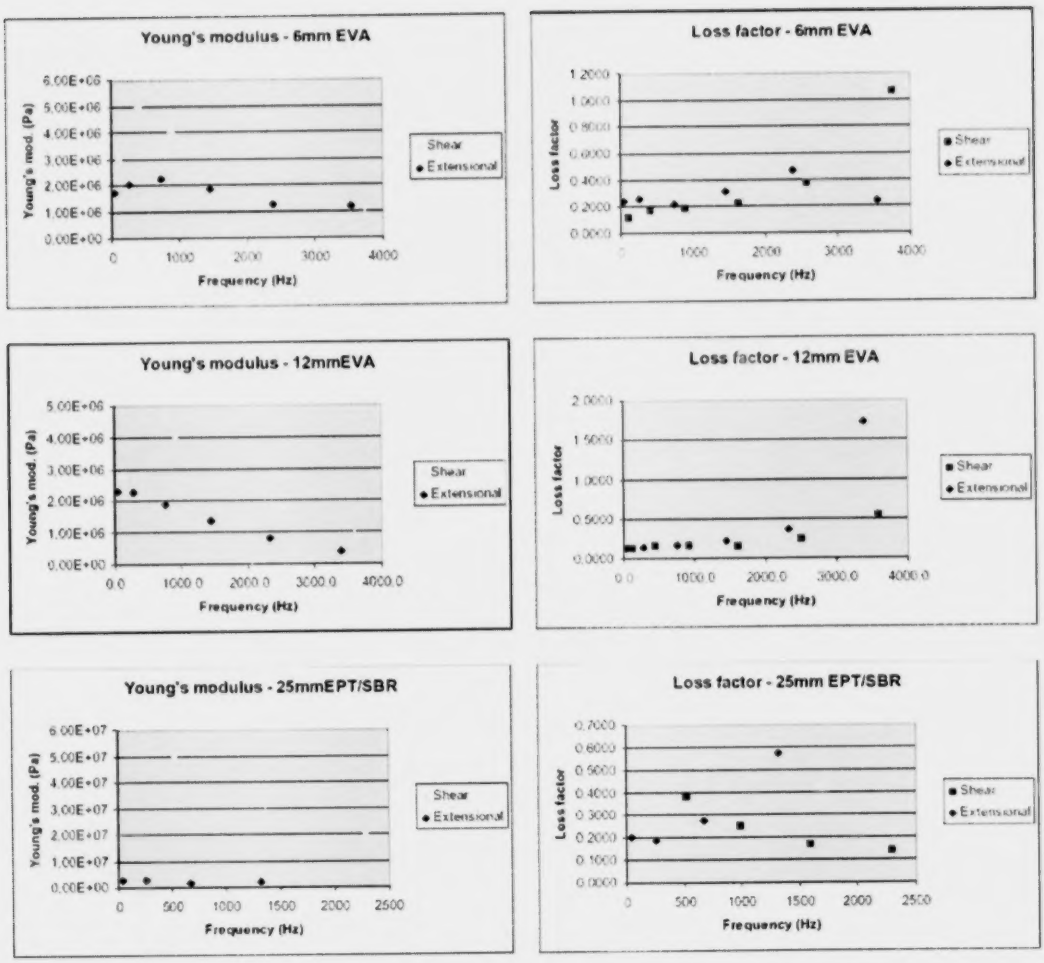

Figure I.11: Comparison of Young's modulus and loss factor frequency dependence obtained with extensional (single-sided) and shear (constrained layer) techniques: 6mm EVA, 12mmEVA and 25mm EPT/SBR

Table I.5 shows the experimental characterisation results obtained from different labs (ref, J.P. Szabo, email of 23/02/01). As a general observation, the modulus values obtained from the Oberst beam technique are larger than those obtained from compression techniques. Since the Oberst beam technique essentially measure the modulus in the in-plane direction of the foam, and compression techniques measure the modulus in the transverse direction, a possible explanation (apart from strictly experimental problems) is the anisotropy of the material.

Table I.5 Dilatational modulus of tested materials obtained by different laboratories

Dilatational Modulus (L) in MPa						
	GAUS	**GAUS**	**GIL**	**TNO**	**DREA**	**DREA**
Frequency Range	0-2kHz	0-2kHz	100- 900 Hz	0 - 200 Hz	0.1 Hz	0.1 - 5 Hz
Method	Oberst	Oberst	Shaker	Shaker	DMTA	Instron
Mode	Extensional	Shear	Compression	Compression	Compression and Shear	Compression
Size of Sample (mm)	150-350 x 25	150-270 x 25	150 diameter	130 diameter	~ 30 diameter	300 diameter
3 mm neoprene foam	2,4-4,8	0,8-3,2		0,68	0,47	
12 mm EVA foam	0,8-3,2	1,6-8	3,00		1,24	
6 mm EVA foam	1,6-3,2	1,6-8	3,00		1,24	
6 mm PVC foam	0,8-1,6	0,8-3,2	0,20		0,16	
25 mm EPT/SBR foam	3,2-4,8	32-80	1,00			0.3 - 0.5

VIBRATION MEASUREMENTS AND COMPARISONS WITH VIBRO

2.1 Experimental set-up

The tested plate and the tested coating are installed in the water tank (Figure II.2). The excitation is provided by a shaker on the air side of the plate, driven by the control computer generator (LMS software) and a power amplifier. The injected force and the acceleration at the driving point on the air side are measured with an impedance head. The vibration measurement both on the water side of the plate and on the air side is made using a laser vibrometer connected to a system of mirrors (Figure II.1) in order to steer the laser beam on the meshing points. The laser beam is pointed between each acquisition on the following meshing point by this mean.

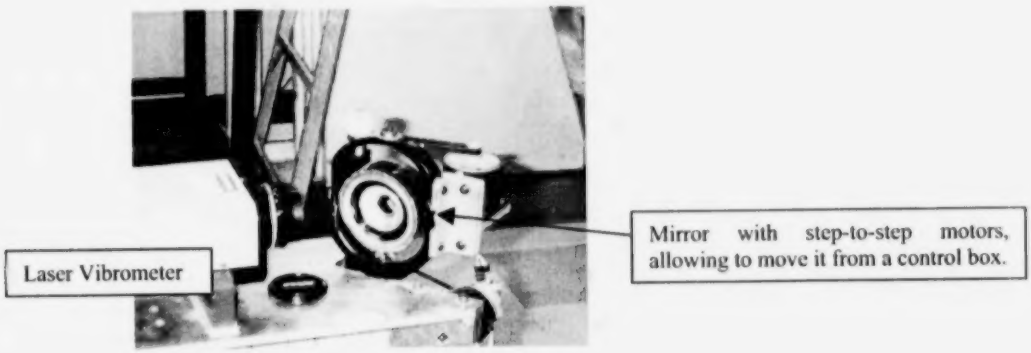

Figure II.1 Close-up of laser vibrometer and mirror

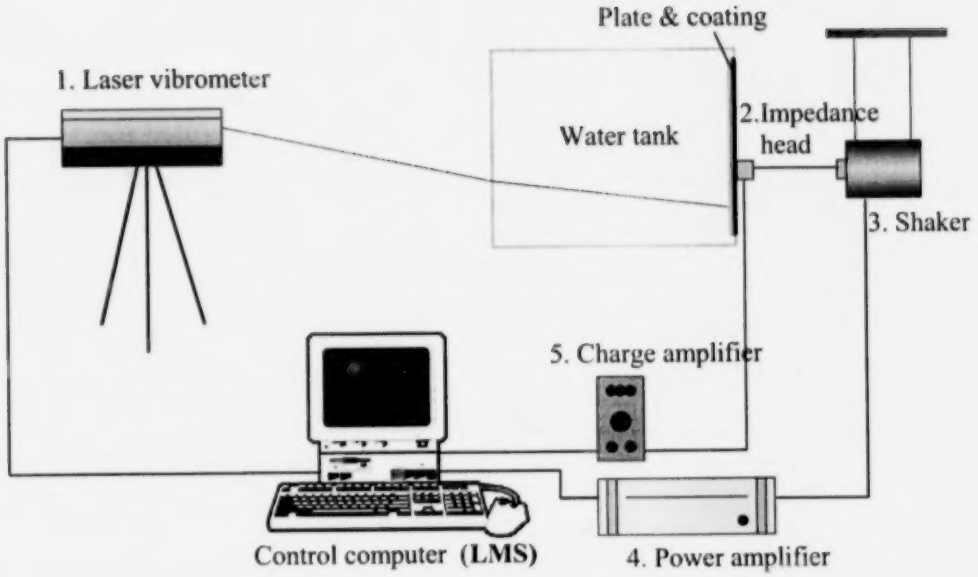

Figure II.2 Experimental set-up

The measurement instrumentation is as follows:

1. Laser Vibrometer Polytec OFV 302
2. Impedance head ICP mod. PCB # 288 D01
3. Shaker Brüel and Kjaer 4810
4. Power amplifier Brüel and Kjaer type 2706
5. Conditioner ICP PCB model 482 A17

The following pictures give an overview of the experimental set-up.

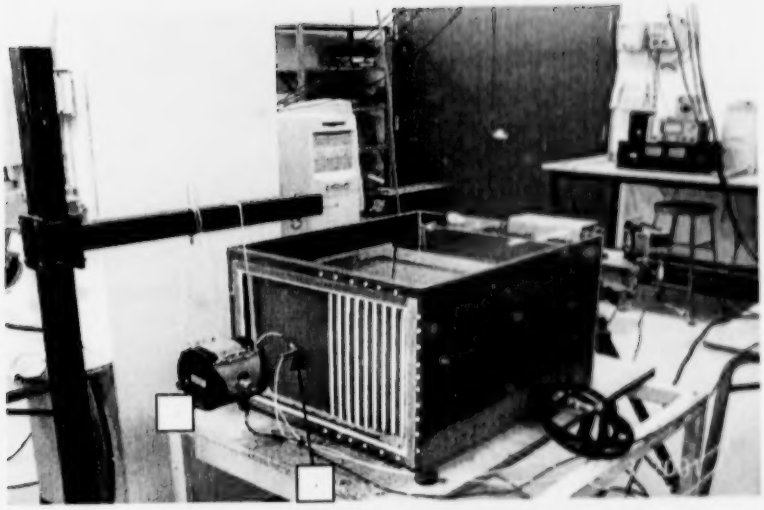

Figure II.3 View of the excitation side of the water tank

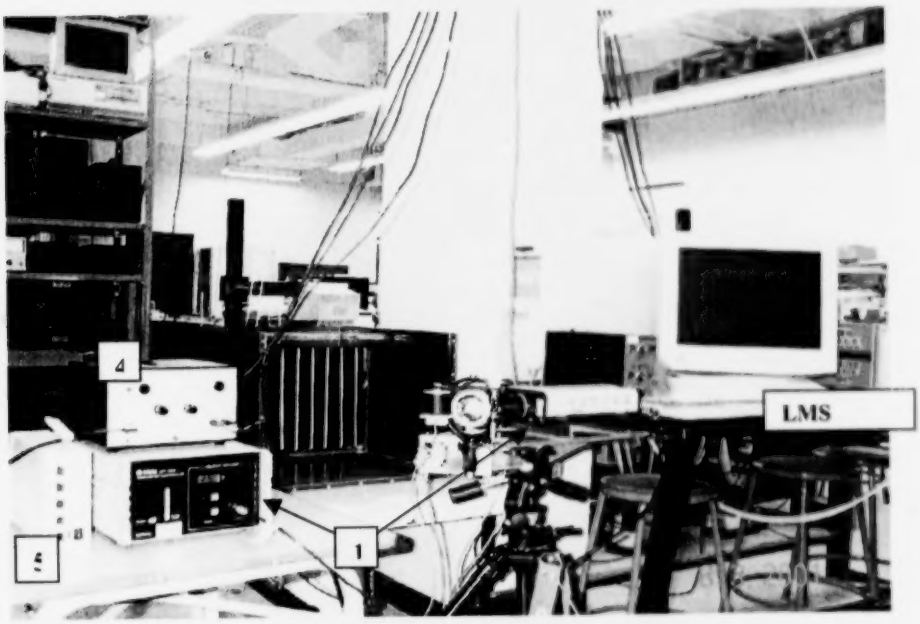

Figure II.4 View of the acquisition/measurement side of the water tank

Water tank and frame The tank is 0.55 x 0.42 x 0.64 m (contenance about 150 L) and is made with PVC. The side opposite to the plate is made of transparent Plexiglas to allow appropriate transmission of the laser beam through it. It is filled with distilled water in order to minimize the air content of the water, and an algaecide (copper sulfate) is added to keep the water clear. On the plate side, the tank is open and a steel frame is inserted to allow the fixation of the plate as described below.

Plate & coating installation and boundary conditions

- The plate dimensions are 0.5 x 0.35 m;
- The plate (plus coating) to be tested is inserted as one side of the tank;
- The plate is mounted on quasi simply supported boundary conditions; in a first instance, the simply supported conditions were realized using thin blades perpendicular to the plate and bonded to the plate edges. These thin aluminum blades are fixed inside a steel frame by the mean of beams and screws to ensure minimum leakage from the tank, as shown in Figure II.5:

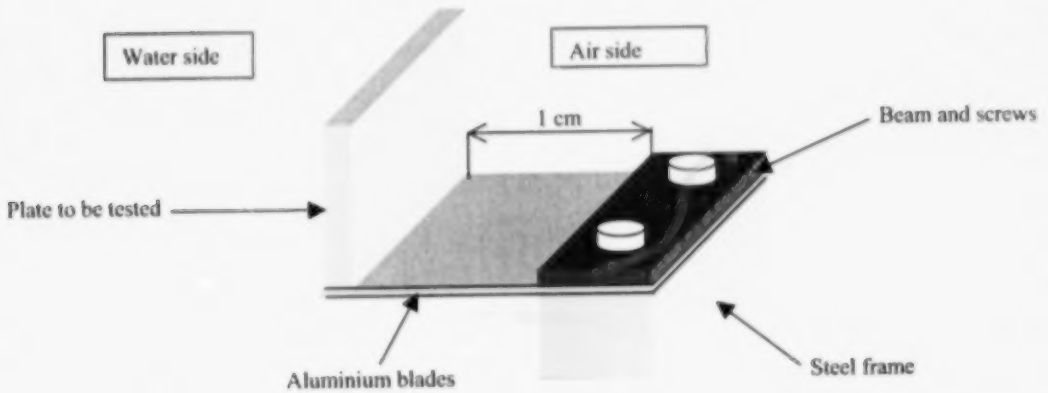

Figure II.5 Experimental boundary conditions for the 2mm steel plate

This mounting procedure worked well for a thin (2mm) steel plate, and was therefore implemented in the experiments involving the 2mm plate. However, for the thicker plate (9.5mm), it was observed that a significant amount of transverse vibration was transmitted to the frame and tank through the supports; also, the small aluminum blades were not rigid enough to ensure a zero transverse displacement at the edges of the plate. As a consequence, the simply-supported boundary condition was not respected for a thick plate. Finally, it was found that in this case, the large vibration transmission to the tank structure resulted in a poor experimental coherence between the applied force to the plate and the plate response.

Consequently, an alternative fixture was used for thick plates. Small aluminum blades coplanar to the plate are inserted between the plate and frame (Figure II.6).

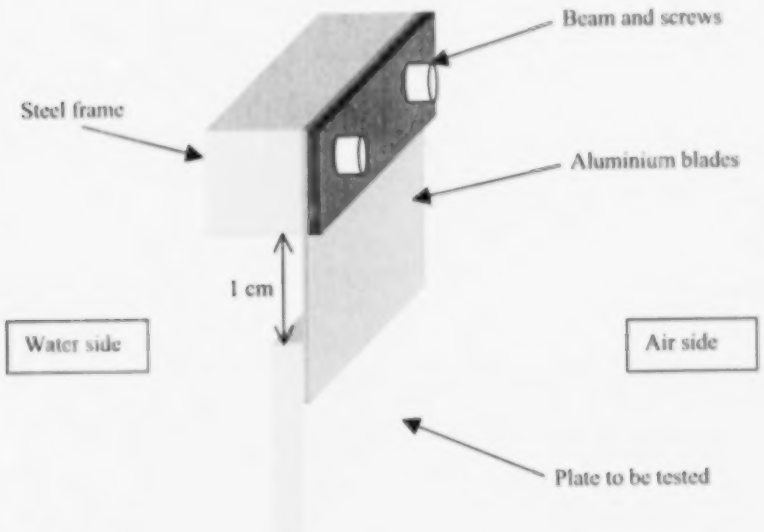

Figure II.6 Experimental boundary conditions for the 9.5mm steel plate

This modification allows to minimize vibration transmission to the tank structure, as the aluminum blades have a low stiffness. However, the boundary conditions are no longer simply supported, as this configuration allows a displacement at the edges of the plate. It is believed however, that boundary conditions of the plate have a moderate impact on the amount of vibration reduction provided by the decoupling coating.

In order to provide sufficient space for the aluminum blades, the size of the 9.5mm plate was slightly reduced (0.48x0.33 m), as compared to the 2mm plate.

The results of Figure II.7 show the vibration transmission between the 9.5mm test plate and the tank structure for the two boundary conditions of Figures II.5 and II.6; the results compare the mean square velocity measured on the plate and on the supporting steel frame for the two fixation systems. The new fixation system provides better vibration isolation of the frame and tank structure.

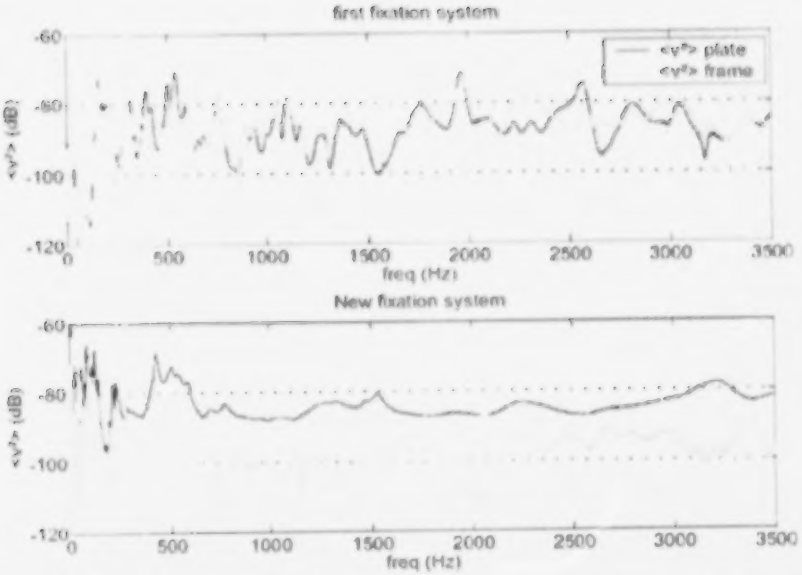

Figure II.7 Comparison of the vibration transmission between the test plate and supporting frame for the two types of plate fixation.

In both configurations, a silicon seal is added at the edges and corners of the plate and aluminum blades to prevent water leakage. Also,

- The tested coating is bonded to the wet side of the tested plate. Note that even though the 3 mm neoprene foam was pre-bonded, an additional layer of glue was necessary in order to provide sufficient bonding in water;
- A reflective film is added on both the water side and the air side to ensure proper reflection to the laser beam.
- The steel plate and frame are prevented from rusting by the use of a lacquer layer, in order to keep a clear transparent water for the laser measurement.

2.2 *Acquisition and analysis*

2.2.1 Acquisition

There are three channels of acquisition :

- Channel 1 : Force (reference channel) } From impedance head through ICP conditioner
- Channel 2 : Acceleration at the driving point } From impedance head through ICP conditioner
- Channel 3 : Velocity from the laser vibrometer

These channels are connected to the control computer through the LMS interface. The laser is manually pointed on a new point between each acquisition. The LMS station is used for the acquisition. It calculates power auto-spectrum for each channel, and Frequency Response Functions (FRF) and coherence between channel 1 and 2, and between channel 1 and 3. The FRF are evaluated with the *H1* estimator, which means that in the case of transverse velocity measurement,

$$FRF = \frac{< vf^* >}{< ff^* >} \qquad \text{(II.1)}$$

where $< vf^* >$ is the power cross-spectrum between the measured velocity and driving force, $< ff^* >$ is the power auto-spectrum of the driving force.

The acquisition parameters are as follows:

- **Frequency range** : LMS only allows to choose the upper frequency and the number of spectral lines (among 2^n values). As the exploitable range of measure is 78.5% of the acquisition range, the upper limit of acquisition should be at least 5120 Hz in order to cover a 0-4000Hz frequency range. However, if the resolution is different to 1 Hz, it is not possible to easily set up the frequency range (this is a problem when the acquisition is done in several bands, see below). To meet those two requirements, the upper frequency was set equal to 8192 Hz, with a resolution of 1 Hz (first 2^n value above 5120 Hz). However, this was not the case for all measurement; the parameters chosen were:

  - 2mm plate: 0-4096 Hz, 1Hz resolution
  - 2mm plate with coating: 0-5120 Hz, 1.25Hz resolution
  - 9.5mm plate without/with coating: 0–8192 Hz, 1Hz resolution.

- **Averaging**: 25 averages per measurement point;

- **Excitation signal**: The excitation is a random noise on the full or partial frequency range, with a burst length of 50% of the measurement duration. The acquisition is triggered on the source.

- **Acquisition in multiples band:** If the measurement shows a good coherence on all the frequency range, the acquisition can be made in only one band. However, as the magnitude of the driving force decreases when frequency increases, it may be necessary to perform the acquisition in multiple successive bands. The figure II.8 below shows that acquisition in multiple bands may have a large impact on the signal/noise ratio.

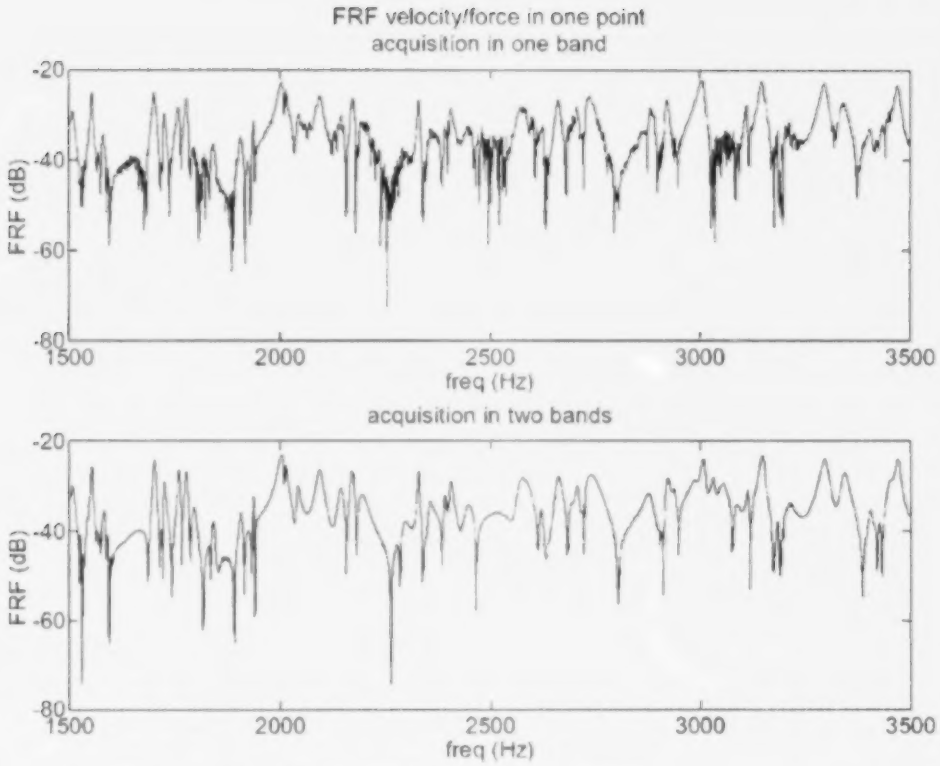

Figure II.8 Single-band vs. multiple-band acquisition.

2.2.2 Analysis

LMS produces at each measurement point, 5 data files of 4096 points (containing real and imaginary part) corresponding to the following results:

- power auto-spectrum of the force
- acceleration/force coherence
- velocity/force coherence
- acceleration/force FRF
- velocity/force FRF.

LMS data are exported as universal files. Useful information is extracted and processed with MATLAB, and results are saved as Matlab files. The results are therefore available in both .UFF and .mat format.

The useful experimental indicators are:

- **Mean square velocity** $< v^2 >= \frac{1}{2}\frac{1}{S}\iint_S |v|^2 dS$

In discrete form:

$$< v^2 >= \frac{1}{2}\frac{1}{S}\sum_{i=1}^{m}\sum_{j=1}^{n}\left|v_{ij}\right|^2 S_{ij} \qquad \text{(II.2)}$$

where v_{ij} is the complex velocity measured at point ij and S_{ij} is the elemental plate area. Assuming the meshing is regular, $S_{ij} = S_e = cte$, and $S = kS_e$, with $N = mn$ the total number of meshing points. Hence:

$$< v^2 >= \frac{1}{2}\frac{1}{N}\sum_{i=1}^{m}\sum_{j=1}^{n}\left|v_{ij}\right|^2 = \frac{1}{2}mean(\left|v_{ij}\right|^2) \qquad \text{(II.3)}$$

For comparisons with the theory, the mean square velocity of the plate is divided by the squared magnitude of the driving force,

$$< v^2 > /|f|^2 = \frac{1}{2}\frac{1}{N}\sum_{i=1}^{m}\sum_{j=1}^{n}\left|v_{ij}\right|^2 /|f|^2 = \frac{1}{2}mean(\left|v_{ij}\right|^2 /|f|^2), \qquad \text{(II.4)}$$

that is,

$$< v^2 > /|f|^2 = \frac{1}{2}mean(FRF(i,j)) \qquad \text{(II.5)}$$

where $FRF(i,j)$ is the force-velocity FRF at point ij. In dB,

$< v^2 > /|f|^2{}_{dB} = 10\log_{10} < v^2 > /|f|^2$

- The **mean square velocity ratio** for a coated plate is defined as ratio of the mean square velocity measured on the air-side and on the water-side:

$$VR = 10\log_{10}\frac{< v^2 > /|f|^2{}_{air-side}}{< v^2 > /|f|^2{}_{water-side}}; \qquad \text{(II.6)}$$

- The **insertion loss** is defined as the ratio of the mean square velocity of the bare plate to the mean square velocity of the coated plate (measured on the water-side):

$$IL = 10\log_{10}\frac{< v^2 >_{bare-plate}}{< v^2 >_{coated-plate,water-side}} \qquad \text{(II.7)}$$

2.2.3 Preliminary tests

Linearity The linearity of the experiment was verified by checking the invariance of the FRF for different levels of excitation.

Coherence Coherence is also a good indicator of the quality of a measurement. The coherence between the driving force and the plate velocity at an arbitrary position (air side and water side) is shown on Figure II.9. The coherence starts to drop in higher frequency, especially when measured on the water side of the plate.

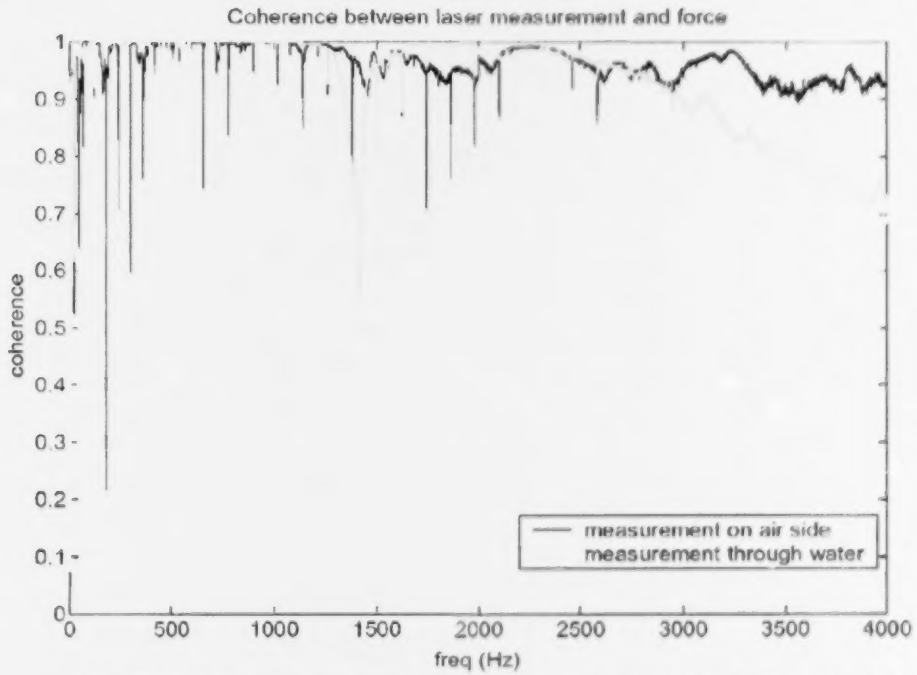

Figure II.9 Coherence measurement between the driving force and the plate velocity.

Laser vibrometry through water The surface velocity measurement on the coating using a laser vibrometer implies that the laser beam crosses three different media : air, the plexiglas side of the tank and water. We have checked that the loss of the reflected signal in this case did not alter the surface velocity measurement, by comparing the mean square

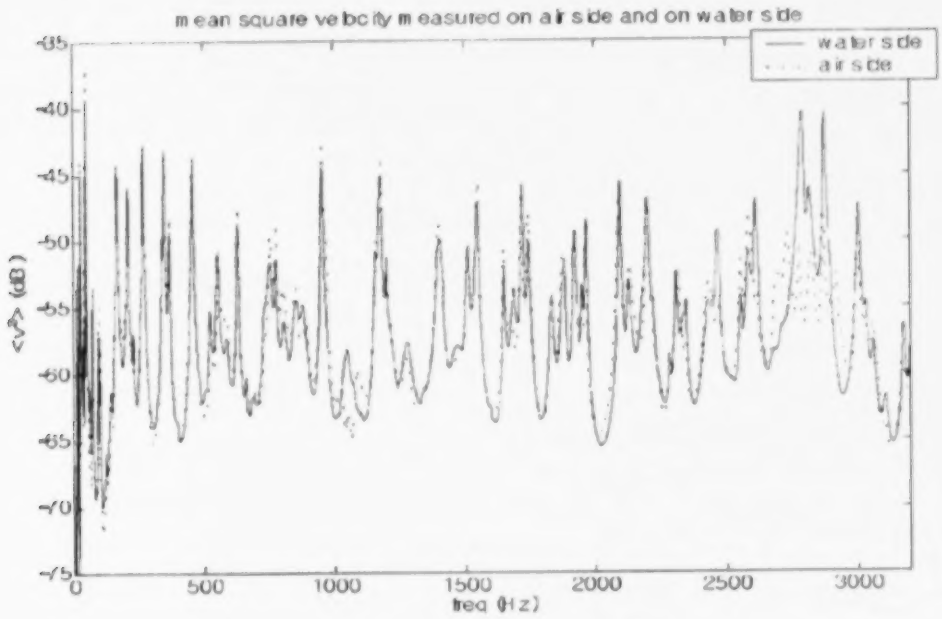

Figure II.10 Mean square velocity of a steel plate measured with the laser vibrometer on the air side and on the water side.

velocity of an uncoated plate measured on the air side and on the water side (Figure II.10). The agreement is generally good, which validates the laser measurement in water.

2.2.4 Characteristics of test plates and of measurements

		Dimensions (m)	Thickness (mm)	Density (kg/m^3)	Young's Modulus (Pa)	Loss factor	Poisson coefficient
Plates	2 mm plate	0.5 x 0.35	1.82	7850	2×10^{11}	0.005	0.3
	9.5 mm plate	0.48 x 0.33	10.00	7850	2×10^{11}	0.005	0.3
Coating materials	3 mm neoprene foam	0.5 x 0.35	3.22	309	Frequency dependant	Frequency dependant	0.45
	6 mm EVA foam	0.5 x 0.35	6.38	74.7	Frequency dependant	Frequency dependant	0.45
	25 mm EPT/SBR foam	0.48 x 0.33	26.8	158	Frequency dependant	Frequency dependant	0.45

The frequency dependant characteristics of decoupling materials (Young's modulus and loss factor) are detailed in section I.2.5

Driving point : the driving point was chosen so that as many plate modes as possible are excited. The driving point was located at the position (0.1625m,0.1625m) from a corner of the plate.

Meshing : The initial criterion to accurately measure the mean square velocity of the plate was 4 measurement points per wavelength at the maximum frequency considered (4kHz). This criterion resulted in 280 points for the 2mm plate and 96 points for the 9.5mm plate. However, since the derivation of mean square velocity does not require phase information, the requirement for the number of data points can be significantly relaxed (See Figure II.11 for tests on the 2mm plate immersed in water). Also, it was verified that measurement points on the air side of the plate can be taken to cover only a limited area of the plate (half the plate instead of the full plate, see Figure II.11). In practice, laser measurements on the air side cannot be performed on the full plate, because of the volume occupied by the shaker and its support.

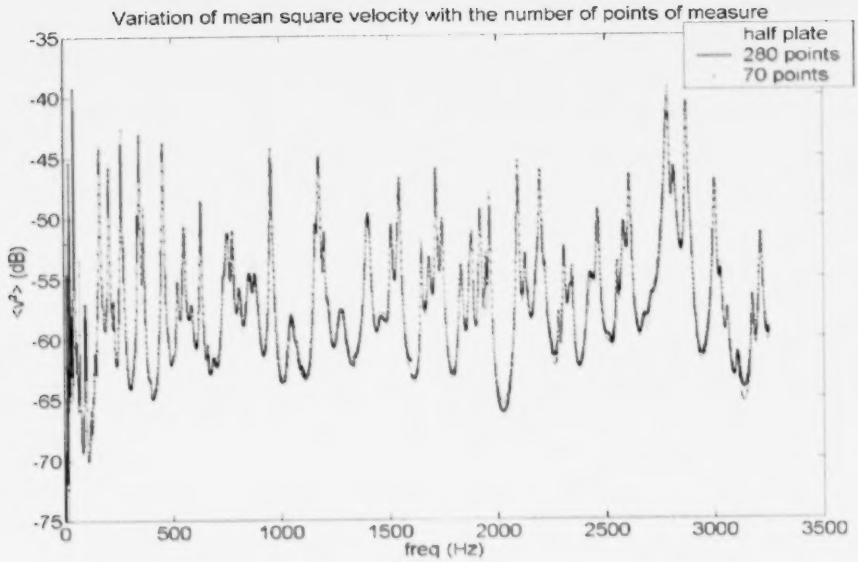

Figure II.11 Mean square velocity measurements on the 2mm steel plate with various meshes.

The final configuration for the excitation and measurement on the plate is shown on Figure II.12

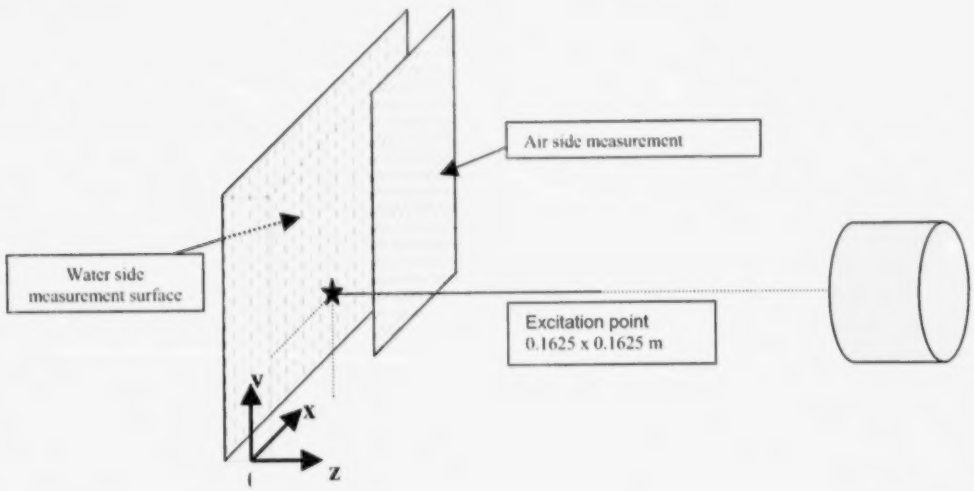

Figure II.12 Measurement configuration on the test plate

The useful measurement parameters are listed in the following table.

Test plate		Meshing			LMS parameters		
		Number of points	Fraction of the plate measured	x-step y-step (cm)	Number of acquisition bands and frequency separation	Frequency range (Hz)	Frequency resolution
2 mm steel plate	Air side	140	Half	2.5 2.5	1	0 – 4096	1 Hz
	Water side	280	Full	2.5 2.5	2 F_s=1600 Hz	0 – 4096	1 Hz
2 mm steel plate + 6 mm EVA foam	Air side	70	Half	2.5 5	1	0 – 5120	1.25 Hz
	Water side	70	Full	5 5	1	0 – 5120	1.25 Hz
2 mm + 3 mm neoprene foam	Air side	70	Half	2.5 5	1	0 – 5120	1.25 Hz
	Water side	70	Full	5 5	1	0 – 5120	1.25 Hz
9.5 mm steel plate	Air side	30	Half	4.8 5.5	2 F_s=2000 Hz	0 – 8192	1 Hz
	Water side						
9.5 mm steel plate + 25 mm EPT/SBR foam	Air side	30	Half	4.8 5.5	2 F_s=2000 Hz	0 – 8192	1 Hz
	Water side	60	Full	4.8 5.5	2 F_s=2000 Hz	0 – 8192	1 Hz

2.3 *Comparisons with VIBRO predictions*

2.3.1 VIBRO parameters

The input parameters of WinVibro are :

Frequency range :

- The frequency range used in each case is 10 – 4000 Hz;
- The frequency resolution used is generally 1 Hz but can be adjusted according to accuracy needs;
- Frequency interpolation for Gauss points integration (fluid-structure coupling): 10 Hz;
- The modal order and the number of Gauss points are adjusted in each case to meet both reasonable requirements of accuracy and computation time.

Characteristics of fluid media :

Medium	Density (kg/m^3)	Sound velocity (m/s)
Air	1.29	340
Water	1000	1460

Characteristics of plate and coating :
The plate and coating properties to be input in the model have been discussed in the previous sections. Note that when the *locally* reacting model is used in VIBRO, the Young's modulus of the material is replaced by the plate modulus calculated from the relation $L = \lambda + 2\mu$, where λ, μ are the Lamé of the material.

Excitation :
The excitation on VIBRO is a point force of amplitude 1N at the location detailed in section II.2.4.

2.3.2 Steel plate in air

As an initial verification, the response of a 2mm steel plate was measured with no water in the tank, in order to make sure that the dynamics of the plate, tank structure and boundary conditions conform to the model, and that the experimental procedure is reliable. The experiment was conducted with 140 measurement points covering half the area of the plate.

VIBRO has been run with following parameters :

Frequency range	Modal order and number of gauss interpolation points	Resolution (Hz)
0 – 1000 Hz	7	1
1000 – 4000 Hz	10	2

The results are presented on figure II.13:

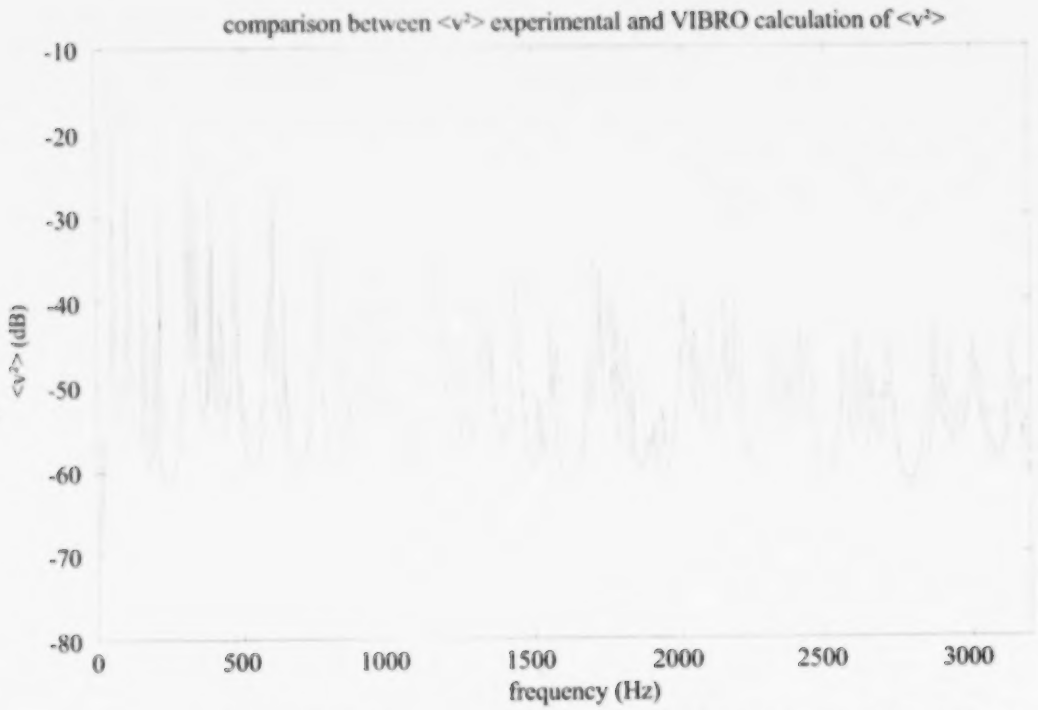

Figure II.13 Mean square velocity of the bare 2mm steel plate in air, VIBRO-experiment comparison.

The experimental curve fits very well with the VIBRO curve. The modal behaviour predicted by VIBRO conforms to the measurement. Note that the amount of damping present in the system in the absence of any coating is very small.

2.3.3 Steel plate in water

2 mm plate Input parameters of VIBRO are as follows:

Frequency range	Modal order	Number of Gauss interpolation points	Resolution (Hz)
10 – 700 Hz	7	7	0.5
700 – 1800 Hz	10	10	1
1800 – 4000 Hz	12	12	1

Figure II.14 shows the VIBRO-experiment comparison. The agreement is satisfactory, as VIBRO is able to capture the complex modal behaviour of the plate coupled to the fluid, especially in low frequency. The free field assumption in VIBRO does not seem to considerably affect the plate response in this case. Note by comparing Figures II.13 and II.14 that the position of the modal peaks is changed by the fluid; also the system is still very reverberant, which implies that the radiation damping is small in this case (the critical frequency of a 2mm steel plate in water is of the order of 100kHz).

9.5 mm plate Input parameters of VIBRO :

Frequency range	Modal order	Number of Gauss interpolation points	Resolution (Hz)
10 – 4000 Hz	9	9	1

When immersed in water, the thick plate has a highly damped measured response (Figure II.15). It was verified that this damping is not related to the boundary conditions of the thick plate: the response was also measured in the absence of water, and showed well defined modes in this case. Therefore, it is suspected that the increased damping in water is related to a strong coupling with the fluid (a 9.5mm steel plate in water has a critical frequency of the order of 20kHz, and is therefore a much more efficient radiator than a 2mm plate in the 0-4kHz frequency range).

The VIBRO predictions in this case show some deviations with the experimental data, although a strong radiation damping is also predicted. Note that in this case, the experimental boundary conditions are probably less rigid than simply supported conditions, which may explain the important mode shifts in low frequency.

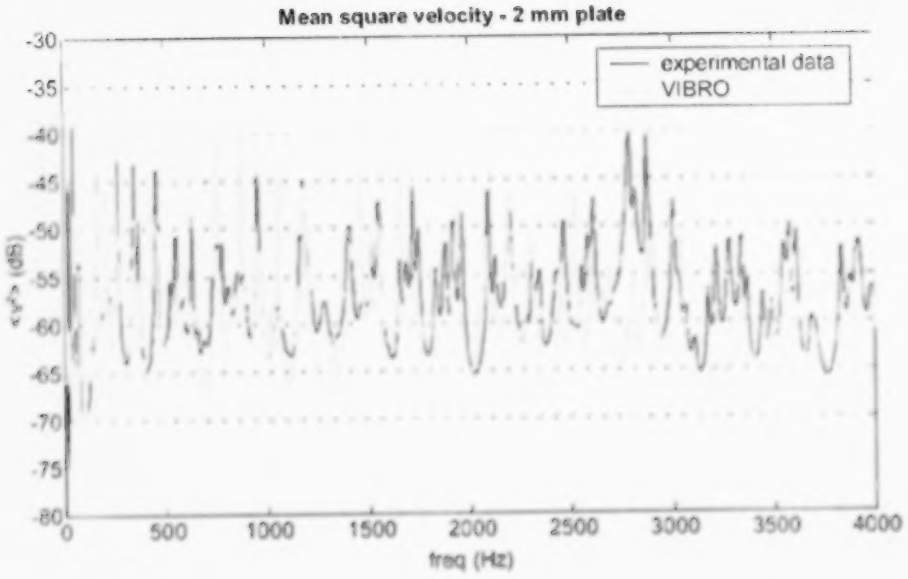

Figure II.14 Mean square velocity of the bare 2mm steel plate in water, VIBRO-experiment comparison.

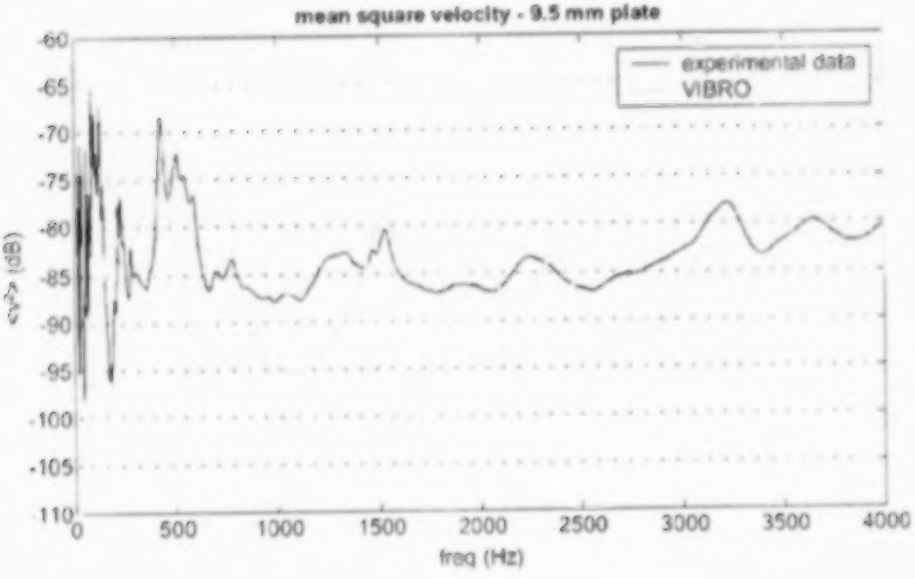

Figure II.15 Mean square velocity of the bare 9.5mm steel plate in water, VIBRO-experiment comparison

2.3.4 2mm steel plate with 3mm neoprene foam

In this configuration as well as in other plate / material configurations, the following data are reported:

- mean square velocity on air side $< v^2 >_{airside}\ |f|^2_{dB} = 10\log_{10} < v^2 >_{airside}\ |f|^2$
- mean square velocity on the material surface
  $< v^2 >_{waterside}\ |f|^2_{dB} = 10\log_{10} < v^2 >_{waterside}\ |f|^2$
- mean square velocity ratio $VR = 10\log_{10} \dfrac{< v^2 > |f|^2_{air-side}}{< v^2 > |f|^2_{water-side}}$
- insertion loss $IL = 10\log_{10} \dfrac{< v^2 >_{bare-plate}}{< v^2 >_{coated-plate,water-side}}$

Comparisons of the experimental results with VIBRO3D (3D elasticity model of the decoupling material) as well as VIBRO1D (locally reacting model) are presented in all cases. In addition, the insertion loss data are compared with the simple model of House, which is briefly recalled below. In some cases, both narrow band and 1/3 octabe band results are shown.

For all comparisons between experiments and theory, the following legend is used :

——	Experimental data
	Model

Recall of theoretical considerations The model of House predicts the insertion loss from the calculation of the sound transmission loss of a multilayer system below:

$$TL_4 = \frac{W_{in}}{W_{trans}} = 20\log_{10}\left[\begin{array}{l}\cos(k_2 l_2)\cos(k_3 l_3)\left(1+\dfrac{z_1}{z_4}\right) - \sin(k_2 l_2)\sin(k_3 l_3)\left(\dfrac{z_3}{z_2}+\dfrac{z_1 z_3}{z_2 z_4}\right) \\ + j\cos(k_2 l_2)\sin(k_3 l_3)\left(\dfrac{z_1}{z_2}+\dfrac{z_3}{z_4}\right) + j\sin(k_2 l_2)\cos(k_3 l_3)\left(\dfrac{z_1}{z_2}+\dfrac{z_3}{z_4}\right)\end{array}\right]$$

where $z_i = \rho_i c_i$ is the acoustic impedance of the medium i, i=1..4 (respectively air, steel plate, coating and water); ρ_i is the density, c_i is the acoustic velocity, $k_i = \dfrac{\omega}{c_i}$ is the acoustic wavenumber; l_2, l_3 are the thickness of the plate and coating, respectively. In the model of House, the insertion loss is defined by:

$$IL = 10\log_{10}\frac{W_{without}}{W_{with}} = W_{trans3} - W_{trans4} = TL_4 - TL_3$$

where TL_3 is obtained by taking $l_3 = 0$. The above definition of IL is not strictly equivalent to the measured IL, which is rather defined in terms of surface velocity data. The model of House predicts a mass-spring mode of the system, at the frequency approximately given by

$F_r = \frac{1}{2\pi}\sqrt{\frac{L_3}{\rho_2 l_2 l_3}}$, where $L_3 = \lambda_3 + 2\mu_3$ is the plate modulus of the coating material.

Coating modes are also singular frequencies of the system; the natural frequency of coating modes is given by:

$$f_n = \frac{nc_L}{2l_3}, \forall n \in [1;\infty[, \text{ with } c_L = \sqrt{\frac{\lambda_3 + 2\mu_3}{\rho_3}}$$

Coating modes are associated with a large velocity response at the surface of the material, and therefore a drop in the decoupling efficiency of the material. The above formula shows that f_n increases with the Young's modulus of the material and is inversely proportional to the material thickness. The following table lists the first coating mode of the tested materials; it appears that the coating modes occur at higher frequencies than investigated in the experiments.

3 mm neoprene foam	**30 823Hz**
6 mm EVA foam	**23 295 Hz**
25 mm EPT/SBR foam	**4 888 Hz**

The input parameters of VIBRO 1D and VIBRO 3D for the 2 mm plate + 3 mm neoprene foam are:

Frequeacy range	Modal order	Number of Gauss interpolation points	Resolution (Hz)
10 – 4000 Hz	9	9	1

The 3 mm neoprene foam is a material with a large loss factor in high frequency; the experimental data show indeed a transition from highly modal response in low frequency to a highly damped, smooth response in high frequency.

The VIBRO3D results should be considered with caution since the code is not able to predict any low frequency mode. It was found that in this case VIBRO3D largely overestimates the resonant frequencies of the system. The modes of the system in this case are shifted to higher frequency and are smoothed out because of the large loss factor of the material. This problem was previously observed in situations where the decoupling material has a large enough rigidity; it is suspected that the origin of the problem is numerical, although it has not been precisely identified yet. However, VIBRO3D gives the correct tendencies for responses on both the air and material side, although it tends to overestimate the vibration attenuation provided by the decoupling material.

In this case the simplified VIBRO1D model seems to better fit; it predicts modes at low frequency, but with an overestimated amplitude, because of massless assumption which provides less damping. The tendencies predicted are also closer to experimental data.

On the airside, the response of the plate shows a dip between 700 and 1000 Hz, that neither VIBRO1D nor VIBRO3D have predicted. This is particularly visible on the mean square velocity ratio (Figure II.18), which shows a frequency range below 1.5kHz where the velocity ratio is negative, whereas predictions show an almost linear progression of the ratio. It was verified that this frequency does not correspond to either the mass-spring mode or a coating mode (which appears on the model of House in the insertion loss at a higher frequency). The appendix C shows additional experimental results obtained with two different water volumes in the water tank (in fact, the z-dimension of the tank, in the direction perpendicular to the plate was modified so that the water volume was half that of the original tank). These results show that the dip on the airside response is not strongly modified by the change of water volume; therefore, this dip is apparently not related to the finite acoustic volume in the tank. The origin of this singularity in the airside response remains unclear; it should be noted here that the updated model of DeJong, however, seems to adequately predict this phenomenon (see next section). In terms of the velocity ratio, VIBRO1D and VIBRO3D are close and, with the exception of the 0-1.5kHz range, fit quite well with experimental data. The amount of vibration reduction reaches 10 dB at 4000 Hz.

The insertion loss is presented on Figure II.19 in third octave band. Experimental data fall between the VIBRO1D and VIBRO3D predictions in low frequencies, and show the same tendencies in higher frequency. The vibration attenuation provided by the material, compared to the bare plate, is around 20 dB at 4000 Hz. It is to be noted that the model of House significantly deviates from experimental data in this case.

Additional theory-experiment comparisons for the 3 coating materials investigated in this work (neoprene, EVA and EPT foams) are presented in Appendix B. In these comparisons, the theoretical predictions are based on properties of the decoupling

material derived from either extensional or shear damping measurements reported in Tables I.1-4, or material data measured by DREA, GIL or TNO. These comparisons show that, in general, our material data derived from shear damping measurement better match the experimental results.

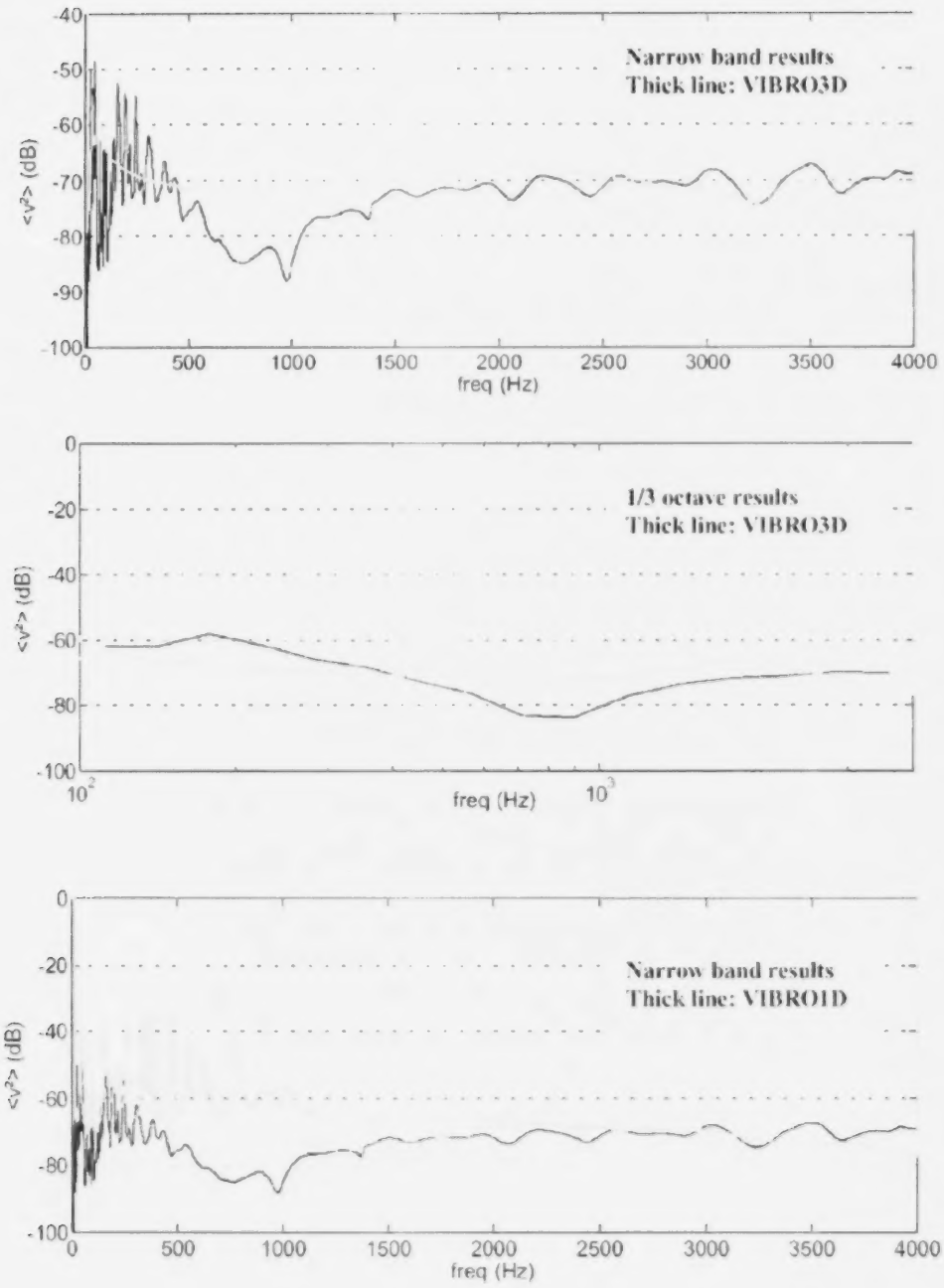

Figure II.16 Mean square velocity on airside of the 2mm steel plate + 3mm neoprene foam, VIBRO-experiment comparison.

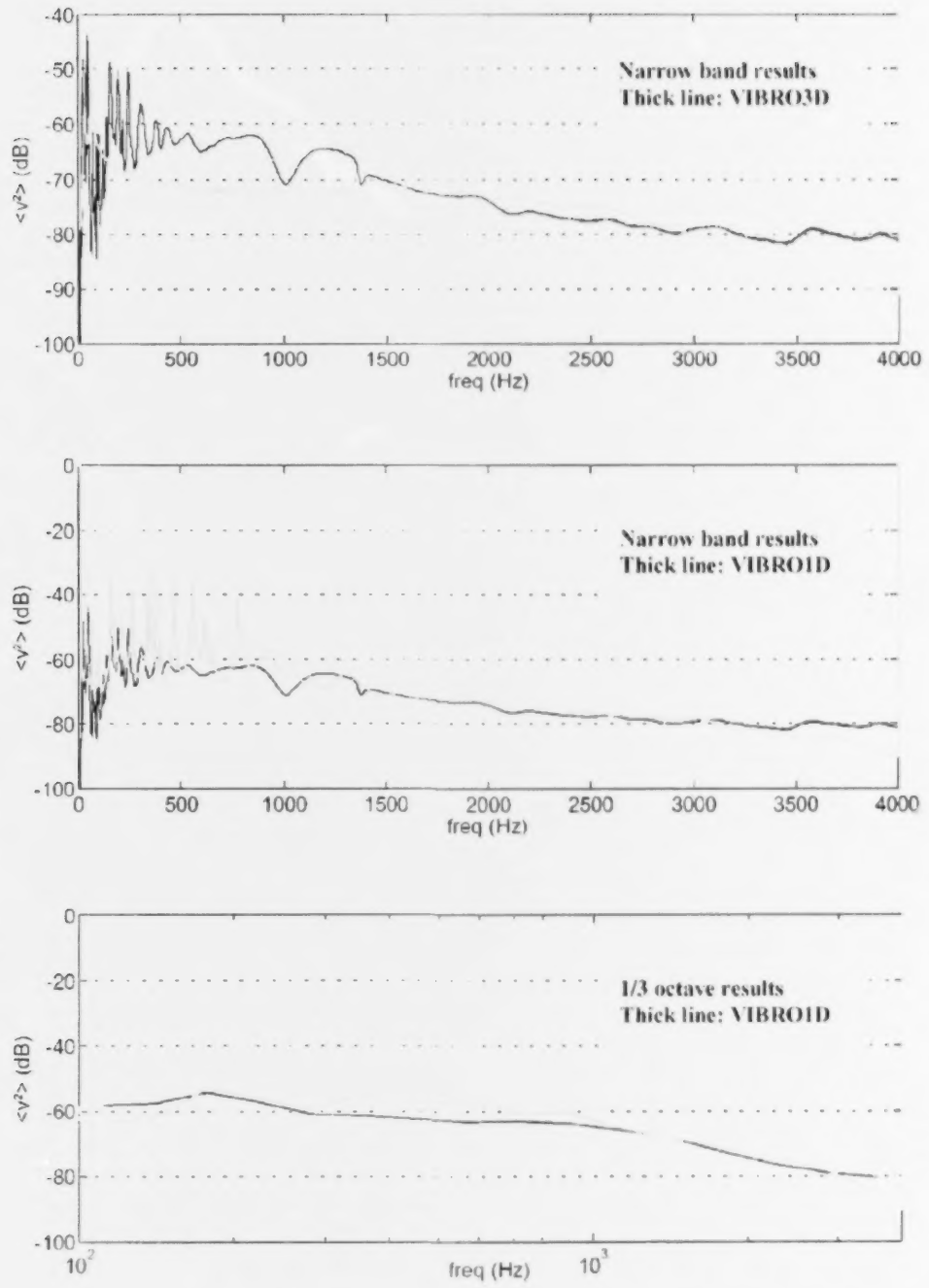

Figure II.17 Mean square velocity on waterside of the 2mm steel plate + 3mm neoprene foam, VIBRO-experiment comparison.

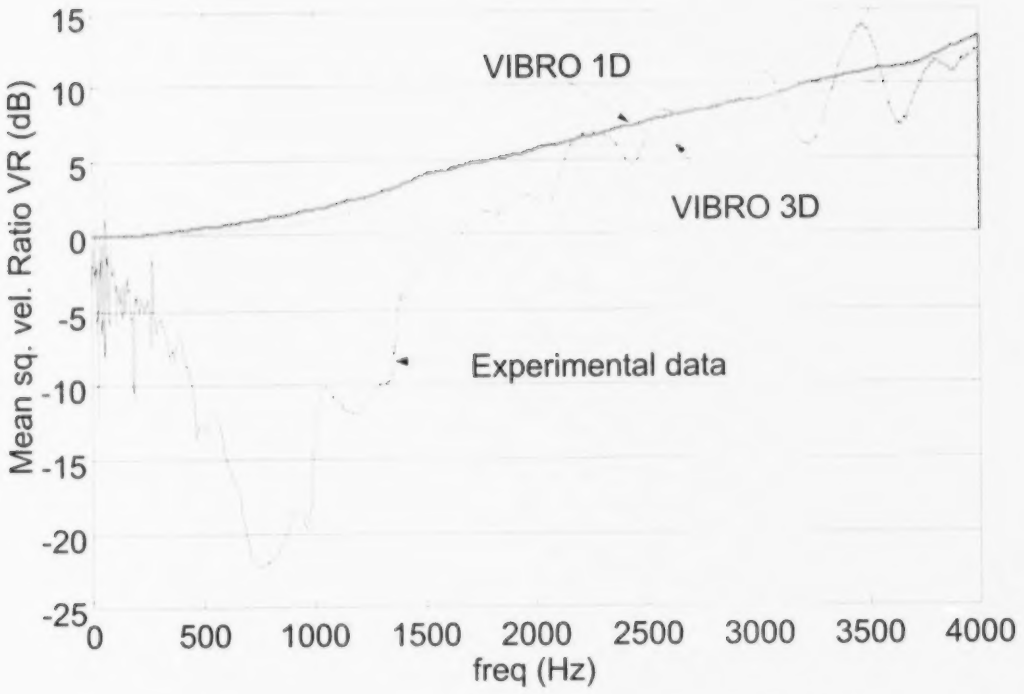

Figure II.18 Mean square velocity ratio $VR = 10\log_{10}\dfrac{<v^2>/|f|^2_{air-side}}{<v^2>/|f|^2_{water-side}}$,

2mm steel plate + 3mm neoprene foam, VIBRO-experiment comparison.

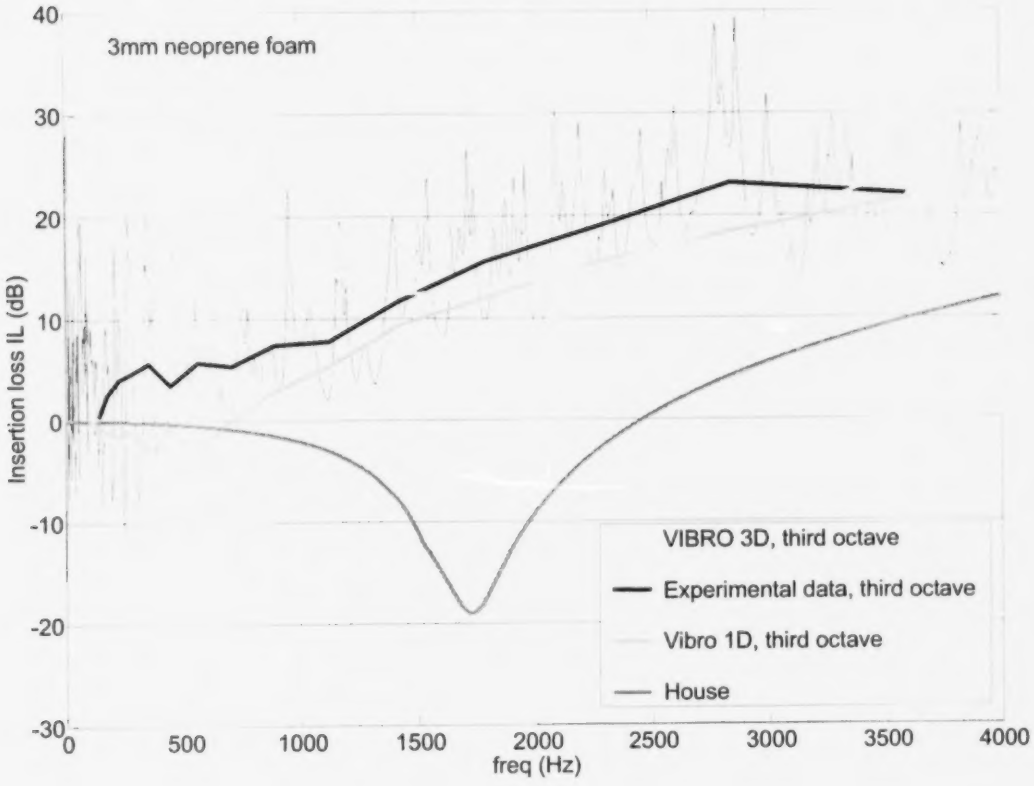

Figure II.19 Insertion loss $IL = 10\log_{10}\frac{< v^2 >_{bare-plate}}{< v^2 >_{coated-plate,water-side}}$, *2mm steel plate + 3mm neoprene foam, VIBRO-experiment comparison.*

Comparison with the model of DeJong DeJong has developed a one-dimensional model to predict the decoupling performance of a compliant coating on an infinite plate[4]. This model is an "updated" version of the original one-dimensional model of House, that accounts for dissipation in the coating and radiation mechanisms of *finite* plates.

Figure II.20 shows the comparison between the measured mean square velocity ratio $VR = 10\log_{10}\frac{<v^2>/|f|^2_{air-side}}{<v^2>/|f|^2_{water-side}}$ and the values predicted by the models of House and of DeJong, for the 2mm steel plate + 3mm neoprene foam. In figure II.20 (a), the complex Young's modulus of the coating has been deduced from the extensional damping measurements (Young's modulus E, loss factor η) of Table I.2 for the 3mm neoprene foam. In figure II.20 (b), the complex Young's modulus of the coating has been deduced from the shear damping measurements (shear modulus G, loss factor η) of Table I.4 for the 3mm neoprene foam. It appears from Figure II.20 that the model of Dejong is much more in agreement with the experiments than the model of House. Additionally, the model of DeJong predicts the *VR* dips which is observed in the experiment.

Figure II.21 shows the comparison between the measured *acoustic* insertion loss IL and the values predicted by the models of House and of DeJong, for the 2mm steel plate + 3mm neoprene foam. In this case, the "measured" acoustic insertion loss is defined (in accordance with the calculated values) as the ratio of the radiated sound power with and without the coating; the radiated sound power was therefore obtained from the experimental surface velocity distributions assuming free-field radiation conditions. Both models satisfactorily agree with the acoustic insertion loss derived from the vibration measurements.

4 The model is detailed in a 11-page document authored by Dr. DeJong and provided to us by Dr. Szabo.

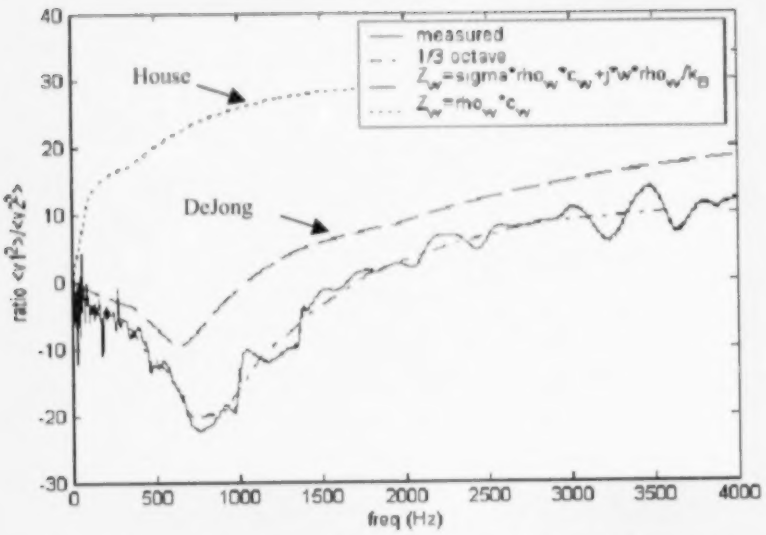

(a) Coating properties derived from extensional damping measurement

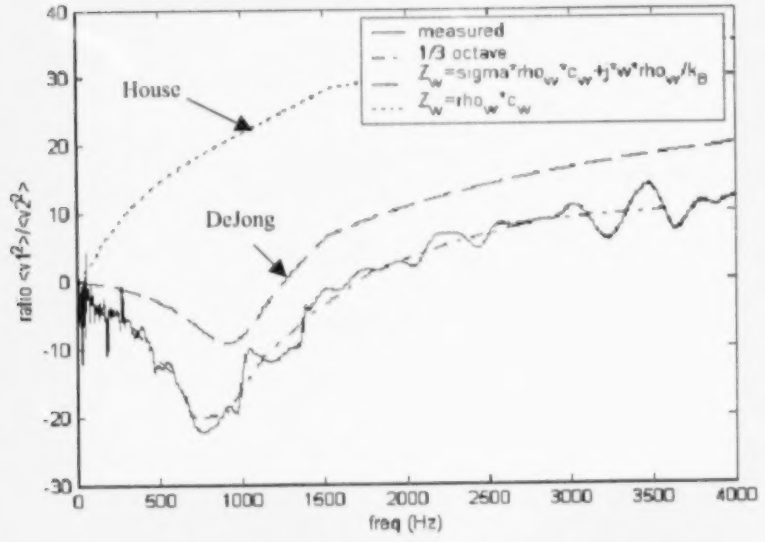

(b) Coating properties derived from shear damping measurement

Figure II.20 Mean square velocity ratio $VR = 10\log_{10}\dfrac{< v^2 > /|f|^2_{air-side}}{< v^2 > /|f|^2_{water-side}}$,

2mm steel plate + 3mm neoprene foam, comparison between experiments and the models of House and Dejong.

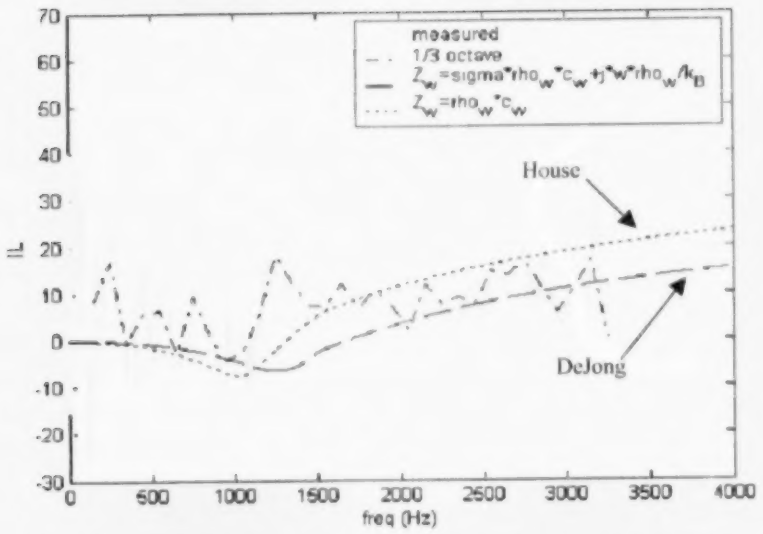

(a) Coating properties derived from extensional damping measurement

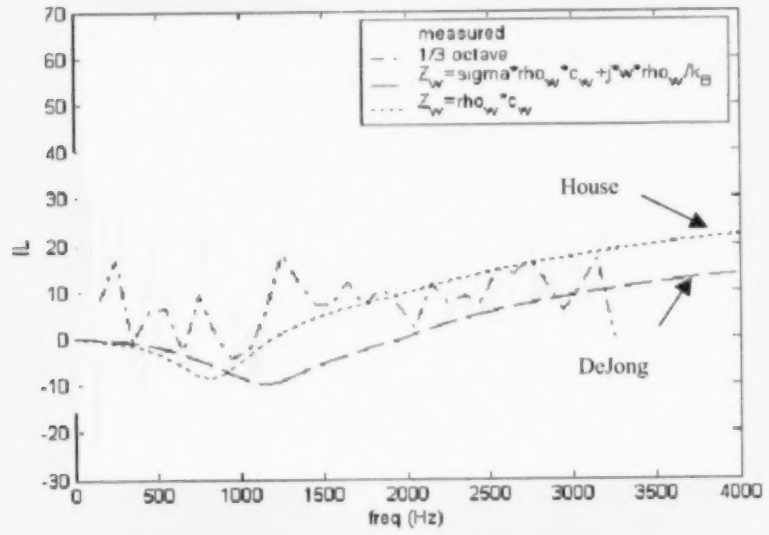

(b) Coating properties derived from shear damping measurement

Figure II.21 Acoustic insertion loss, 2mm steel plate + 3mm neoprene foam, comparison between experiments and the models of House and Dejong.

2.3.5 2mm steel plate with 6mm EVA foam

The input parameters of VIBRO1D and VIBRO3D are:

Frequency range	Modal order	Number of Gauss interpolation points	Resolution (Hz)
10 - 4000 Hz	10	10	1

The 6 mm EVA foam has a modulus similar to the 3 mm neoprene foam, but a much lower density. As for the 3mm neoprene foam, it is suspected that VIBRO3D results are not reliable in this case. VIBRO1D results are generally in better agreement with the experiment.

The same dip in the air side response is noticeable between 700 and 1000 Hz, producing an important difference between experimental velocity ratio and predictions of VIBRO (Figure II.22). Again, above 2000 Hz, predictions agree quite well with the experimental data (Figure II.24); VIBRO1D slightly overestimates the vibration reduction. The amount of vibration reduction reaches 10 dB at 4000 Hz.

Insertion loss results (Figures II.25, II.26) also show a good agreement between experimental data and VIBRO1D, especially in high frequency. Again, the model of House significantly deviates from the experiments.

Figures II.27, II.28 show comparison between experimental data and the models of House and DeJong in terms of the mean square velocity ratio (Figure II.27) and acoustic insertion loss (Figure II.28) (in the latter case, the free-field sound power was calculated from surface velocity distributions as explained in II.3.4). Again the model of DeJong adequately describes both the vibration and radiation phenomena. It is worthwhile noticing that coating material properties derived from shear damping measurements seem to better fit with the experimental data (Figure II.27-b).

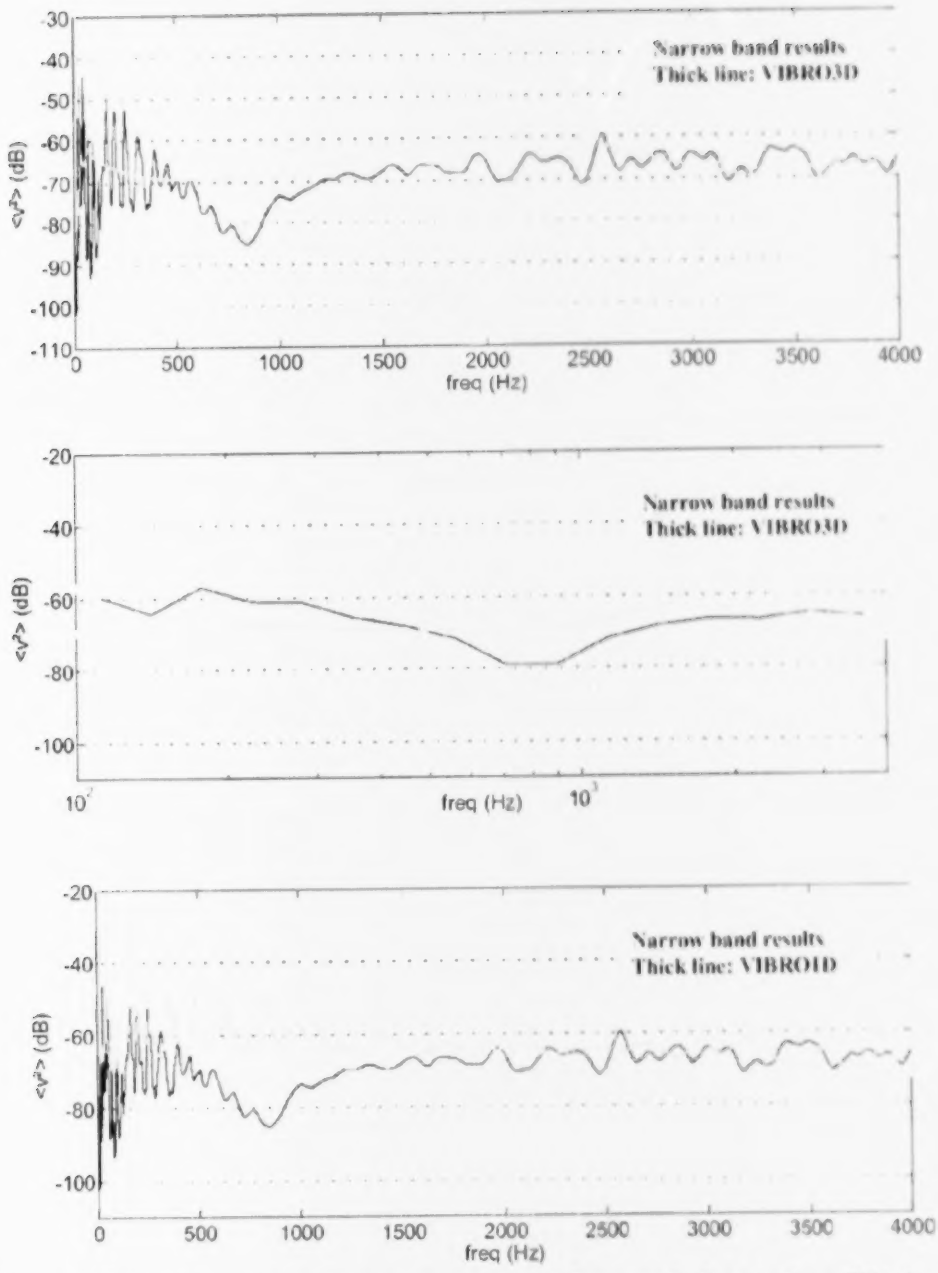

Figure II.22 Mean square velocity on airside of the 2mm steel plate + 6mm EVA foam, VIBRO-experiment comparison.

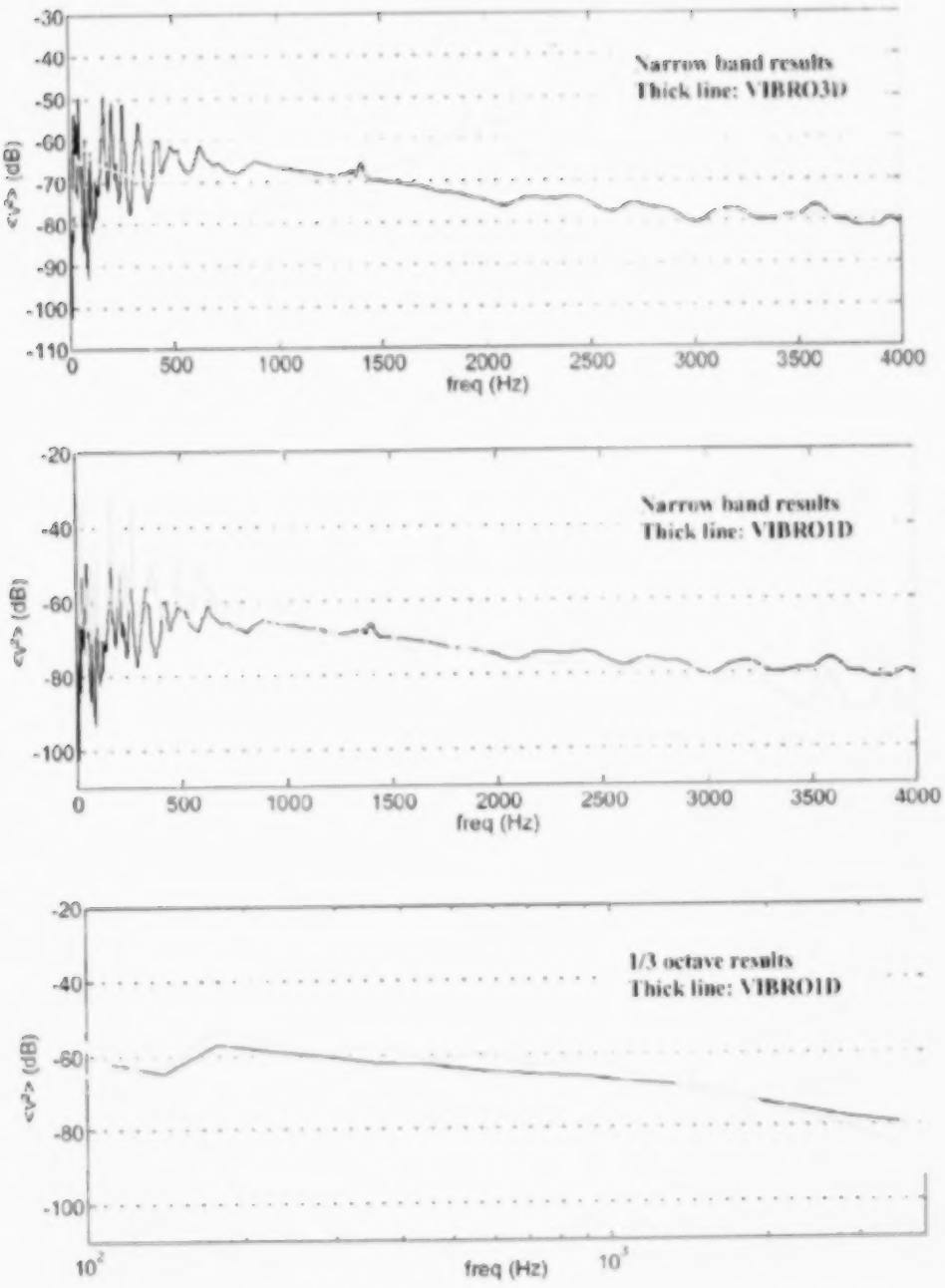

Figure II.23 Mean square velocity on waterside of the 2mm steel plate + 6mm EVA foam, VIBRO-experiment comparison

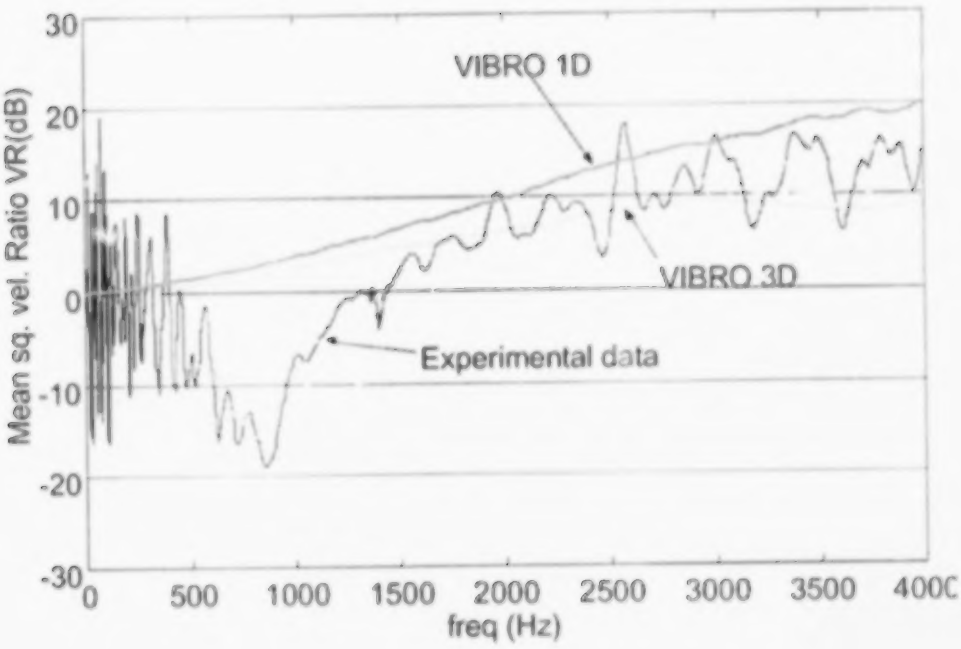

Figure II 24 Mean square velocity ratio $VR = 10\log_{10}\frac{\langle v^2 \rangle |f|^2_{air-side}}{\langle v^2 \rangle |f|^2_{water-side}}$.

2mm steel plate + 6mm EVA foam. VIBRO-experiment comparison.

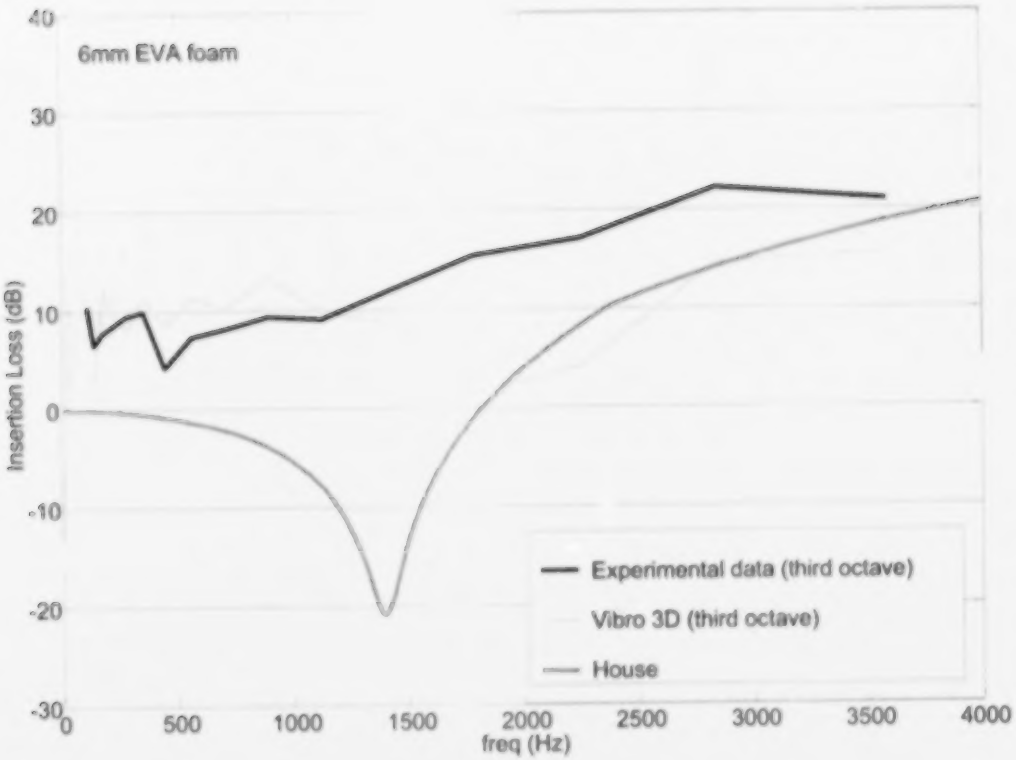

Figure II.25 Insertion loss $IL = 10\log_{10}\frac{< v^2 >_{bare-plate}}{< v^2 >_{coated-plate,water-side}}$, *2mm steel plate + 6mm EVA foam, VIBRO3D-experiment comparison.*

Figure II.26 Insertion loss IL $10\log_{10}\frac{v_{\text{bare plate}}}{v_{\text{coated plate,water side}}}$*, 2mm steel plate + 6mm EVA foam, VIBRO1D-experiment comparison.*

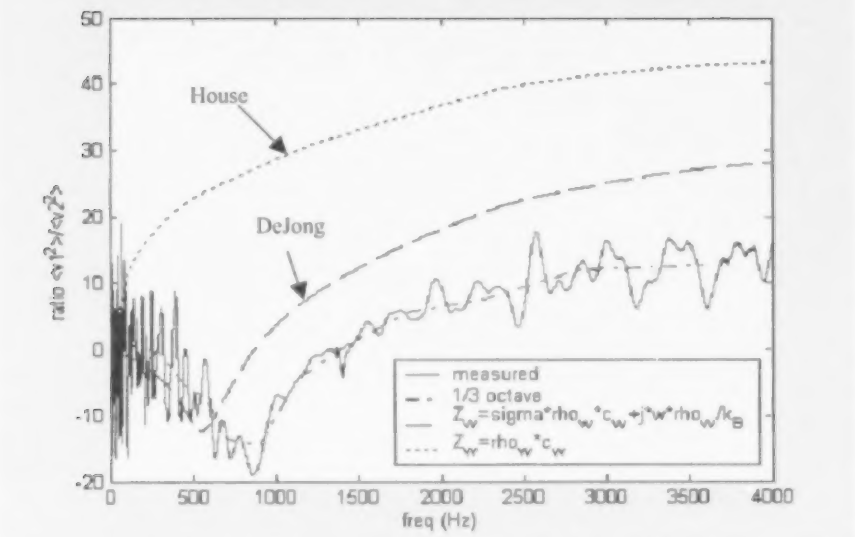

(a) Coating properties derived from extensional damping measurement

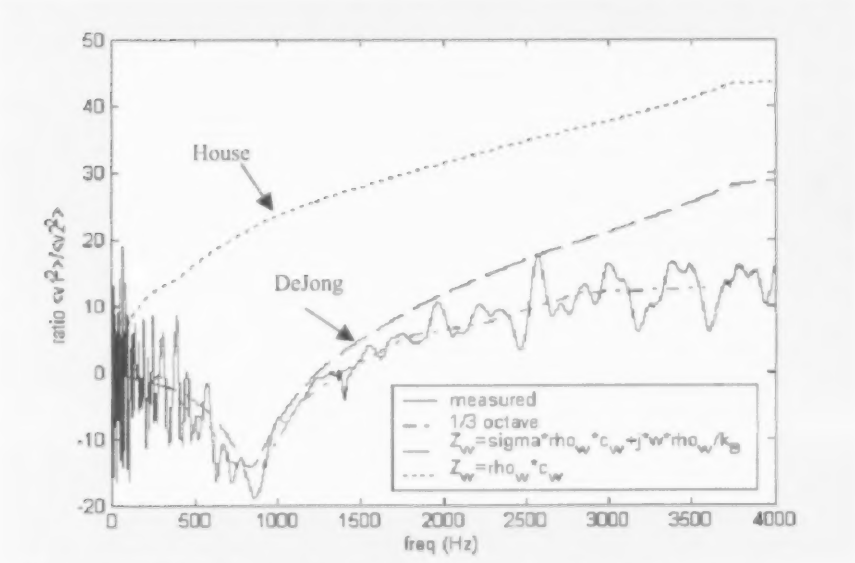

(b) Coating properties derived from shear damping measurement

Figure II.27 Mean square velocity ratio $VR = 10\log_{10}\dfrac{<v^2>/|f|^2_{air-side}}{<v^2>/|f|^2_{water-side}}$, *2mm steel plate + 6mm EVA foam, comparison between experiments and the models of House and Dejong.*

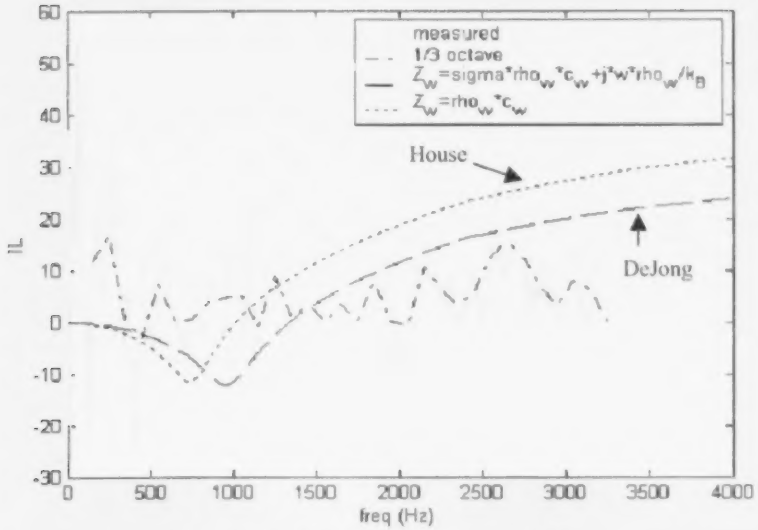

(a) Coating properties derived from extensional damping measurement

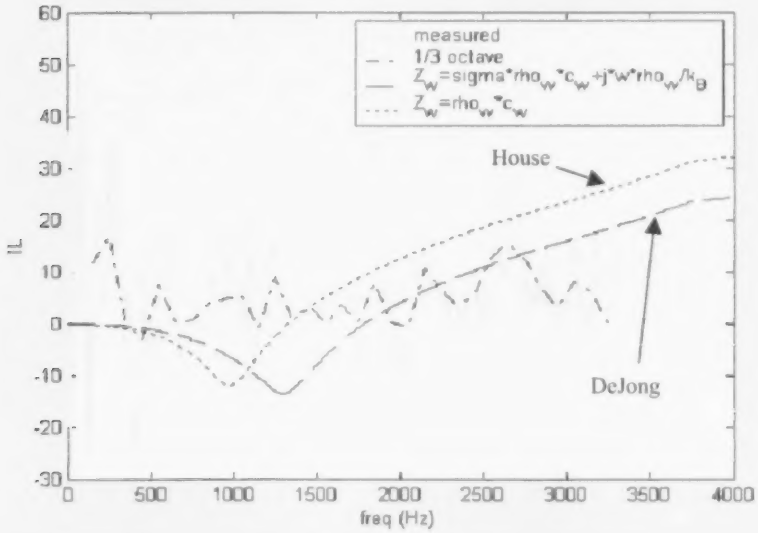

(b) Coating properties derived from shear damping measurement

Figure II.28 Acoustic insertion loss, 2mm steel plate + 6mm EVA foam, comparison between experiments and the models of House and Dejong.

2.3.6 9.5mm steel plate with 25 mm EPT/SBR foam

Input parameters of VIBRO1D and VIBRO3D:

Frequency range	Modal order	Number of Gauss interpolation points	Resolution
10 – 4000 Hz	7	7	1

In this case, the plate and the coating material are far thicker that in the two previous cases. It results in a lower modal density and a lower response level, too. As already pointed, the experimental boundary conditions in this case deviate from simply supported, which makes the comparisons with the theory more difficult.

The experimental response on the material side does not decrease progressively when frequency increases but rather presents a drop around 1000 Hz, and then keeps a relatively constant level (Figure II.30). In contrast, VIBRO predicts a monotonic decrease with the frequency, which results in a large over-estimation of the vibration reduction. VIBRO3D overestimates the velocity ratio by 10 to 15 dB (Figure II.31), and the insertion loss by 10 dB (Figures II.32, II.33), whereas VIBRO1D overestimates the velocity ratio by 15 to 20 dB and the insertion loss by 20 dB.

Figures II.34, II.35 present comparisons with the model of DeJong. As a general trend, theoretical results based on shear damping characterisation of the material seem to better agree with the experiments.

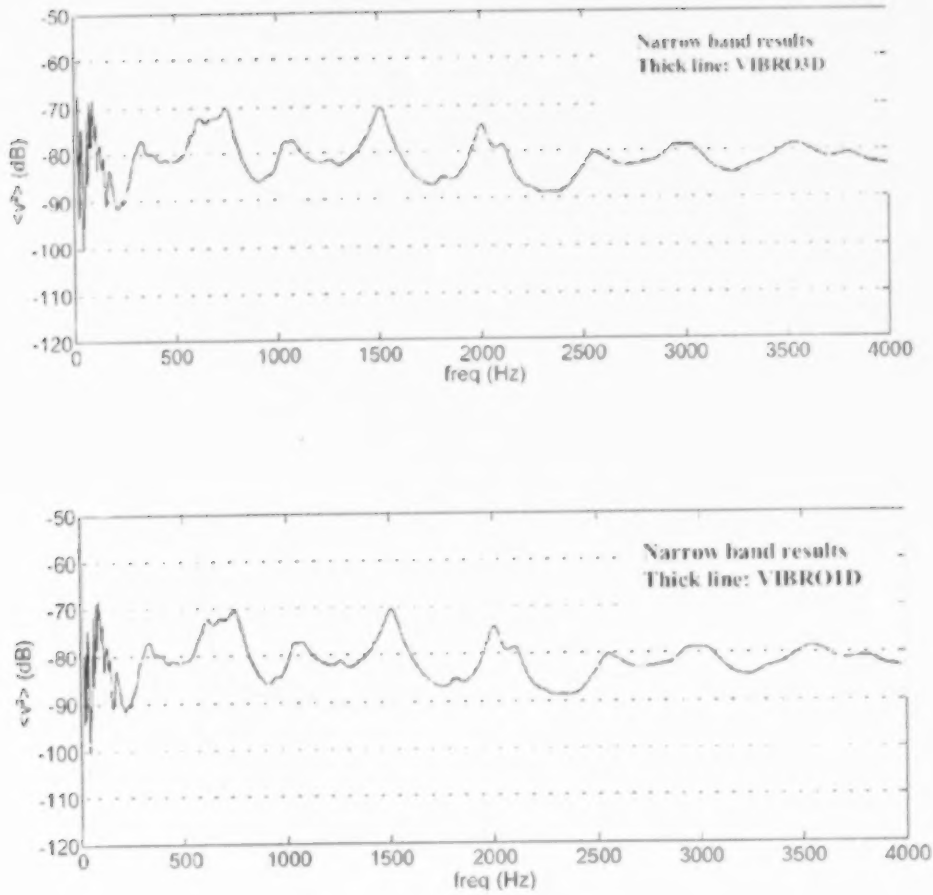

Figure II.29 Mean square velocity on airside of the 9.5mm steel plate + 25 mm EPT/SBR foam, VIBRO-experiment comparison.

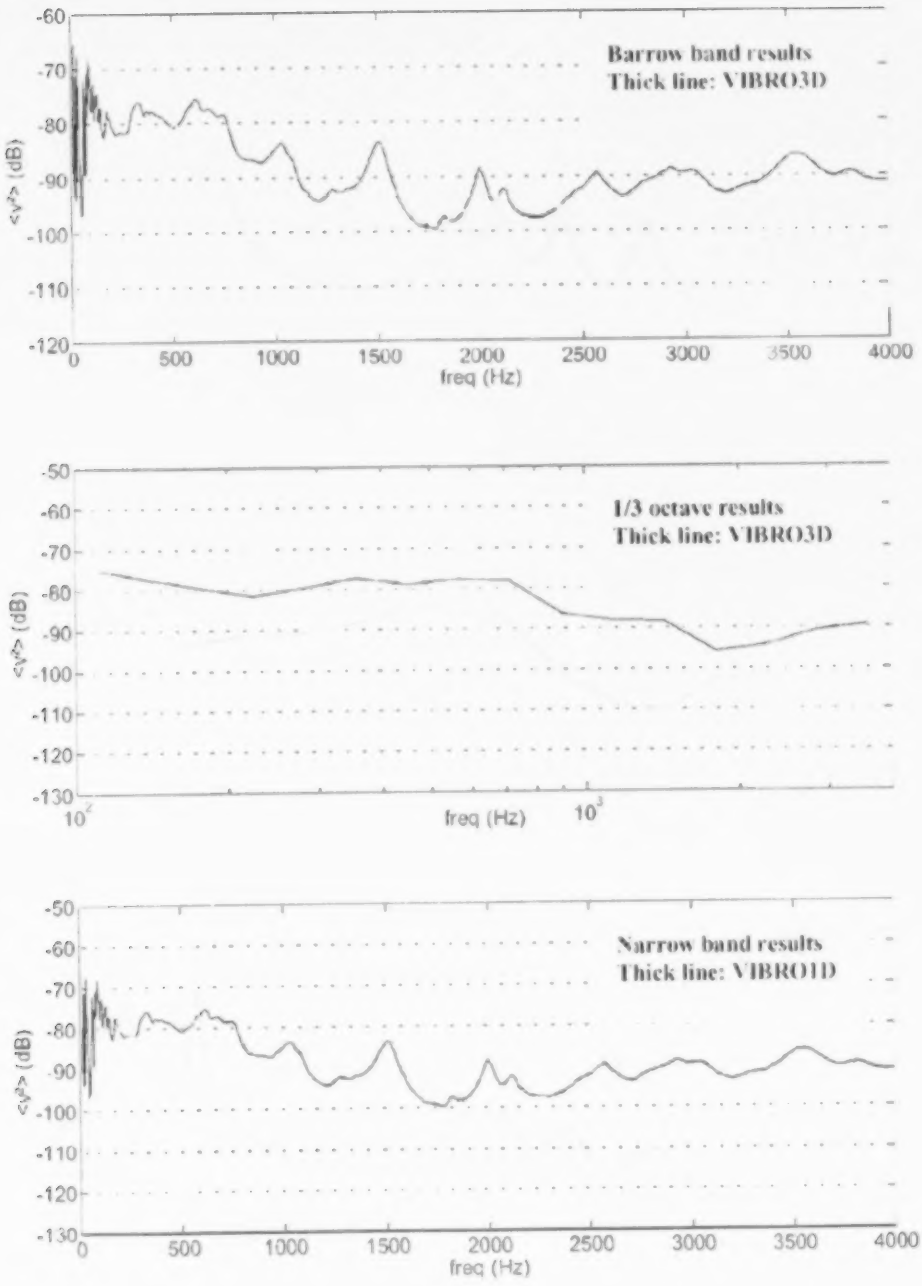

Figure II.30 Mean square velocity on waterside of the 9.5mm steel plate + 25 mm EPT/SBR foam, VIBRO-experiment comparison.

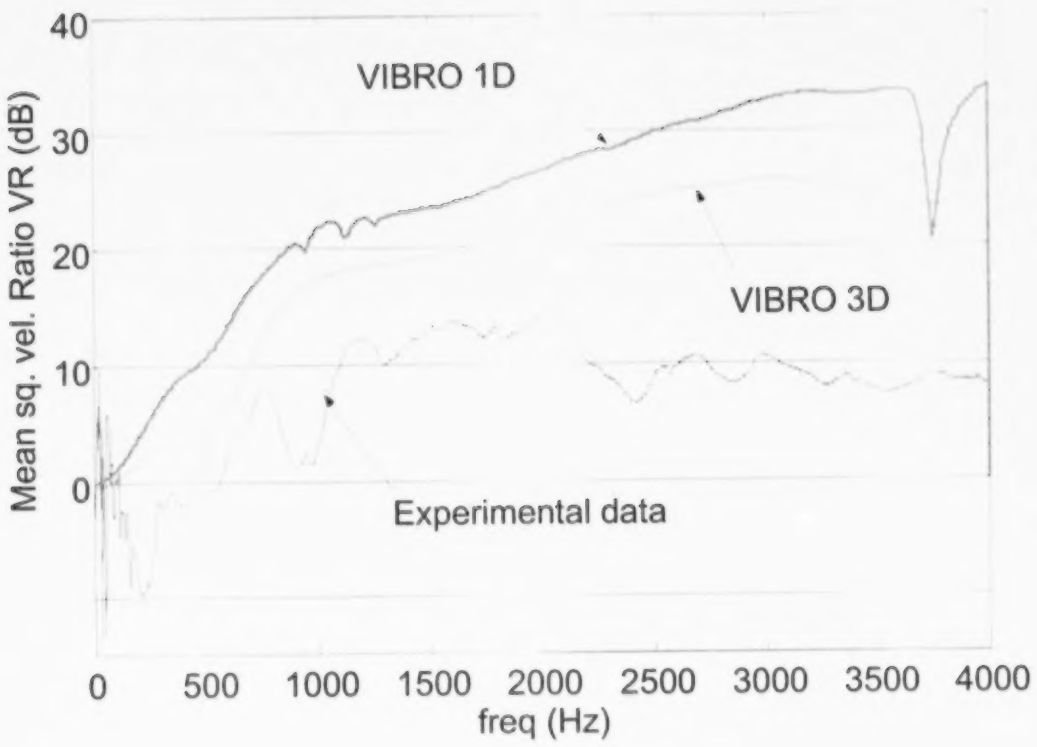

Figure II.31 Mean square velocity ratio $VR = 10\log_{10}\dfrac{<v^2>/|f|^2_{air-side}}{<v^2>/|f|^2_{water-side}}$,

9.5mm steel plate + 25mm EPT/SBR foam, VIBRO-experiment comparison.

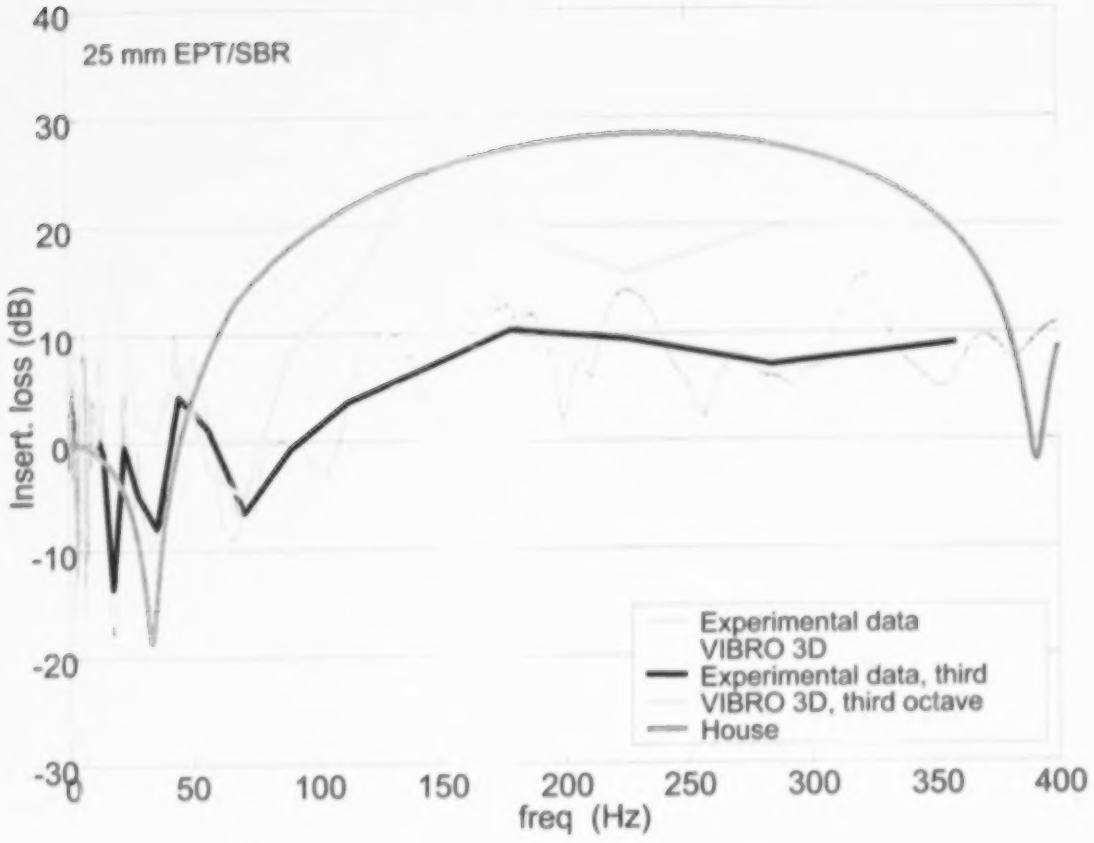

Figure II.32 Insertion loss $IL = 10\log_{10}\frac{< v^2 >_{bare-plate}}{< v^2 >_{coated-plate,water-side}}$, *9.5mm steel plate + 25mm EPT/SBR foam, VIBRO3D-experiment comparison.*

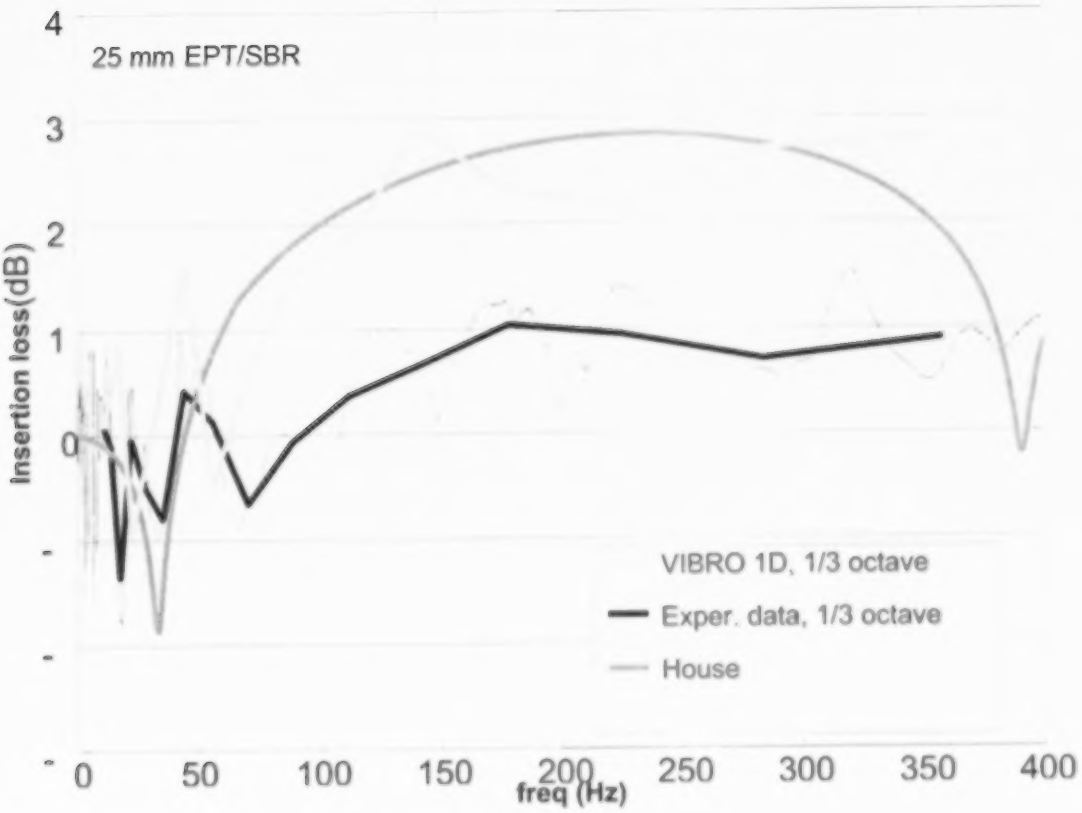

Figure II.33 Insertion loss $IL = 10\log_{10}\frac{< v^2 >_{bare\ plate}}{< v^2 >_{coated-plate,water-side}}$, *9.5mm steel plate + 25mm EPT/SBR foam, VIBRO1D-experiment comparison.*

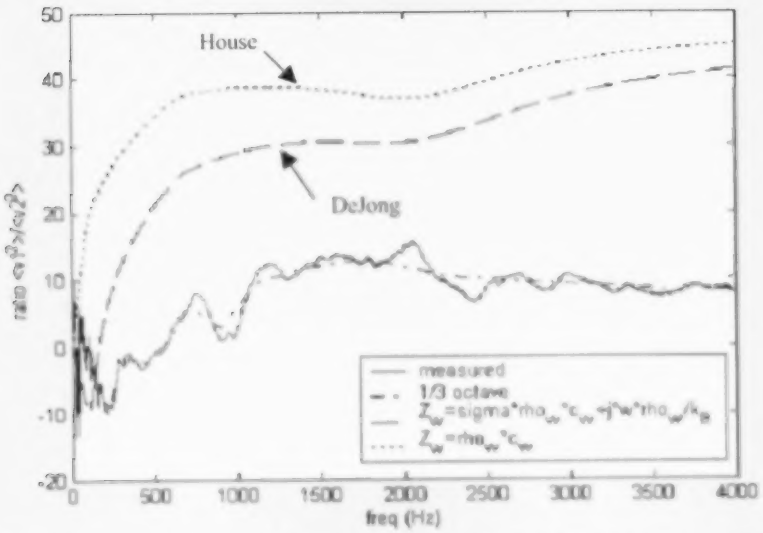

(a) Coating properties derived from extensional damping measurement

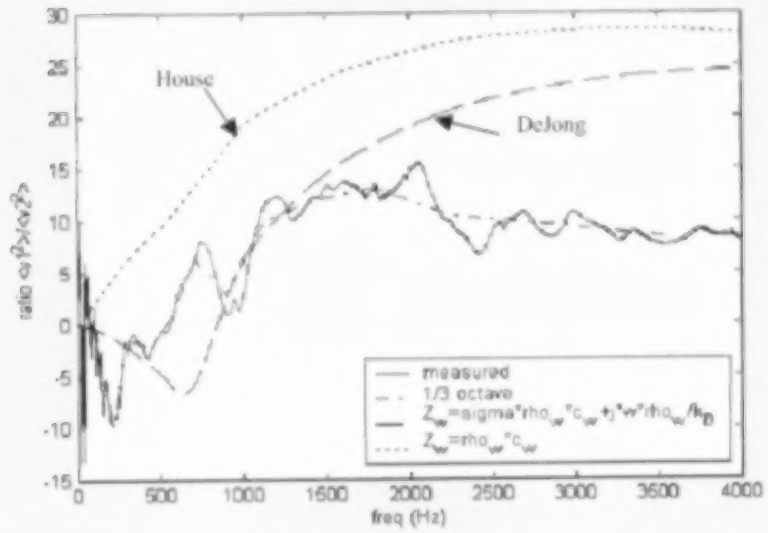

(b) Coating properties derived from shear damping measurement

Figure II.34 Mean square velocity ratio $VR = 10\log_{10}\dfrac{< v^2 > /|f|^2_{air-side}}{< v^2 > /|f|^2_{water-side}}$,

9.5mm steel plate + 25mm EPT foam, comparison between experiments and the models of House and Dejong.

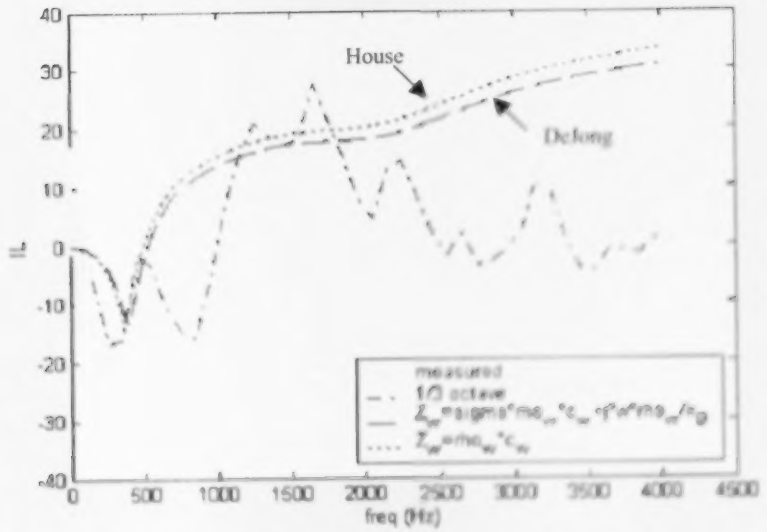

(a) Coating properties derived from extensional damping measurement

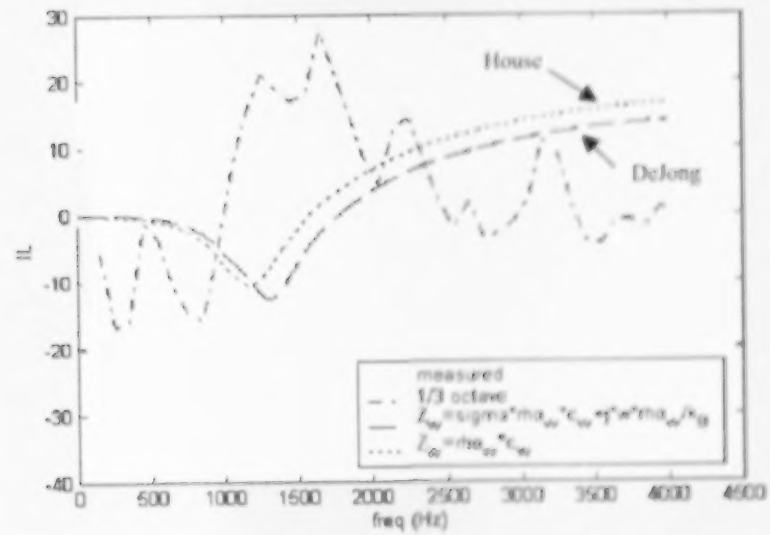

(b) Coating properties derived from shear damping measurement

Figure II.35 Acoustic insertion loss, 9.5mm steel plate + 25mm EPT foam, comparison between experiments and the models of House and Dejong.

CONCLUSIONS

The Table below summarises the general observations in terms of comparison between the experimental data gathered in the various test configurations, and the various modelling tools tested.

Note that the conclusions below are based essentially on the **experimental results for 2mm steel plates**. The experimental results for a 9mm steel plate + 25 mm foam material need to be taken with caution (uncertain plate boundary conditions, stiffness of tank structure not sufficient, material characterisation method not appropriate for thick materials).

	VIBRO*	House	DeJong
Mean Square Velocity Ratio[1]	Good fit in HF	Not available	Good fit
Vibration Insertion Loss[2]	Good fit	Bad fit	Not available
Acoustic insertion Loss[3]	Not available	Not available	Good fit
Base Plate Vibration Ratio[4]	Not tested		

[1] Ratio of base plate velocity to velocity at free surface of material;
[2] Ratio of base plate velocity (uncoated) to velocity at free surface of material;
[3] Ratio of base plate sound power (uncoated) to sound power of coated plate;
[4] Ratio of base plate velocity (uncoated) to base plate velocity (coated).

*VIBRO3D results may not be reliable for the 2mm steel plate + 3mm neoprene or 6 mm EVA (Numerical problems have been observed with the 3D model when the added stiffness of the material is "large enough" as compared to the base plate stiffness).

The main conclusions that can be drawn from the 2mm plate data are as follows:

- VIBRO1D has been found to reliably predict the "high frequency" response both in terms of Mean Square Velocity Ratio and Vibration Insertion Loss. However, the low frequency dip visible on the airside response and Mean Square Velocity Ratio was not predicted by VIBRO.
- The simple model of House was found to be incorrect in general.
- The updated model of DeJong agrees well with experimental data in terms of Mean Square Velocity Ratio and Acoustic Insertion Loss. Especially, this model picks up the low frequency dip of the airside response.
- The Oberst beam shear damping measurement technique seems to be more reliable than the extensional damping measurement, both in terms of sensitivity and agreement between theory and experiments.

APPENDIX A: SHEAR DAMPING EQUATIONS

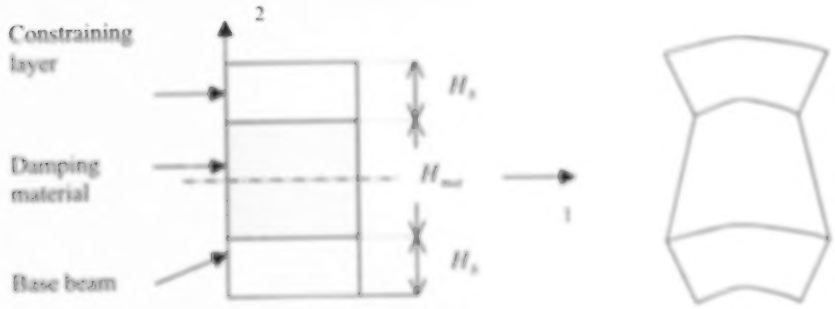

Constrained-layer treatment

The kinematic assumptions for the constrained-layer treatment are that the base base beam and constraining layer have pure bending deformation and the damping material experiences bending and shear deformation. Also, it is assumed that the base beam and constraining layer are identical. The displacements of each layer (base beam *b*, damping material *mat*, constraining layer *c*) in the cartesian system (1-2) passing through the symmetry axis of the composite beam are given by:

Beam:
$$\begin{cases} u_1^b(x_1,x_2,t) = -(x_2 + \dfrac{H_b + H_{mat}}{2})\dfrac{\partial w}{\partial x_1} \\ u_2^b(x_1,x_2,t) = w(x_1,t) \end{cases} \quad \text{(A-1)}$$

Constraining layer:
$$\begin{cases} u_1^c(x_1,x_2,t) = -(x_2 - \dfrac{H_b + H_{mat}}{2})\dfrac{\partial w}{\partial x_1} \\ u_2^c(x_1,x_2,t) = w(x_1,t) \end{cases} \quad \text{(A-2)}$$

Material:
$$\begin{cases} u_1^{mat}(x_1,x_2,t) = x_2 \dfrac{H_b}{H_{mat}}\dfrac{\partial w}{\partial x_1} \\ u_2^{mat}(x_1,x_2,t) = w(x_1,t) \end{cases} \quad \text{(A-3)}$$

According to the above kinematic assumptions, the Hamilton functional of the system is given by:

$$H(w) = \int_{t_0}^{t_1}\int_{0}^{L}\left(\frac{1}{2}\rho_{mat}A_{mat} + \rho_b A_b\right)\left(\frac{\partial w}{\partial t}\right)^2 dx_1 dt - \int_{t_0}^{t_1}\int_{0}^{L}\left(\frac{1}{2}\tilde{E}_{mat}I_{mat}\frac{H_b^{\,2}}{H_{mat}^{\,2}} + \tilde{E}_b I_b\right)\left(\frac{\partial^2 w}{\partial x_1^{\,2}}\right)^2 dx_1 dt$$

$$- \int_{t_0}^{t_1}\int_{0}^{L}\frac{1}{2}\tilde{G}_{mat}A_{mat}\left(1 + \frac{H_b}{H_{mat}}\right)^2\left(\frac{\partial w}{\partial x_1}\right)^2 dx_1 dt \qquad \text{(A-4)}$$

where ρ_{mat} and ρ_b are the density of the damping material and base beam (or constraining layer), respectively. The first term in equation A-4 accounts for the kinetic energy, the second term for the flexural energy and the last term for the shear deformation energy. The associated equation of motion for free vibration of the composite beam is:

$$\alpha\frac{\partial^2 w}{\partial t^2} - \gamma\frac{\partial^2 w}{\partial x_1^{\,2}} + \beta\frac{\partial^4 w}{\partial x_1^{\,4}} = 0 \qquad \text{(A-5)}$$

with:

$$\alpha = \frac{1}{2}\rho_{mat}A_{mat} + \rho_b A_b$$

$$\beta = \frac{1}{2}\tilde{E}_{mat}I_{mat}\frac{H_b^{\,2}}{H_{mat}^{\,2}} + \tilde{E}_b I_b$$

$$\gamma = \frac{1}{2}\tilde{G}_{mat}A_{mat}\left(1 + \frac{H_b}{H_{mat}}\right)^2$$

In the following, the solution of equation A-5 (eigenfunctions and eigenfrequencies) is derived in the case of simply-supported boundary conditions of the beam; even though the experimental boundary conditions are rather free-free, the simply-supported case is more convenient to derive the expression of the equivalent flexural rigidity in terms of the properties of the individual layers. For the simply-supported case, the eigenfunctions are given by

$$w(x_1, t) = \sin(k_n x_1)e^{j\omega_n t} \qquad \text{(A-6)}$$

with $k_n = \frac{n\pi}{L}$. Substituting equation A-6 into equation A-5 allows the eigenfrequencies to be derived,

$$\omega_n = k_n \sqrt{\frac{\gamma + \beta k_n^{\,2}}{\alpha}} = k_n \sqrt{\frac{\frac{1}{2}\widetilde{G}_{mat} A_{mat} (1 + \frac{H_b}{H_{mat}})^2 + \left(\frac{1}{2} \widetilde{E}_{mat} I_{mat} \frac{H_b^{\,2}}{H_{mat}^{\,2}} + \widetilde{E}_b I_b \right) k_n^{\,2}}{\frac{1}{2}\rho_{mat} A_{mat} + \rho_b A_b}} \tag{A-7}$$

In most cases, the damping material has a much lower rigidity than the base or constraining layer, such that $\widetilde{E}_{mat} I_{mat} \frac{H_b^{\,2}}{H_{mat}^{\,2}} << \widetilde{E}_b I_b$, and equation A-7 can be simplified to

$$\omega_n = k_n \sqrt{\frac{\frac{1}{2}\widetilde{G}_{mat} A_{mat} (1 + \frac{H_b}{H_{mat}})^2 + \widetilde{E}_b I_b k_n^{\,2}}{\frac{1}{2}\rho_{mat} A_{mat} + \rho_b A_b}} \tag{A-8}$$

The equivalent flexural rigidity of the composite beam $\widetilde{EI}$ can be deduced by identifying equation A-8 with $\omega_n = k_n^{\,2} \sqrt{\frac{\widetilde{EI}}{\rho_{mat} A_{mat} + 2\rho_b A_b}}$. It follows that

$$\widetilde{EI} = \widetilde{G}_{mat} A_{mat} (1 + \frac{H_b}{H_{mat}})^2 / k_n^{\,2} + 2\widetilde{E}_b I_b \tag{A-9}$$

APPENDIX B: Theory-experiment comparison for various material characterisation data

- 2mm steel plate + 3mm neoprene foam

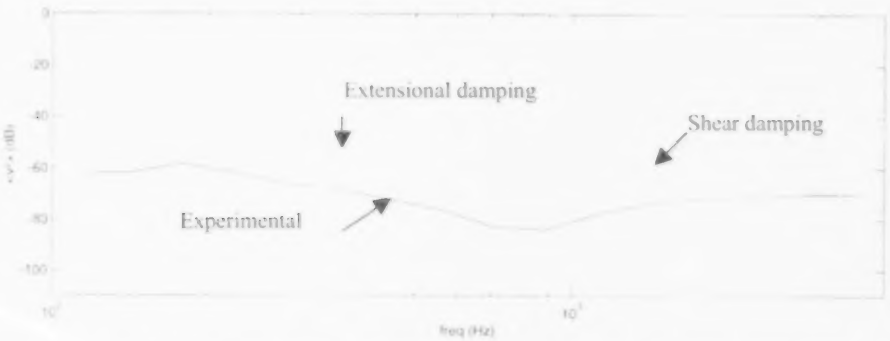

Figure B.1: Mean square velocity on airside of the 2mm steel plate + 3mm neoprene foam (1/3 octave results) , comparison between experimental results and VIBRO1D with material properties derived from extensional or shear damping measurements.

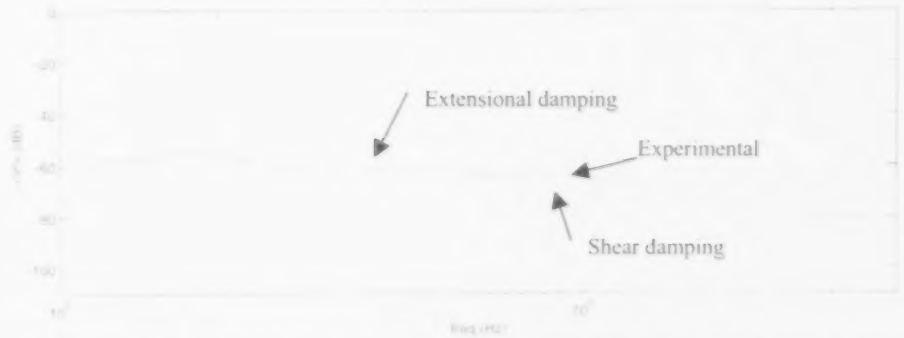

Figure B.2: Mean square velocity on water side of the 2mm steel plate + 3mm neoprene foam (1/3 octave results) , comparison between experimental results and VIBRO1D with material properties derived from extensional or shear damping measurements.

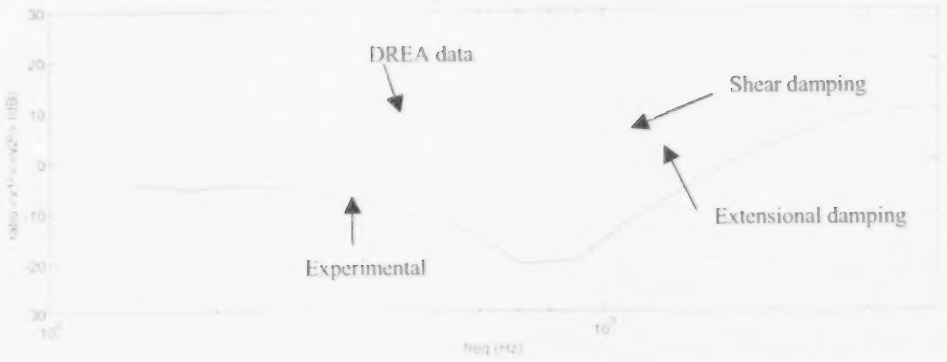

Figure B.3: Mean square velocity ratio (airside/waterside) of the 2mm steel plate + 3mm neoprene foam (1/3 octave results) , comparison between experimental results and VIBRO3D with material properties derived from extensional measurements, shear damping measurements or DREA data.

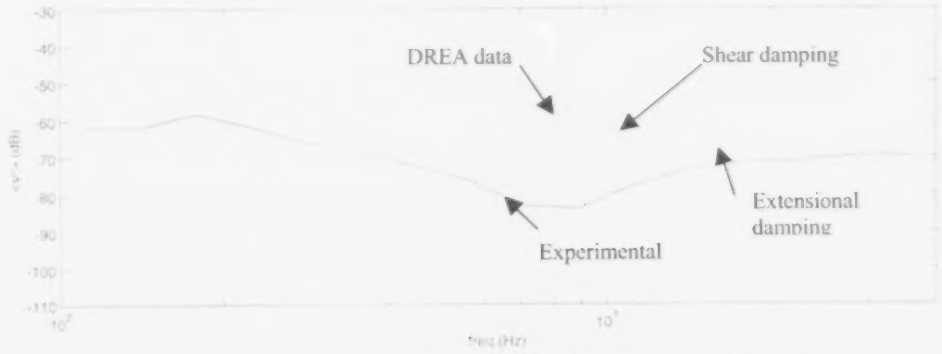

Figure B.4: Mean square velocity on airside of the 2mm steel plate + 3mm neoprene foam (1/3 octave results) , comparison between experimental results and VIBRO3D with material properties derived from extensional measurements, shear damping measurements or DREA data.

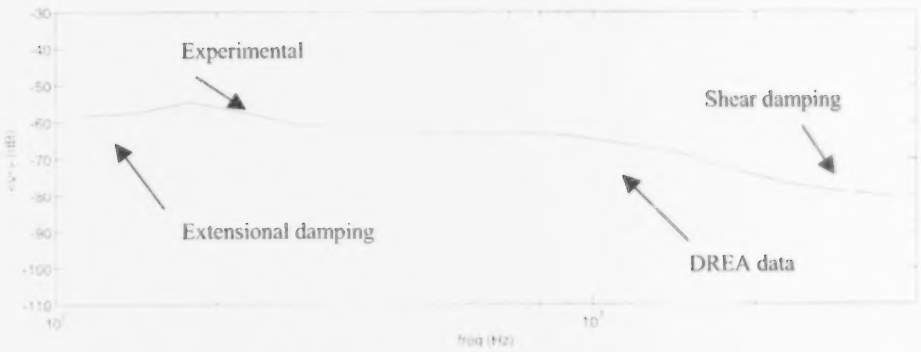

Figure B.5: Mean square velocity on waterside of the 2mm steel plate + 3mm neoprene foam (1/3 octave results) , comparison between experimental results and VIBRO3D with material properties derived from extensional measurements, shear damping measurements or DREA data.

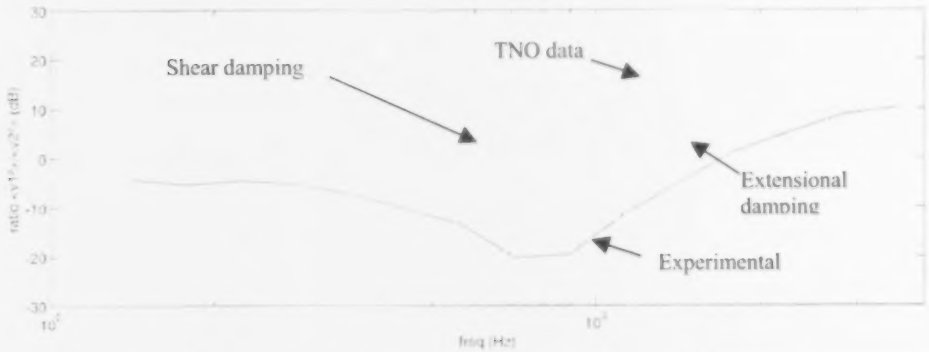

Figure B.6: Mean square velocity ratio (water side/airside) of the 2mm steel plate + 3mm neoprene foam (1/3 octave results) , comparison between experimental results and VIBRO3D with material properties derived from extensional measurements, shear damping measurements and TNO data.

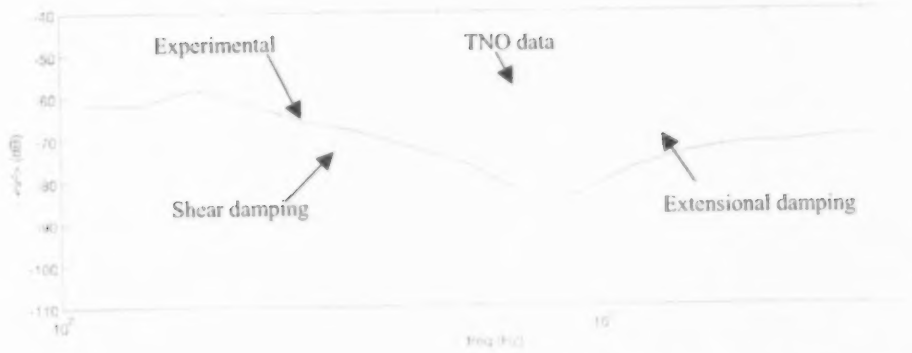

Figure B.7: Mean square velocity on the airside of the 2mm steel plate + 3mm neoprene foam (1/3 octave results) , comparison between experimental results and VIBRO3D with material properties derived from extensional measurements, shear damping measurements and TNO data.

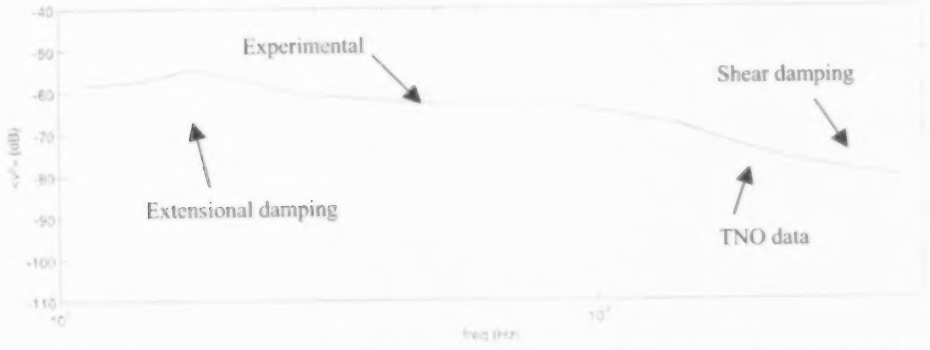

Figure B.8: Mean square velocity on the water side of the 2mm steel plate + 3mm neoprene foam (1/3 octave results) , comparison between experimental results and VIBRO3D with material properties derived from extensional measurements, shear damping measurements and TNO data.

- 2mm steel plate + 6mm EVA foam

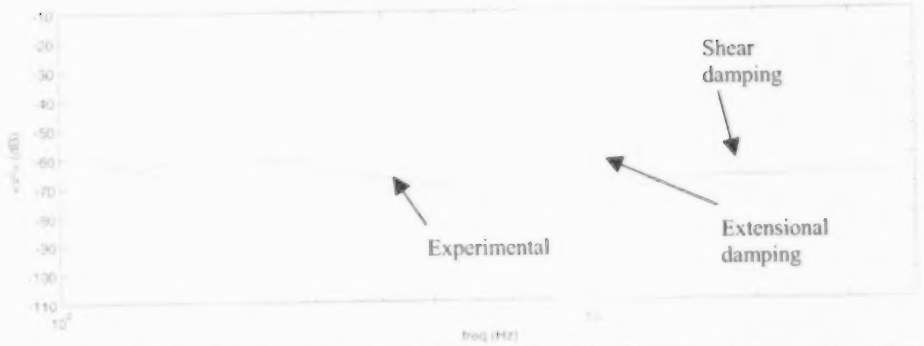

Figure B.9: Mean square velocity on airside of the 2mm steel plate + 6mm EVA foam (1/3 octave results) , comparison between experimental results and VIBRO1D with material properties derived from extensional or shear damping measurements.

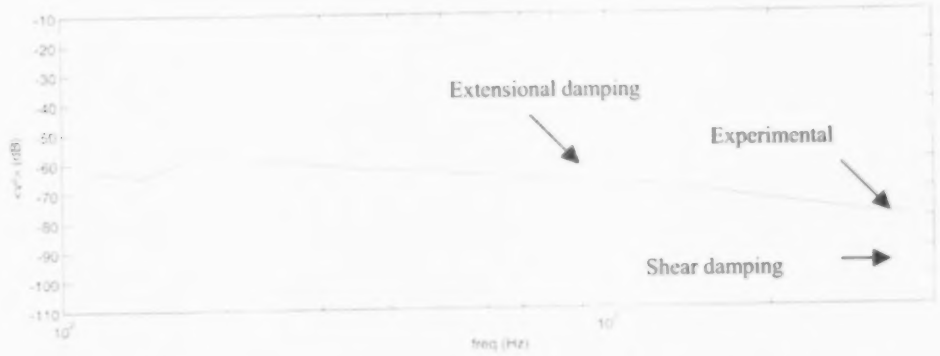

Figure B.10: Mean square velocity on water side of the 2mm steel plate + 6mm EVA foam (1/3 octave results) , comparison between experimental results and VIBRO1D with material properties derived from extensional or shear damping measurements.

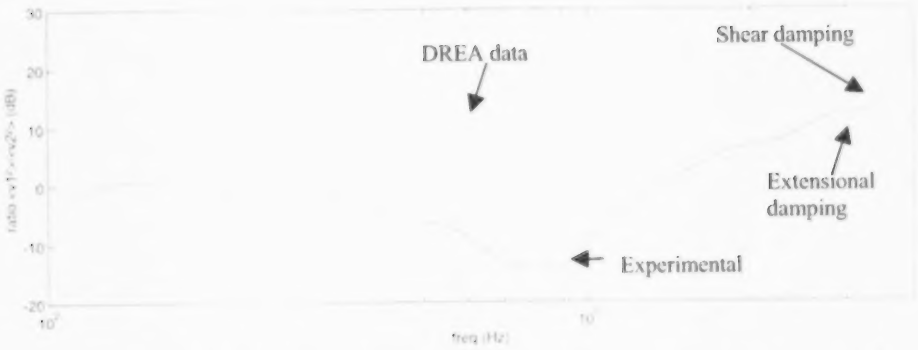

Figure B.11: Mean square velocity ratio (airside/waterside) of the 2mm steel plate + 6mm EVA foam (1/3 octave results) , comparison between experimental results and VIBRO3D with material properties derived from extensional measurements, shear damping measurements or DREA data.

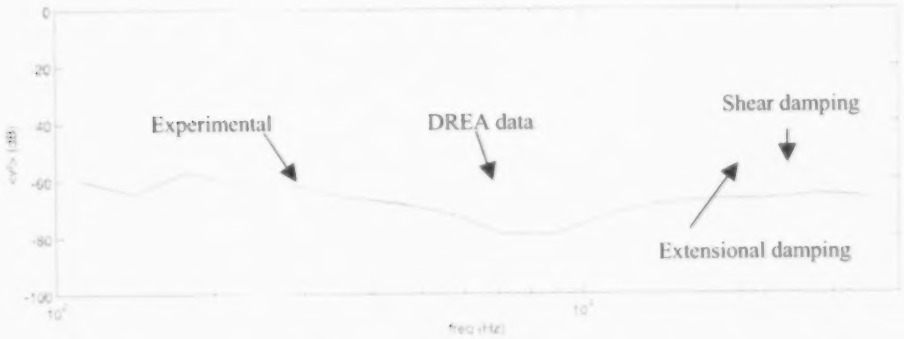

Figure B.12: Mean square velocity on airside of the 2mm steel plate + 6mm EVA foam (1/3 octave results) , comparison between experimental results and VIBRO3D with material properties derived from extensional measurements, shear damping measurements or DREA data.

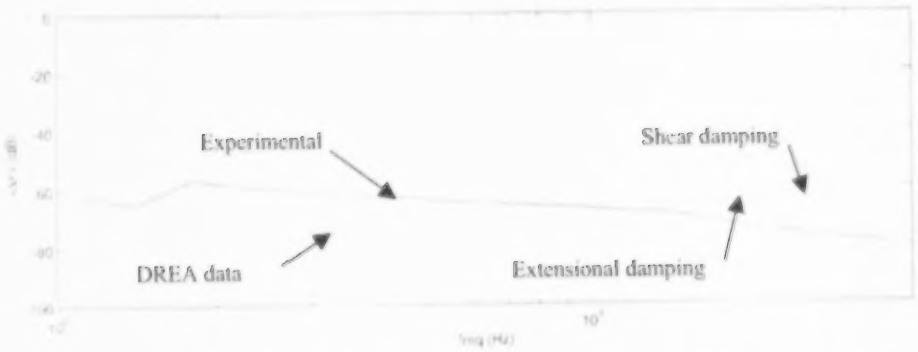

Figure B.13: Mean square velocity on water side of the 2mm steel plate + 6mm EVA foam (1/3 octave results) , comparison between experimental results and VIBRO3D with material properties derived from extensional measurements, shear damping measurements or DREA data.

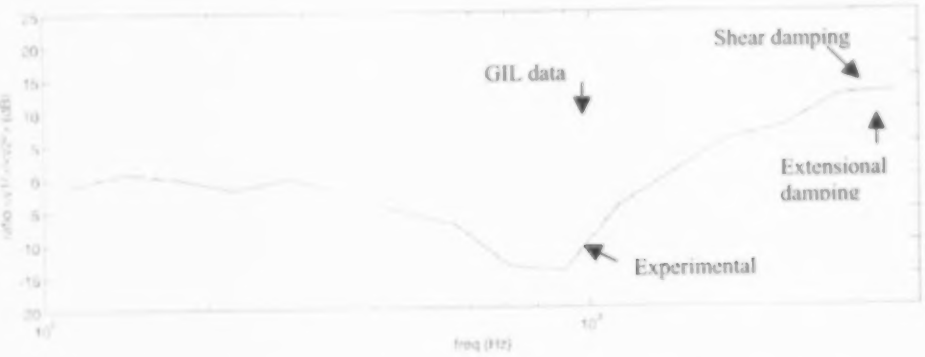

Figure B.14: Mean square velocity ratio (water side/airside) of the 2mm steel plate + 6mm EVA foam (1/3 octave results) , comparison between experimental results and VIBRO3D with material properties derived from extensional measurements, shear damping measurements and GIL data.

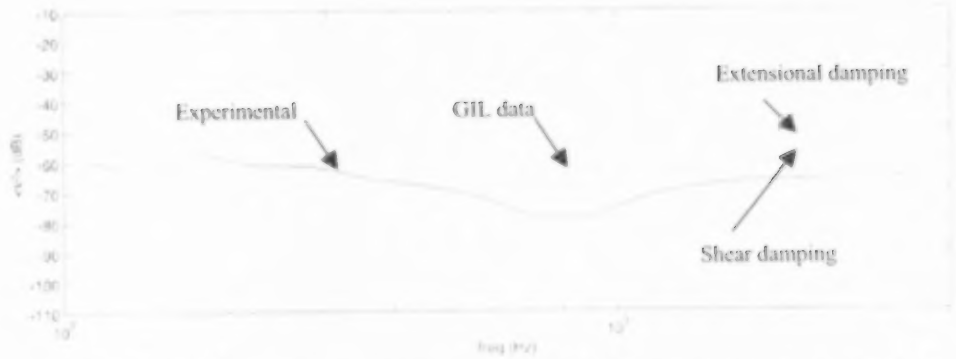

Figure B.15: Mean square velocity on the airside of the 2mm steel plate + 6mm EVA foam (1/3 octave results) , comparison between experimental results and VIBRO3D with material properties derived from extensional measurements, shear damping measurements and GIL data.

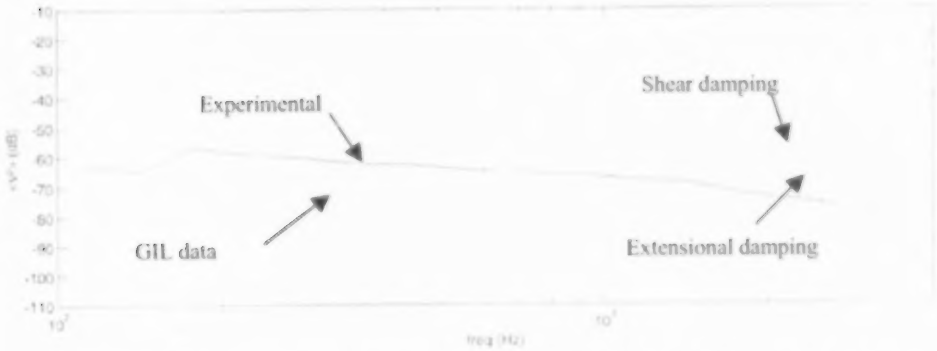

Figure B.16: Mean square velocity on the water side of the 2mm steel plate + 6mm EVA foam (1/3 octave results) , comparison between experimental results and VIBRO3D with material properties derived from extensional measurements, shear damping measurements and GIL data.

- 9.5mm steel plate + 25 EPT foam

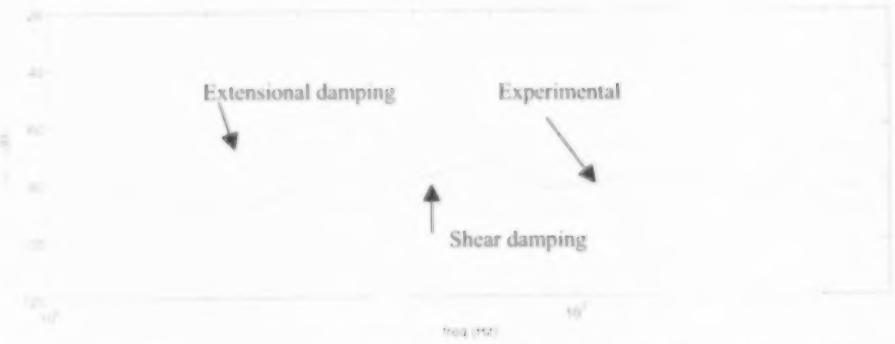

Figure B.17: Mean square velocity on airside of the 9.5mm steel plate + 25mm EPT foam (1/3 octave results) , comparison between experimental results and VIBRO1D with material properties derived from extensional or shear damping measurements.

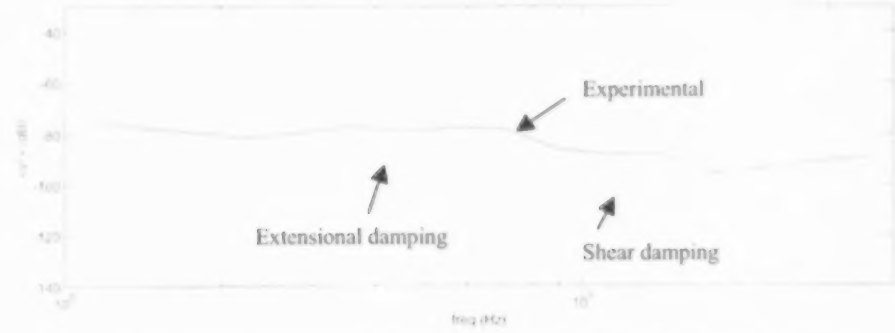

Figure B.18: Mean square velocity on water side of the 9.5mm steel plate + 25mm EPT foam (1/3 octave results) , comparison between experimental results and VIBRO1D with material properties derived from extensional or shear damping measurements.

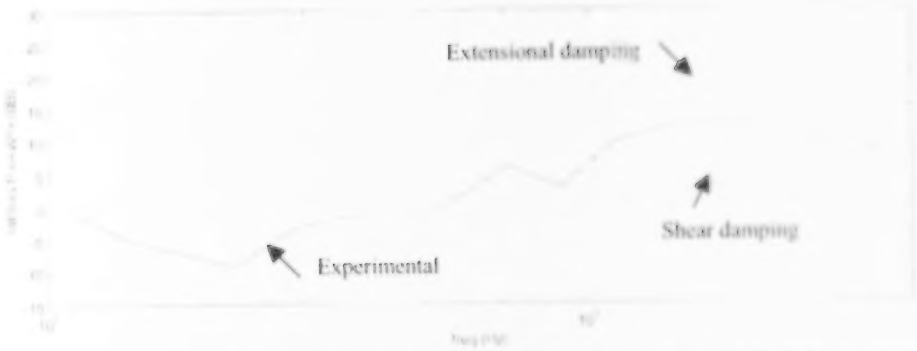

Figure B.19: Mean square velocity ratio (airside/water side) of the 9.5mm steel plate + 25mm EPT foam (1/3 octave results) , comparison between experimental results and VIBRO1D with material properties derived from extensional measurements, and shear damping measurements.

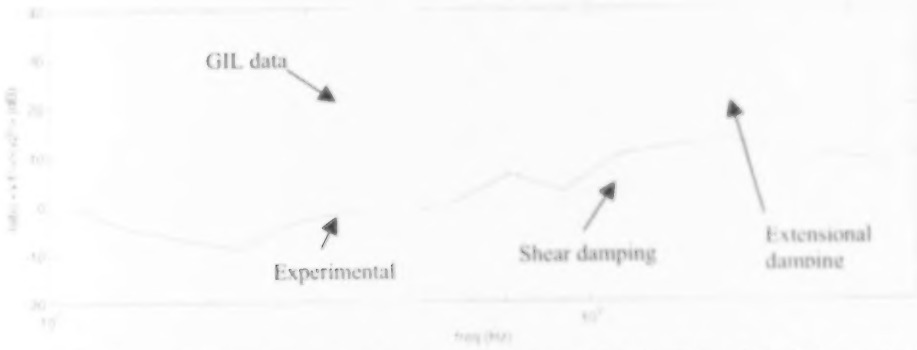

Figure B.20: Mean square velocity ratio (waterside/air side) of the 9.5mm steel plate + 25mm EPT foam (1/3 octave results) , comparison between experimental results and VIBRO3D with material properties derived from extensional measurements, shear damping measurements and GIL data.

Figure B.21: Mean square velocity on the airside of the 9.5mm steel plate + 25mm EPT foam (1/3 octave results) , comparison between experimental results and VIBRO3D with material properties derived from extensional measurements, shear damping measurements and GIL data.

Figure B.22: Mean square velocity on the water side of the 9.5mm steel plate + 25mm EPT foam (1/3 octave results) , comparison between experimental results and VIBRO3D with material properties derived from extensional measurements, shear damping measurements and GIL data.

Figure B.23: Mean square velocity on the water side of the 9.5mm steel plate + 25mm EPT foam (1/3 octave results) , comparison between experimental results and VIBRO3D with material properties derived from extensional measurements, shear damping measurements and DREA data.

APPENDIX C: Influence of the volume of water on the vibration response

Figure C: Mean square velocity ratio on the water side of the 2mm steel plate + 3mm neoprene foam (1/3 octave results) , with 2 different water volumes in the tank.

DOCUMENT CONTROL DATA

(Security classification of title, body of abstract and indexing annotation must be entered when the overall document is classified)

1. ORIGINATOR (the name and address of the organization preparing the document. Organizations for whom the document was prepared, e.g. Establishment sponsoring a contractor's report, or tasking agency, are entered in section 8.)

University of Sherbrooke
Sherbrooke, Quebec, Canada J1K 2R1

2. SECURITY CLASSIFICATION (overall security classification of the document including special warning terms if applicable).

UNCLASSIFIED

3. TITLE (the complete document title as indicated on the title page. Its classification should be indicated by the appropriate abbreviation (S,C,R or U) in parentheses after the title).

VIBRO Software Experimental Validation

4. AUTHORS (Last name, first name, middle initial. If military, show rank, e.g. Doe, Maj. John E.)

Berry, Alain , Wojtowicki, Jean-Luc, Berry, Samuel, Panneton, Raymond

5. DATE OF PUBLICATION (month and year of publication of document)

July 2002

6a. NO .OF PAGES (total containing information Include Annexes, Appendices, etc)

134 (approx.)

6b. NO. OF REFS (total cited in document)

7. DESCRIPTIVE NOTES (the category of the document, e.g. technical report, technical note or memorandum. If appropriate, enter the type of report, e.g. interim, progress, summary, annual or final. Give the inclusive dates when a specific reporting period is covered).

CONTRACTOR REPORT

8. SPONSORING ACTIVITY (the name of the department project office or laboratory sponsoring the research and development. Include address).

DRDC Atlantic
PO Box 1012
Dartmouth, NS, Canada B2Y 3Z7

9a. PROJECT OR GRANT NO. (if appropriate, the applicable research and development project or grant number under which the document was written. Please specify whether project or grant).

11gh14

9b. CONTRACT NO. (if appropriate, the applicable number under which the document was written).

W7707-0-8313

10a. ORIGINATOR'S DOCUMENT NUMBER (the official document number by which the document is identified by the originating activity. This number must be unique to this document.)

2000-R28b

10b. OTHER DOCUMENT NOs. (Any other numbers which may be assigned this document either by the originator or by the sponsor.)

DREA CR 2001-054

11. DOCUMENT AVAILABILITY (any limitations on further dissemination of the document, other than those imposed by security classification)

(X) Unlimited distribution
( ) Defence departments and defence contractors; further distribution only as approved
( ) Defence departments and Canadian defence contractors; further distribution only as approved
( ) Government departments and agencies; further distribution only as approved
( ) Defence departments; further distribution only as approved
( ) Other (please specify):

12. DOCUMENT ANNOUNCEMENT (any limitation to the bibliographic announcement of this document. This will normally correspond to the Document Availability (11). However, where further distribution (beyond the audience specified in (11) is possible, a wider announcement audience may be selected).

13. ABSTRACT (a brief and factual summary of the document. It may also appear elsewhere in the body of the document itself. It is highly desirable that the abstract of classified documents be unclassified. Each paragraph of the abstract shall begin with an indication of the security classification of the information in the paragraph (unless the document itself is unclassified) represented as (S), (C), (R), or (U). It is not necessary to include here abstracts in both official languages unless the text is bilingual).

The University of Sherbrooke's Acoustics and Vibration Group (GAUS) have developed a computer code called VIBRO for modelling the effect of damping and decoupling coatings on the sound radiation from fluid loaded plates. In this work, laser vibrometry was used to measure the vibration on both the wet and dry sides of plates backed by a water filled cavity. VIBRO accurately predicted the mean square velocity spectra of bare 2 mm steel plates in air, both in terms of peak positions and magnitudes. The agreement between experimental data and VIBRO model predictions was not quite as good for the corresponding experiment of the bare plate in water, but peak positions still matched closely. A modified Oberst beam method was used to determine the complex Young's and shear modulus of four different types of foam materials: 3 mm neoprene, 6 mm ethylvinylacetate, 12 mm ethylvinylacetate, and 25 mm EPT/SBR foam. For plates coated with these foams, the VIBRO model predictions were generally very good on the water side of the plate. However, the VIBRO model calculations did not capture a dip in the mean square velocity spectrum that was observed on the air side of coated plates. The results suggest that VIBRO is a useful tool for prediction of the vibration insertion loss and acoustic insertion loss as vibroacoustic indicators. The experimental results related to the effect of the decoupling coatings on the vibration at the plate/ air interface could not be explained in terms of the VIBRO model.

14. KEYWORDS, DESCRIPTORS or IDENTIFIERS (technically meaningful terms or short phrases that characterize a document and could be helpful in cataloguing the document. They should be selected so that no security classification is required. Identifiers, such as equipment model designation, trade name, military project code name, geographic location may also be included. If possible keywords should be selected from a published thesaurus, e.g. Thesaurus of Engineering and Scientific Terms (TEST) and that thesaurus-identified. If it not possible to select indexing terms which are Unclassified, the classification of each should be indicated as with the title).

Noise reduction
Decoupling
VIBRO

Defence R&D Canada

Canada's leader in defence
and national security R&D

R & D pour la défense Canada

Chef de file au Canada en R & D
pour la défense et la sécurité nationale

www.drdc-rddc.gc.ca